Upper Extremity Kinetics during Lofstrand Crutch-Assisted Gait in Children

Neha Bhagchandani
Marquette University

UPPER EXTREMITY KINETICS DURING LOFSTRAND CRUTCH-ASSISTED GAIT IN CHILDREN

by

Neha Bhagchandani B.E.

"A Thesis submitted to the Faculty of the Graduate School,
Marquette University,
in Partial Fulfillment of the Requirements for
the Degree of Master of Science"

Milwaukee, Wisconsin,

May 2010

ABSTRACT
UPPER EXTREMITY KINETICS DURING LOFSTRAND
CRUTCH-ASSISTED GAIT IN CHILDREN

Neha Bhagchandani, B.E.

Marquette University, 2010

Complete biomechanical analysis helps evaluate the motion during various gait patterns for the upper and lower extremities. Extensive studies have been performed to evaluate unassisted gait patterns, but very little has been accomplished for studying assisted motion. Children with pathologies such as osteogenesis imperfecta, spinal cord injury, and cerebral palsy use assistive devices such as anterior and posterior walkers, canes, Lofstrand and axillary crutches for ambulation purposes.

Statistics show that there are currently about 566,000 crutch users in the United States. The long-term crutch users in this population can suffer various upper limb pathologies associated with extensive upper extremity (UE) loading. Better knowledge of UE dynamics in crutch users may ultimately help to prevent injuries due to excessive loading or inappropriate gait patterns. These evaluations may ultimately assist in pre-treatment planning and post-treatment rehabilitation.

Currently, there is no validated system for the assessment of UE joint kinetics during Lofstrand crutch-assisted gait in children. To address these needs two aims will be accomplished:

1. A novel crutch system will be designed and validated to accurately evaluate the UE joint kinetics in children and young adults.
2. A kinetic model will be demonstrated for the newly developed crutch system during Lofstrand crutch-assisted gait in children with osteogenesis imperfecta, spinal cord injury, and cerebral palsy.

ACKNOWLEDGEMENTS

Neha Bhagchandani, B.E.

I would like to express my sincere appreciation for all the support and encouragement to my advisor, Dr. Gerald Harris and my committee members, Dr. Brooke Slavens, Dr. Mei Wang and Dr. Peter Smith for their enormous support and guidance. Owing to their guidance and support I was able to encapsulate the complete experience of my graduate school education. I am very grateful for all the help and encouragement from my very good friend, Ronak Dunung. I am also grateful for my parents, Dr. Suresh and Anjulika Bhagchandani, and my sister Reema Bhagchandani without whom this would not have been possible. I would also like to thank my colleague Dr. Jason Long at the motion analysis lab at the Medical College of Wisconsin for all his help. I would like to thank the Shriners Hospital for Children-Chicago motion analysis laboratory team, Sahar Hassani, Adam Graf, Joseph Krzak, Kathy Reiners, and Vicky Young, for their assistance. This work is supported by the Orthopedic and Rehabilitation Engineering Center, (OREC), Shriners Hospitals for Children and Dr. Ralph and Marian Falk Medical Trust.

TABLE OF CONTENTS

LIST OF TABLES

Chapter 2: Upper Extremity Kinetics during Lofstrand Crutch-Assisted Gait in Children

LIST OF FIGURES

Chapter 1: INTRODUCTION

1.1 Background

While biomechanical analysis has been extensively used to study unassisted motion during gait, little has been accomplished to characterize upper extremity (UE) dynamics during assisted gait. Motion analysis is a noninvasive and painless technique that allows evaluation of multi-planar motion during functional activities [1, 2]. Improved motion analysis technology and modeling software has allowed more rapid development of complex biomechanical models such as those needed to study the UEs during assisted gait.

The prescription of an appropriate assistive device is an essential component for ambulation purposes. In the selection of an ambulatory aid, the goal of the therapist and patient is to maximize maneuverability and independence, while maintaining safety and stability [3]. Walkers are traditionally thought to provide more stability, and thus maximize safety [4]. Compared to walkers, crutches are less cumbersome and are believed to allow patients to maneuver in small spaces easily. Also, they might decrease the appearance of disability [5]. The weight bearing loads associated with assistive devices can be substantial. At the shoulder, in ten adult incomplete SCI subjects, it has been shown that crutches present significantly higher loads than walkers [5]. Melis et al. showed that crutches supported up to 50% body weight, providing lateral stability and anterior–posterior restraint [6].

With underarm crutches, a condition known as crutch paralysis or crutch palsy can arise from pressure on nerves in the armpit, or axilla [7]. Thus, Lofstrand crutches are more common in populations who require long-term crutch usage.

1.2. Significance

There are about 566,000 crutch users estimated in the United States [8]. Among these 36,000 are under 18 years of age [8]. Extensive weight bearing due to long-term crutch usage in this pediatric population can lead to various upper extremity (UE) pathologies such as shoulder arthropathy, arthritis and carpel tunnel syndrome [9,10]. It has also been shown that with repetitive impulse loading, combined with prolonged wrist extension and radial deviation, are proposed risk factors associated with the use of crutches [11]. They have also reported that the use of forearm crutches may lead to hand pain and sensory disturbances [11]. Study done by Sie et al. indicated that walking aids are a causative factor in developing shoulder pain [12].

Evaluating the UE dynamics of Lofstrand crutch users may ultimately help prevent injuries due to excessive loading or inappropriate gait patterns. These evaluations may also assist in pre-treatment planning and post-treatment rehabilitation.

1.3 Pediatric crutch user populations

Lofstrand crutches are common in populations who present partial use of their lower extremities. This population includes children suffering from incomplete spinal cord injury (SCI), cerebral palsy (CP), osteogenesis imperfecta (OI) and myelomeningocele (MM). In this study, subjects with SCI, CP and OI were studied. There are five different gait patterns common with Lofstrand crutch usage [13]. These patterns are depicted in the Figure 1.

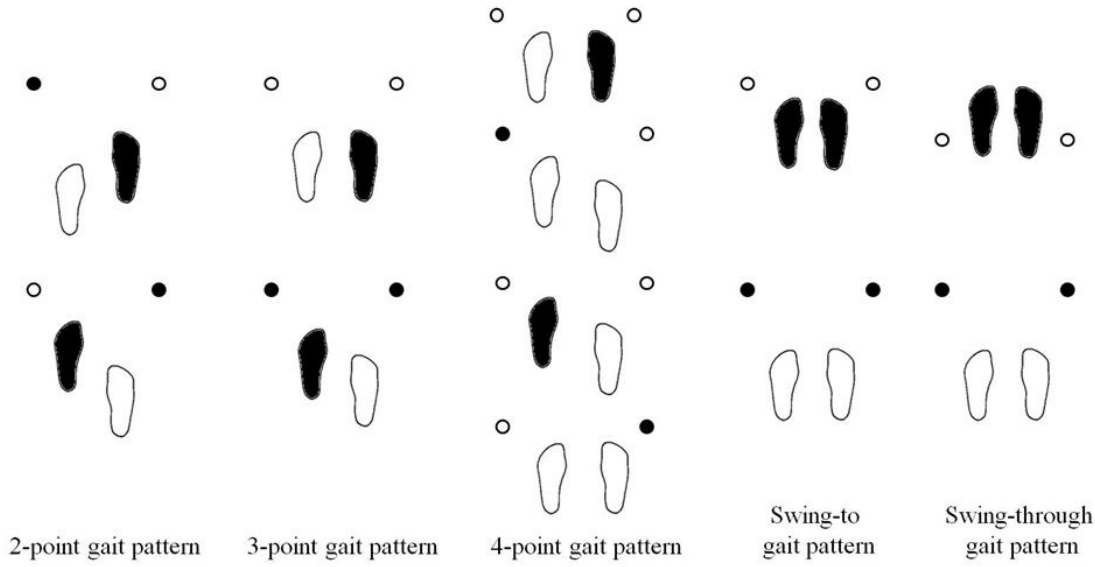

Figure 1: Gait patterns with Lofstrand crutches. The dark represent the entity that was moved forward [13].

1.3.1 Spinal Cord Injury (SCI)

There are about 227,080 to 300,938 persons with SCI in the United States [14]. With improved medical attention at the scene of accident and rehabilitation most spinal cord injuries are incomplete. These survivors present weak lower extremities but are able to ambulate with various assistive devices and can become functional walkers. Musculoskeletal problems are frequent in people who have suffered spinal cord injury as children. According to Vogel, et al., the most common complaint was pain (69%), spasticity (57%), shoulder pain (48%), scoliosis (40%), hip contractures (23%), and back pain (22%) [15]. Thus, long-term crutch usage, causes UE loading which can exacerbate the existing issues.

1.3.2 Cerebral Palsy (CP)

Subjects with CP present an inability to move in a coordinated way since this disorder affects their muscle tone, movement and motor skills. In these patients, the part of the brain that controls muscle tone is affected [16].There is no cure for CP, but

treatment, therapy, special equipment, and, in some cases, surgery can help children living with this condition. In the United States 3 to 4 children per 1000 live births present with CP [17]. This disorder affects the lower extremities more severely than the UEs. Increased levels of spasticity of muscles impairs normal gait in this population. Due to this, children suffering from CP use assistive devices such walkers and crutches for ambulation purposes. In fact, in these children, higher mobility can help maintain joint function and muscle strength [18]. Studies have demonstrated that the effects of long-term crutch usage could be harmful if excessive loading is seen on the UEs [9-12]. Thus, an appropriate assessment of UE loading would be beneficial for this population.

1.3.3 Osteogensis Imperfecta (OI)

This a genetic disorder characterized by fragile bones. OI is caused by an error called a mutation on a gene that affects the body's production of the collagen found in bones, and other tissues [19]. In addition to fractures, people with OI often have muscle weakness, hearing loss, fatigue, joint laxity, curved bones, scoliosis, blue sclerae, dentinogenesis imperfecta (brittle teeth), and short stature [20]. There are about 25,000-50,000 OI cases in the United States [20]. OI is divided into eight types (I, II, III, IV, V, VI, VII and VIII) based on clinical, radiographic and genetic characteristics. Type I OI is the mildest form of OI and the most common in this population. These children suffer from mild fractures but shoulder and elbow dislocation are more common than normal healthy children [20]. Children with type I OI commonly use assistive devices for community ambulation. Children using Lofstrand crutches present a possibility of recurrent fractures due to excessive and repetitive loading of the UEs.

1.4 Hypothesis and Specific Aims

Studies defining UE loading patterns in Lofstrand crutch-assisted gait have been limited. Identification of potential causes and implication of long-term crutch usage on the UEs in pathologies such as SCI, CP and OI would require a comprehensive three dimensional (3D) biomechanical dynamic model. This requires a complete set of kinematics and kinetics which describes UE motion. For the kinematics, the motion of all the UE joints will be defined and kinetics will be computed will the help of reaction forces and moments occurring at the points of contact between the UEs and the crutches.

Previous study done by our group, presented dynamics of reciprocal and swing-through gait pattern, using Lofstrand crutches, in subjects with MM [21]. The instrumented crutch system was equipped with one load cell placed at the tip of each crutch. This system only allowed incorporation of forces and moments at one point of contact (i.e. handle of the crutch). The first goal of this study was to enhance this instrumented crutch system so that it can include forces and moments at the handle, as well as at the cuff. The second aim was to validate the system for future usage. Lastly, the kinetic model will be demonstrated in children with SCI, CP and OI.

The hypothesis of the study was to model a Lofstrand crutch system that can detect joint loading patterns from individual patients and/or pathologies.

1.5 Previous Work

Dynamics of Lofstrand crutch-assisted in a pediatric population has been limited. Unlike lower extremity motion, UE motion is less reproducible and thus difficult to standardize and compare data across various studies. The International Society of Biomechanics (ISB) has established recommendations for standardizing UE joint

coordinate systems [22]. With the help of this, communication across researchers and physicians has been simplified and can aid further studies to follow these standards. Due to the limitation of number of sensors on the Lofstrand crutch previous studies have not been able to include tri-axial forces and moments occurring at the cuff in evaluating the UE kinetics. It is important to include these inputs in the model to accurately estimate the kinetics of the wrist and elbow joints.

Opila et al. pioneered the work for studying the kinetics of UEs during assistive gait using Lofstrand crutches and canes [9]. They tested 12 subjects presenting three different pathologies (total hip replacement (4), tibial fracture (4) and paraplegia (4)).The two systems consisted of a six-axis strain gauge transducer placed on the shaft of each of the assistive devices used to measure axial and shear forces applied to the aids. A 3D video analysis was used to measure the distance from the crutch resultant force vector to the joint centers and subsequently compute shoulder and elbow moments. They did not provide for any analysis during crutch swing. This study showed that strengthening the specific UE musculature required to balance the moments due to loads by these assistive devices can lead to effective use of crutches.

In a study done by Liggins et al., sagittal plane crutch motion, superior/inferior and fore/aft crutch forces seen by the load cell were presented [23]. A six-axis load cell was placed at the crutch tip. This study presented two subjects with two different pathologies, incomplete SCI and CP. The subject with incomplete SCI demonstrated higher forces in the sagittal plane. But the loading patterns in the sagittal plane were different in both the subjects. This preliminary study presented a basis for developing an UE biomechanical system to study crutch motion and ground reaction forces.

Requejo et al. presented a comprehensive study quantifying the UE dynamics in a SCI subject using Lofstrand crutches [24]. The kinetic system used for this study consisted of a six-axis load cell placed just below the handle which reduced the inertial loads. A strain gauge was placed near the cuff which was used to evaluate the cuff moments. The cuff forces were derived from cuff moments. The subject presented an asymmetry in loading pattern consistent with lower extremity strength. The study presented a validated kinetic system for evaluating UE joint loads. Highest superior forces were seen at the wrist, elbow and shoulder.

A study done by Haubert et al., compared the forces in an adult SCI population using Lofstrand crutches and walkers [5]. The study evaluated the mean forces, peak forces, rate of loading, and force time integral at the shoulder. The shoulder forces and rate of loading seen during crutch usage was higher than walker usage. This study failed to quantify forces and moments occurring at the other UE joints.

Previous work done by Slavens et al. presented a 3D biomechanical model in accordance with the ISB recommendation [21]. The kinematic model consisted of nine segments (seven for the UE and one for each of the crutches) whose local coordinates were used to describe the UE extremity motion. A Vicon motion analysis system with 14 infrared cameras was used to evaluate the kinematic motion of the UE segments. For the joint kinetics a six-axis load cell was placed at the crutch-tip. The reaction forces from the load cell were used to evaluate the tri-axial forces and moments at the UEs. Also, due to the placement of the load cells inertial loads were introduced. The involvement of cuff forces and moments was not incorporated in this system. This system was completely evaluated for further reliable usage. This study presented a comparison between

reciprocal and swing-through gait pattern in subjects with MM. The swing-through gait pattern used by this pediatric population presented higher forces and moments than the reciprocal gait pattern.

Chapter 2: UPPER EXTREMITY KINETICS DURING LOFSTRAND CRUTCH-ASSISTED GAIT IN CHILDREN

A version of this chapter is planned for submission to a peer-reviewed journal.

2.1 ABSTRACT

Extensive three dimensional (3D) biomechanical models have been developed to study lower extremity assisted gait. These models have been very useful for pre and post surgical treatment planning. But very little have been accomplished in studying upper extremity (UE) motion during assisted gait. The goal of this study was to develop an instrumented Lofstrand crutch system which completely defines the UE kinematics and kinetics. The kinematic model developed was based on previous studies and was compliant with the International Society of Biomechanics (ISB) recommended standards. The kinetic model consisted of forces and moments and was derived using the kinematic data, anthropometric data, reaction forces and moments generated from the load cells. The novel crutch system has also been validated for accuracy of computing the reaction force and moments. The system and its applications were demonstrated in children with incomplete spinal cord injury (SCI), cerebral palsy (CP) and osteogenesis imperfecta (OI). Evaluating the UE dynamics of these crutch users may ultimately help to reduce long-term pathologies due to excessive loading or inappropriate gait patterns.

2.2 INTRODUCTION

Recognition of upper extremity (UE) arthropathy and degenerative arthritis associated with long-term assistive device usage has been reported in current literature [9-12, 25]. Individuals with weaker lower extremities frequently rely on assistive devices such as walkers, canes and Lofstrand crutches for ambulation. Among these, walkers provide the most support but require large amount of UE strength [6]. Canes provide the

least support [26]. Lofstrand crutches strike a balance between support and freedom required to perform activities of daily living [6].

A few previous studies have quantified UE dynamics during Lofstrand crutch-assisted gait. Among those, Slavens et al. investigated a pediatric myelomeningocele (MM) population and established a standardized UE inverse dynamics model [21]. However, the cuff forces and moments were considered negligible in this model [21]. Also, the placement of the sensor at the tip of the crutch increased the inertial loads. Requejo et al. presented a system with reduced inertial loads by locating the sensor proximal to the handle of the crutch [24]. Yet, this system evaluated only the cuff moments, from which the cuff forces were derived [24]. This crutch model was applied to a single adult incomplete spinal cord injury (SCI) subject. In the study done by Liggins et al., a crutch system similar to Slavens et al. was used but did not fully quantify the UE dynamics [23].

The goal of this study was to develop a pediatric Lofstrand crutch model, which provides a quantitative description of the UE dynamics during crutch-assisted gait. This model will be standardized based on recommendations by the International Society of Biomechanics (ISB) [22] and will include both cuff forces and moments. The system will be versatile for application with various pediatric pathologies performing reciprocal gait pattern. The system can evaluate repetitive loading during ambulation and may prove helpful to develop gait strategies for safer, long-term crutch usage. Studies have shown that Lofstrand crutches require loading of the UEs up to 50% of body weight (BW), without including the involvement of the cuff forces and moments [6]. Evaluation of the UE kinetics in a pediatric population of osteogenesis imperfecta (OI), SCI and cerebral

palsy (CP) is used in this study to gain further insight into the demands placed on the UEs. We hypothesize that the Lofstrand crutch system can detect joint loading patterns from individual patients and/or pathologies.

2.3 METHODS

2.3.1 Crutch Design

Based on previous studies and their limitations (number of sensors, sensor location, and sensor characteristics) five important aspects were considered while designing the crutch system:

1. Increase the number of sensors for evaluating tri-axial forces and moments can at all points of contact on the Lofstrand crutch (handle and cuff) and reduce the overall weight of the system.
2. The location of the 1st load cell, which includes the reaction forces and moments near the handle, should not introduce high inertial loads on the system.
3. The location of the 2nd load cell will be such that all the forces and moments seen at the cuff will be included in the model.
4. The system should be designed in such a way that it could be used by various subjects. This implies that it has to be adjustable to accommodate subjects with varying heights and different forearm sizes. (See appendix for drawings of this crutch system)
5. The system should follow ISB recommendations

Addressing the first concern of more sensors in order to capture all the kinetic data, two six-axis load cells were instrumented on each crutch. These sensors evaluated tri-axial forces and moments occurring at the handle and cuff. The sensors weighed only

0.1 kg. Thus, the whole crutch weighed only 0.2 kg more than the actual weight of the crutch. The weight of sensors included in this study was considerably less than the ones used in the previous studies [5, 21 and 24].

The second aim was to improve the placement of the load cell that are used for evaluating the reaction forces at the handle of the Lofstrand crutch so as to reduce inertial loads which were seen in the previous studies. In order to achieve this goal, the 1st load cell was placed just below the handle. This was referred to as the lower load cell.

To study the involvement of the cuff forces and moments, the 2nd load cell was placed just below the cuff. This allowed capture of tri-axial forces and moments occurring at the cuff. This load cell was referred to as the upper load cell. Due to the placement of the load cells, the lower load cell demonstrated a combined effect of the forces and moments seen at both the load cells. This issue was dealt with while designing the software in such a way that all force and moment components of the upper load cell were subtracted out of the equation while computing the handle forces. This allowed isolation of the forces and moments seen at the cuff and handle.

The next concern was the adjustability of the system to accommodate various subjects with variable height and forearm sizes. The lower load cell was placed such that the upper portion of the crutch shaft was maintained with the holes for adjustable pins which allowed using variable shaft sizes for the lower portion of the crutch and thus making it height adjustable. A similar approach was used for the cuff portion where the load cell was placed just above the handle, allowing the use of various cuff sizes to match the one used by the subject. The last aspect was that the system followed ISB recommendation for which the original crutch axis was flipped according to the ISB

recommendations (See Appendix 1 for details).

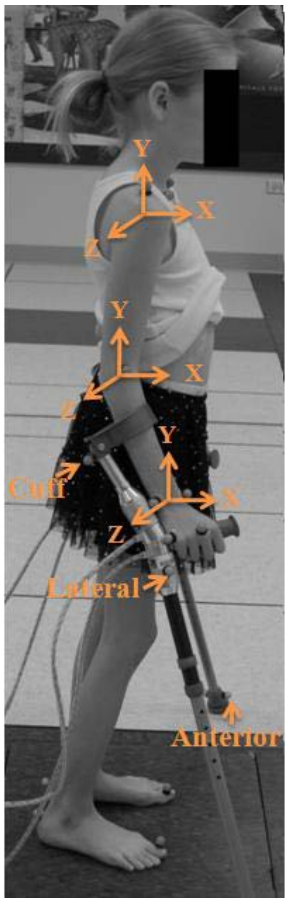

Figure 2: Axis orientation

2.3.2. Kinematic model

The UEs were modeled using seven rigid body segments which were the thorax, upper arms, forearms, and hands. The UE segments were connected by a three degree of freedom (dof) shoulder joint, a two dof elbow joint and a three dof wrist joint. Eighteen reflective markers were used to define these segments (Figure 3). These markers were placed on bony anatomical landmarks to reduce skin and soft tissue motion between bones and markers. Each crutch was modeled using three rigid body segments defined by

the cuff, handle and lower crutch segment. In order to determine crutch kinematics five reflective markers were placed on each crutch.

Joint coordinate segment axes were setup based on ISB recommended standards [22]. The X-axis was directed anteriorly (abduction/adduction axis), Y-axis was directed superiorly (internal/external rotation axis), and the Z-axis was directed laterally to the right (flexion/extension axis). All joints were assumed to have fixed centers of rotation. Euler rotation sequence of Z-X-Y was used to define rotations of the segments. The rotations of the distal coordinate system were defined with respect to the proximal coordinate system, while the crutch and the thorax were referenced to the lab coordinate system.

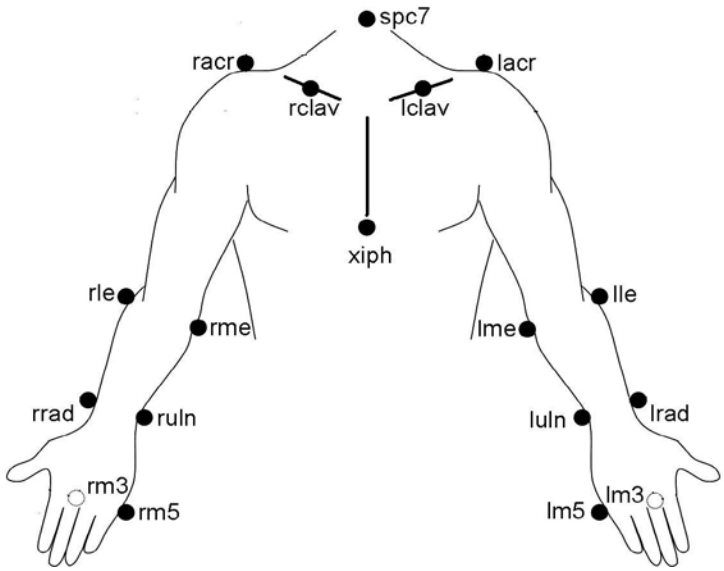

Figure 3: Marker placement for defining the UE segments [21].

2.3.2.1. Joint Centers

Joint centers were calculated using the markers and subject specific anthropometric data (Table 1). The thorax model was based on the study done by Nyugen

et al., for analyzing thorax kinematics in children with MM [28]. The markers situated in the clavicles ($\overline{m}_{rclav}$ and $\overline{m}_{lclav}$), C7 spinous process ($\overline{m}_{spc7}$) and xiphoid process ($\overline{m}_{xi}$) were used to define the thorax movement. Among the thorax markers the clavicles and the C7 spinous process were used to define the thorax center. The thorax center ($\overline{t_c}$) was evaluated halfway between the center of the clavicles and the C7 spinous process.

The upper arm was defined using the markers placed on the acromions ($\overline{m}_{racr}$ and $\overline{m}_{lacr}$), medial ($\overline{m}_{rme}$ and $\overline{m}_{lme}$) and lateral elbow epicondyles ($\overline{m}_{rle}$ and $\overline{m}_{lle}$). The radius of the shoulder joint was estimated by measuring the circumference around the shoulder. The distance equal to the radius of the shoulder plus the radius of the marker (0.007 m) was subtracted from the acromion marker acting in the negative Y direction ($\overline{Y}$) was determined as the shoulder joint center ($\overline{s_c}$) [31-35] .

The forearm segment was defined by medial ($\overline{m}_{rme}$ and $\overline{m}_{lme}$) and lateral elbow epicondyles ($\overline{m}_{rle}$ and $\overline{m}_{lle}$); radius ($\overline{m}_{rrad}$ and $\overline{m}_{lrad}$) and ulnar styloids ($\overline{m}_{ru\ln}$ and $\overline{m}_{lu\ln}$). The midpoint of the lateral and the medial epicondyles was defined as the elbow joint center ($\overline{e_c}$).

Similarly, the wrist segment was defined by radial ($\overline{m}_{rrad}$ and $\overline{m}_{lrad}$) and ulnar styloids ($\overline{m}_{ru\ln}$ and $\overline{m}_{lu\ln}$); 3rd ($\overline{m}_{rm3}$ and $\overline{m}_{lm3}$) and 5th metacarpal ($\overline{m}_{rm5}$ and $\overline{m}_{lm5}$). The midpoint of the radial and ulnar styloids was defined as the wrist joint center ($\overline{w_c}$).

Table 1: Upper extremity joint centers

	Wrist ($\overline{w_c}$)	Elbow ($\overline{e_c}$)	Shoulder ($\overline{s_c}$)	Thorax($\overline{t_c}$)
Joint Centers	$\frac{(\overline{m}_{rrad} + \overline{m}_{ru\ln})}{2}$	$\frac{(\overline{m}_{rme} + \overline{m}_{rle})}{2}$	$\overline{m}_{acr} - \overline{Y}(0.007 + r)$	$\frac{\frac{1}{2}\left(\overline{m}_{rclav} + \overline{m}_{lclav}\right) + \overline{m}_{spc7}}{2}$

2.3.2.2. Segment coordinate axis

Segment coordinate axis was setup for each of the 7 segments of the UEs and 6 segments of the crutches. The relative motion between two adjacent segments was used to define the joint angles. ISB recommendations were implemented for developing the segment coordinate axis [22]. All coordinate axes followed the right hand rule where, X-axis was directed anteriorly, Y-axis was directed superiorly and Z-axis was directed laterally to the right. The vectors used to evaluate each of the segment coordinate axis are described below.

2.3.2.2.1 Thorax

The thorax coordinate system was setup with the help of a temporary coordinate axis and virtual point [21, 28]. The temporary coordinate axis had its origin at the xiphoid process ($\overline{m}_{xiph}$). This temporary coordinate axis is represented below:

$$\overline{Y}_{temp} = \frac{\overline{m}_{spc7} - \overline{m}_{xiph}}{\left|\overline{m}_{spc7} - \overline{m}_{xiph}\right|} \tag{1}$$

$$\overline{X}_{temp} = \frac{\left(\overline{m}_{rclav} + \overline{m}_{lclav}\right)/2 - \overline{m}_{xiph}}{\left|\left(\overline{m}_{rclav} + \overline{m}_{lclav}\right)/2 - \overline{m}_{xiph}\right|} \times \overline{Y}_{temp} \tag{2}$$

$$\overline{Z}_{temp} = \overline{X}_{temp} \times \overline{Y}_{temp}$$

The virtual point ($\bar{t}_{virtualpoint}$) was the translated 10 mm in the direction of the temporary X-axis.

$$\bar{t}_{virtualpoint} = \overline{t}_c + 0.01 \times \overline{X}_{temp} \tag{3}$$

The thorax center ($\overline{t}_c$) was the origin for the thorax coordinate system which is presented below.

$$\overline{X}_{Thorax} = \frac{\left(\overline{m}_{rclav} + \overline{m}_{lclav}\right)/2 - \overline{m}_{spc7}}{\left|\left(\overline{m}_{rclav} + \overline{m}_{lclav}\right)/2 - \overline{m}_{spc7}\right|} \quad (4)$$

$$\overline{Y}_{Thorax} = \frac{\bar{t}_{virtualpoint} - \bar{t}_c}{\left|\bar{t}_{virtualpoint} - \bar{t}_c\right|} \times \overline{X}_{Thorax} \quad (5)$$

$$\overline{Z}_{Thorax} = \overline{X}_{Thorax} \times \overline{Y}_{Thorax} \quad (6)$$

2.3.2.2.2. Upper Arm

The shoulder joint center ($\overline{s_c}$) was the origin for the upper arm segment coordinate axis. The vectors defining this segment coordinate axis are described in the Figure 2.

$$\overline{Y}_{Upperarm} = \frac{\bar{s}_c - \bar{e}_c}{\left|\bar{s}_c - \bar{e}_c\right|} \quad (7)$$

$$\overline{Z}_{Upperarm} = \frac{\overline{m}_{uln} - \bar{e}_c}{\left|\overline{m}_{uln} - \bar{e}_c\right|} \times \overline{Y}_{Upperarm} \quad (8)$$

$$\overline{X}_{Upperarm} = \overline{Z}_{Upperarm} \times \overline{Y}_{Upperarm} \quad (9)$$

2.3.2.2.3. Forearm

The elbow joint center ($\overline{e_c}$) was the origin for the forearm segment coordinate axis. The vectors defining this segment coordinate axis are described in the Figure 2. The design of the elbow to constrain varus and valgus was similar to the method reported by Rab and Schmidt [29, 30 and 39].

$$\overline{Y}_{Forearm} = \frac{\bar{e}_c - \overline{m}_{uln}}{\left|\bar{e}_c - \overline{m}_{uln}\right|} \quad (10)$$

$$\overline{X}_{Forearm} = \frac{\overline{m}_{u\ln} - \overline{m}_{rad}}{\left|\overline{m}_{u\ln} - \overline{m}_{rad}\right|} \times \overline{Y}_{Forearm} \quad (11)$$

$$\overline{Z}_{Forearm} = \overline{X}_{Forearm} \times \overline{Y}_{Forearm} \quad (12)$$

2.3.2.2.4 Hand

The hand coordinate system was setup similar to the thorax segment where a temporary coordinate axis and virtual point were used to compute the hand coordinate system. The temporary coordinate axis had its origin at the ulnar styloid ($\overline{m}_{u\ln}$). This temporary coordinate axis is represented below:

$$\overline{Y}_{temp} = \frac{\overline{m}_{u\ln} - \overline{m}_{m5}}{\left|\overline{m}_{u\ln} - \overline{m}_{m5}\right|} \quad (13)$$

$$\overline{X}_{temp} = \frac{\overline{m}_{u\ln} - \overline{m}_{rad}}{\left|\overline{m}_{u\ln} - \overline{m}_{rad}\right|} \times \overline{Y}_{temp} \quad (14)$$

$$\overline{Z}_{temp} = \overline{X}_{temp} \times \overline{Y}_{temp} \quad (15)$$

The virtual point ($\overline{h}_{virtualpo\text{int}}$) was then translated in the direction of the temporary X-axis and that distance was equivalent to subject specific width of the hand divided by 2 ($w/2$) and radius of the marker (7mm).

$$\overline{h}_{virtualpo\text{int}} = \overline{\overline{m}_{m3}} + \left(\frac{w}{2} + 0.007\right) \times \overline{X}_{temp} \quad (16)$$

The wrist center ($\overline{\overline{w}_c}$) was the origin for the hand coordinate system which is presented below (Figure 2) [22 and 24].

$$\overline{Y}_{Hand} = \frac{\overline{w}_c - \overline{h}_{virtualpo\text{int}}}{\left|\overline{w}_c - \overline{h}_{virtualpo\text{int}}\right|} \quad (17)$$

$$\overline{X}_{Hand} = \frac{\overline{m}_{u\ln} - \overline{m}_{rad}}{\left|\overline{m}_{u\ln} - \overline{m}_{rad}\right|} \times \overline{Y}_{Hand} \tag{18}$$

$$\overline{Z}_{Hand} = \overline{X}_{Hand} \times \overline{Y}_{Hand} \tag{19}$$

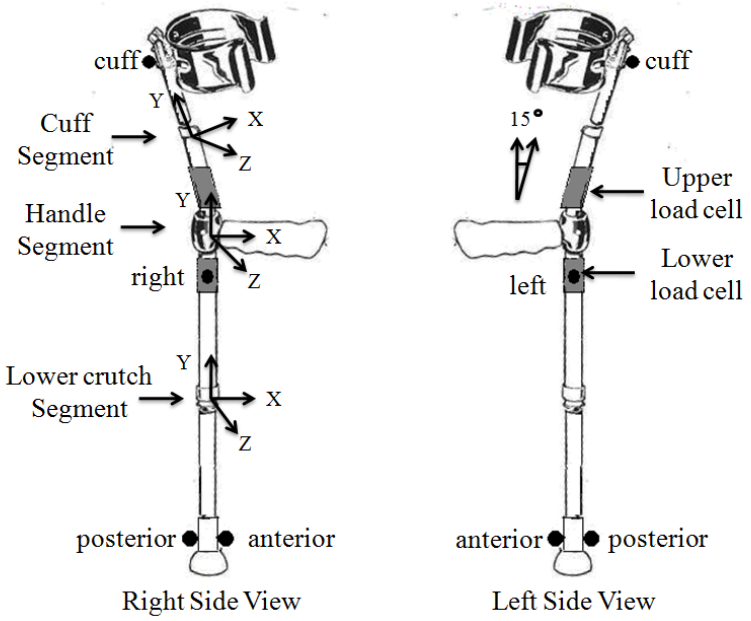

Figure 4: Crutch segment definitions and axis orientation

2.3.2.2.4 Crutch

The crutch kinematics was divided into three segments: lower crutch, crutch handle and the cuff (Figure 4). Since the crutch is a rigid segment only one main crutch segment was defined which was then appropriately modified using spatial coordinate transformation to compute the kinematics of all the three segments.

2.3.2.2.4.1 Handle

The crutch handle segment consisted of the crutch handle, upper and lower load cells. The crutch maker setup is shown in the Figure 4.The origin of the handle segment ($\overline{lc}_c$) was defined by the computing the midpoint of the lower load cell. A midpoint of

the crutch tip was computed as a virtual point ($\bar{c}_{virtualpoint}$), which was further used for defining the segment coordinate axis.

$$\overline{lc}_c = \frac{(\overline{m}_{lateral} + \overline{m}_{medial})}{2} \tag{20}$$

$$\bar{c}_{virtualpoint} = \frac{(\overline{m}_{anterior} + \overline{m}_{posterior})}{2} \tag{21}$$

$$\overline{Y}_{Handle} = \frac{\overline{lc}_c - \bar{c}_{virtualpoint}}{\left|\overline{lc}_c - \bar{c}_{virtualpoint}\right|} \tag{22}$$

$$\overline{X}_{Handle} = \frac{\overline{m}_{medial} - \overline{m}_{lateral}}{\left|\overline{m}_{medial} - \overline{m}_{lateral}\right|} \times \overline{Y}_{Handle} \tag{23}$$

$$\overline{Z}_{Handle} = \overline{X}_{Handle} \times \overline{Y}_{Handle}$$

2.3.2.2.4.2 Lower Crutch

The midpoint of the lower load cell ($\overline{lc}_c$) and the virtual point ($\bar{c}_{virtualpoint}$) was used to compute the origin for the crutch tip segment ($\overline{Ctip}_c$).

$$\overline{Ctip}_c = \frac{(\overline{lc}_c + \bar{c}_{virtualpoint})}{2} \tag{24}$$

$$\overline{Y}_{LowerCrutch} = \frac{\overline{lc}_c - \overline{Ctip}_c}{\left|\overline{lc}_c - \overline{Ctip}_c\right|} \tag{25}$$

$$\overline{X}_{LowerCrutch} = \frac{\overline{m}_{medial} - \overline{m}_{lateral}}{\left|\overline{m}_{medial} - \overline{m}_{lateral}\right|} \times \overline{Y}_{LowerCrutch} \tag{26}$$

$$\overline{Z}_{LowerCrutch} = \overline{X}_{LowerCrutch} \times \overline{Y}_{LowerCrutch}$$

2.3.2.2.4.3 Cuff

First a temporary segment was setup which was positively rotated along the Z-axis by an angle of 15 degrees. The 15 degree angle was chosen since the cuff is 15 degrees rotated with reference to vertical shaft (Figure 4). For the origin of the cuff

segment the midpoint of the upper load cell was estimated by shifting the lower load cell midpoint by 9 cm in the Y direction of the temporary axis. The cuff segment had the same orientation as the temporary axis but with the origin of this coordinate axis was the midpoint of the upper load cell. The temporary axis definitions, origin of the cuff segment and the coordinate axis of the cuff segment are given below.

$$\overline{Z}_{temp} = \overline{Z}_{Handle} \tag{27}$$

$$\overline{X}_{temp} = \overline{X}_{Handle} * \cos(15^{o}) - \overline{Y}_{Handle} * \sin(15^{o}) \tag{28}$$

$$\overline{Y}_{temp} = \overline{X}_{Handle} * \sin(15^{o}) + \overline{Y}_{Handle} * \cos(15^{o}) \tag{29}$$

$$\overline{cuff}_{c} = \left(\overline{lc}_{c} + 0.09\right) \times \overline{Y}_{temp} \tag{30}$$

$$\overline{Z}_{cuff} = \overline{Z}_{temp} \tag{31}$$

$$\overline{X}_{cuff} = \overline{X}_{temp} \tag{32}$$

$$\overline{Y}_{cuff} = \overline{Y}_{temp} \tag{33}$$

2.3.2.3 Euler angle sequence

Z-X-Y Euler rotation sequence was used to evaluate the UE joint kinematics [35]. The rotation matrix used for this study is given below.

$$R = \begin{bmatrix} -\sin(\theta 1)\sin(\theta 2)\sin(\theta 3) + \cos(\theta 1)\cos(\theta 3) & -\sin(\theta 1)\cos(\theta 2) & \sin(\theta 1)\sin(\theta 2)\cos(\theta 3) + \cos(\theta 1)\sin(\theta 3) \\ \cos(\theta 1)\sin(\theta 2)\sin(\theta 3) + \sin(\theta 1)\cos(\theta 3) & \cos(\theta 1)\cos(\theta 2) & -\cos(\theta 1)\sin(\theta 2)\cos(\theta 3) + \sin(\theta 1)\sin(\theta 3) \\ -\cos(\theta 2)\sin(\theta 3) & \sin(\theta 2) & \cos(\theta 2)\cos(\theta 3) \end{bmatrix} \tag{34}$$

2.3.3. Kinetic model

The crutch and the UE forces are evaluated by the kinetic model. The kinetic model was developed using the inverse dynamics Newton-Euler approach [35]. The reaction forces and the moments from the instrumented crutches were used to evaluate the 3D forces and moments occurring at the crutch, wrist, elbow and shoulder. The joint forces and moments were expressed in the local (segmental) coordinate frame.

2.3.3.1. Instrumentation

Crutches were custom designed and instrumented with FS-6 load cells (AMTI, Watertown, MA) to measure the applied reaction forces and moments. These load cells measured tri-axial forces and moments. Each crutch consisted of two load cells placed above and below the handle (Figures 2 and 4). The load cells were made from high-strength aluminum alloy. Strain gages and bridge circuits were incorporated in the load cells to evaluate the forces and moments. Thin co-axial cables were used to multiplex crutch data for data acquisition. The load cells had high sensitivity, high stiffness, low cross talk and long-term stability. The analog data from the load cells were amplified using AMTI MSA-6 high gain amplifiers. The weight of the load cells was 0.10 kg each and the weight of the crutch used for this study was 0.43 kg.

2.3.3..2. Kinetic Inputs

In order to evaluate the kinetics of the UEs, inputs such as angular joint velocities and accelerations were needed. These were computed by means of Euler angles obtained from kinematics for the wrist, elbow, shoulder and trunk. The center of mass (CoM) of the segments and the inertial properties of the UE segments was determined by the marker positions and inertial properties of human body segments [36]. The crutch was assumed to be composed of cylindrical shells and solid cylinder for the load cells. This assumption was used to define the center of mass and the moment of inertia of the crutches. Segmental masses, segmental acceleration of the CoM, distal forces and moments were used as inputs for the inverse dynamic equations to evaluate the forces and moments at the proximal segments. The Newton-Euler equations used for an individual joint are given below:

$$\bar{F}_{i+1} = \bar{F}_i - m\bar{g} - m\bar{a} \quad (35)$$

$$\dot{H} = [I]\,\ddot{\theta} + \dot{\theta} \times \left([I]\,\dot{\theta} \right) \quad (36)$$

$$\bar{M}_{i+1} = \dot{H} - \bar{M}_i - r_i \times \bar{F}_i - r_{i+1} \times \bar{F}_{i+1} \quad (37)$$

where forces $\bar{F}$, $\dot{H}$ and $\bar{M}$ are the forces, rate of change of angular momentum and the moment acting on a segment *i* where *i* represents the distal joint and *i+1* represents the proximal joint [36]. Mass of the particular segment is given by *m*. $\bar{g}$ is the acceleration due to gravity and $\bar{a}$ is the acceleration of the i^{th} segment. $[I]$is the inertia matrix of a body, whose origin is located at the CoM of the body. For an angle θ formed between two segments, $\dot{\theta}$ is the angular velocity, and $\ddot{\theta}$ is the angular acceleration.

2.3.3.3. Kinetic equations

The kinetics equations were computed with the inverse dynamics Newton-Euler approach [39]. The reaction forces and moments from the two load cells in each crutch were used recursively to solve the kinetic equations one after the other starting from the most distal segment. The proximal forces were computed from the known distal forces, mass and acceleration of a segment. After which the proximal moments where computed from known distal moments, rate of change of angular momentum of the segment, moment arms and moment contribution of the distal and proximal forces. The free body diagrams for each segment are shown (Figures 5-7). The kinetic equations for each segment are described below. All these equations were applied separately in the x, y and z directions.

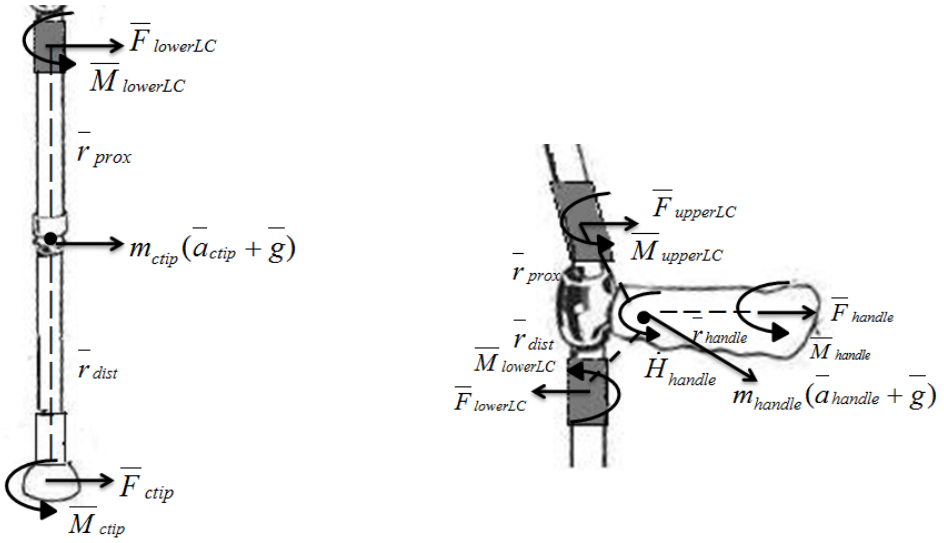

Figure 5: Free body diagram of crutch tip and crutch handle

2.3.3.3.1. Lower Crutch Segment

The lower crutch segment consisted of lower load cell and the lower shaft of the crutch. The force and moment from the lower load cell were used to evaluate the force and moment contribution at the crutch tip (Figure 5).

$$\overline{F}_{ctip} = -m_{ctip}(\bar{a}_{ctip} + \bar{g}) - \overline{F}_{lowerLC} \tag{38}$$

$$\overline{M}_{ctip} = \dot{H}_{ctip} - \overline{M}_{lowerLC} - \bar{r}_{dist} \times \overline{F}_{ctip} - \bar{r}_{prox} \times \overline{F}_{lowerLC} \tag{39}$$

where $\overline{F}_{ctip}$ and $\overline{M}_{ctip}$ are the unknown force and moment occurring at the crutch tip. m_{ctip} and $\bar{a}_{ctip}$ are the mass and the linear acceleration of the lower crutch segment. $\bar{g}$ is the acceleration due to gravity. $\overline{F}_{lowerLC}$ and $\overline{M}_{lowerLC}$ are the known force and moment seen at the lower load cell. $\dot{H}_{ctip}$ in this equation is zero since the angular velocities and accelerations are zero for a rigid body. $\bar{r}_{dist}$ is the distance from the crutch tip and $\bar{r}_{prox}$ is the distance from the center of the lower load cell to the CoM of the lower segment.

2.3.3.3.2. Handle Segment

This segment consisted of the crutch handle, lower and upper load cell. The force and moment from the lower and upper load cell was used to evaluate the force and moment contribution at the handle (Figure 5).

$$\overline{F}_{handle} = -m_{handle}(\bar{a}_{handle} + \bar{g}) + \overline{F}_{lowerLC} - \overline{F}_{upperLC} \tag{40}$$

$$\overline{M}_{handle} = \dot{H}_{handle} + \overline{M}_{lowerLC} - \overline{M}_{upperLC} + \bar{r}_{dist} \times \overline{F}_{lowerLC} - \bar{r}_{prox} \times \overline{F}_{upperLC} - \bar{r}_{handle} \times \overline{F}_{handle} \tag{41}$$

where $\overline{F}_{handle}$ and $\overline{M}_{handle}$ are the unknown force and moment occurring at the point of contact between the hand the crutch handle. m_{handle} and $\bar{a}_{handle}$ are the mass and the linear acceleration of the handle segment. $\overline{F}_{lowerLC}$ and $\overline{M}_{lowerLC}$ are the known force and moment seen at the lower load cell. $\overline{F}_{upperLC}$ and $\overline{M}_{upperLC}$ are the known force and moment seen at the upper load cell. $\dot{H}_{handle}$ is the rate of change of angular momentum of the handle segment. $\bar{r}_{dist}$ is the distance from the CoM of the lower loadcell, $\bar{r}_{prox}$ is the distance from the Com of the upper load cell and $\bar{r}_{handle}$ is the distance from the point of contact of the hand on the crutch handle to the CoM of the handle segment.

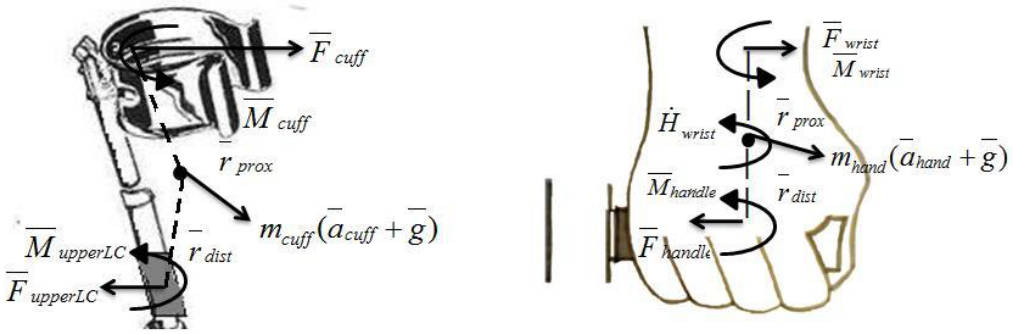

Figure 6: Free body diagram of cuff and hand

2.3.3.3.3. Cuff Segment

The cuff segment consisted of upper load cell and the cuff. The force and moment from the upper load cell were used to evaluate the force and moment contribution at the cuff (Figure 6).

$$\overline{F}_{cuff} = -m_{cuff}(\bar{a}_{cuff} + \bar{g}) + \overline{F}_{upperLC} \tag{42}$$

$$\overline{M}_{cuff} = \dot{H}_{cuff} - \overline{M}_{upperLC} + \bar{r}_{dist} \times \overline{F}_{upperLC} - \bar{r}_{prox} \times \overline{F}_{cuff} \tag{43}$$

where $\overline{F}_{cuff}$ and $\overline{M}_{cuff}$ are the unknown force and moment occurring at the point of contact of the cuff. m_{cuff} and $\bar{a}_{cuff}$ are the mass and the linear acceleration of the cuff segment. $\overline{F}_{upperLC}$ and $\overline{M}_{upperLC}$ are the known force and moment seen at the upper load cell. $\dot{H}_{cuff}$ in this equation is zero since the angular velocities and accelerations are zero for a rigid body. $\bar{r}_{dist}$ is the distance from the CoM of the upper load cell and $\bar{r}_{prox}$ is the distance from the point of contact at the cuff to the CoM of the cuff segment.

2.3.3.3.4. Hand Segment

The hand segment consisted of the hand. The force and moment from the lower load cell were used to evaluate the force and moment contribution at the wrist (Figure 6).

$$\overline{F}_{wrist} = -m_{hand}(\bar{a}_{hand} + \bar{g}) + \overline{F}_{handle} \tag{44}$$

$$\overline{M}_{wrist} = \dot{H}_{wrist} + \overline{M}_{handle} + \bar{r}_{dist} \times \overline{F}_{handle} - \bar{r}_{prox} \times \overline{F}_{wrist} \tag{45}$$

where $\overline{F}_{wrist}$ and $\overline{M}_{wrist}$ are the unknown force and moment occurring at the wrist joint. m_{wrist} and $\bar{a}_{wrist}$ are the mass and the linear acceleration of the wrist segment. $\overline{F}_{handle}$ and $\overline{M}_{handle}$ are the known force and moment at the point of contact between the hand and crutch handle. $\dot{H}_{wrist}$ is the rate of change of angular momentum of the wrist segment.

$\bar{r}_{dist}$ is the distance from the point of contact between the hand and crutch handle and $\bar{r}_{prox}$ is the distance from the wrist joint center to the CoM of the wrist segment.

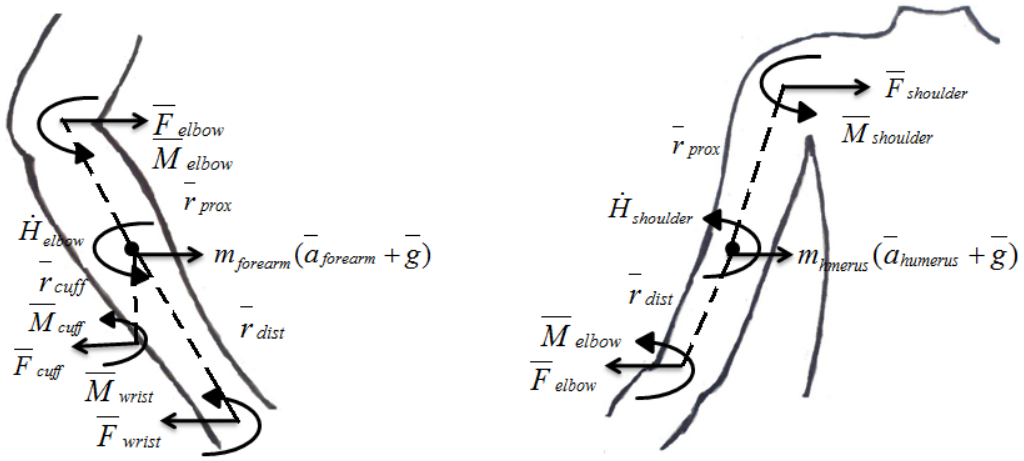

Figure 7: Free body diagram of forearm and upper arm

2.3.3.3.5. Forearm Segment

This segment consisted of the forearm. The force and moment from the wrist joint and point of contact at the cuff were used to evaluate the force and moment contribution at the elbow (Figure 7).

$$\bar{F}_{elbow} = -m_{forearm}(\bar{a}_{forearm} + \bar{g}) + \bar{F}_{wrist} + \bar{F}_{cuff} \tag{46}$$

$$\bar{M}_{elbow} = \dot{H}_{elbow} + \bar{M}_{wrist} + \bar{M}_{cuff} + r_{dist} \times \bar{F}_{wrist} + r_{cuff} \times \bar{F}_{cuff} - r_{prox} \times \bar{F}_{wrist} \tag{47}$$

where $\bar{F}_{elbow}$ and $\bar{M}_{elbow}$ are the unknown force and moment occurring at the elbow joint. m_{elbow} and $\bar{a}_{elbow}$ are the mass and the linear acceleration of the forearm segment. $\bar{F}_{wrist}$ and $\bar{M}_{wrist}$ are the known force and moment at the wrist joint. $\bar{F}_{cuff}$ and $\bar{M}_{cuff}$ are the known force and moment at the point of contact of the cuff. $\dot{H}_{elbow}$ is the rate of change of angular momentum of the elbow joint. $\bar{r}_{dist}$ is the distance from the wrist joint center,

$\bar{r}_{prox}$ is the distance from the elbow joint center and $\bar{r}_{cuff}$ is the distance from the point of contact at the cuff to the CoM of the elbow segment.

2.3.3.3.6. Upper arm Segment

The upper arm segment consisted of the humerus. The force and moment from the elbow joint were used to evaluate the force and moment contribution at the shoulder (Figure 7).

$$\overline{F}_{shoulder} = -m_{hmerus}(\bar{a}_{humerus} + \bar{g}) + \overline{F}_{elbow} \quad (48)$$

$$\overline{M}_{shoulder} = \dot{H}_{shoulder} + \overline{M}_{elbow} + \bar{r}_{dist} \times \overline{F}_{elbow} - \bar{r}_{prox} \times \overline{F}_{shoulder} \quad (49)$$

where $\overline{F}_{shoulder}$ and $\overline{M}_{shoulder}$ are the unknown force and moment occurring at the shoulder joint. $m_{humreus}$ and $\bar{a}_{humerus}$ are the mass and the linear acceleration of the upper arm segment. $\overline{F}_{elbow}$ and $\overline{M}_{elbow}$ are the known force and moment at the elbow joint. $\dot{H}_{shoulder}$ is the rate of change of angular momentum of the shoulder joint. $\bar{r}_{dist}$ is the distance from the elbow joint center and $\bar{r}_{prox}$ is the distance from the shoulder joint center to the CoM of the upper arm segment.

2.3.4. System validation

A stand was built for performing validation protocols and initial zeroing of the load cells before testing (See Appendix 1 for diagrams). Two sets of validation trials were performed. First, static validation was performed by applying known loads to the instrumented crutch system. Five trials were performed for each load applied to the system. During the static validation, the crutch was supported by the stand; clamped at the handle and held above the ground (See Appendix 1 for photos). The original axes of the sensors were oriented differently than the required ISB recommendations. Thus, for

testing, the software was modified in order to re-orient the load cell axis in accordance with the ISB recommendations (See Appendix 1 for original axes of the sensors).

Secondly, dynamic validation of the system was performed by walking with the crutches on a force plate and comparing the resultant forces evaluated by both systems. Five trials were performed with each crutch for this validation protocol. Percentage RMS error (% RMS Error) and standard deviation (STD) was computed for the validation protocols. The RMS error for the dynamic validation was reported as a percentage of the force recorded from the force plate.

The load cells were zeroed before every testing session to maintain repeatability between sessions. During zeroing the crutches, they were supported similar to the technique used for supporting the crutches during static validation i.e. they were held vertical, clamped at the handle and held above the ground.

2.3.5. Patient Population

Three subjects with prior experience using Lofstrand crutches participated in this study. The subjects belonged to three different pathologies which consisted of incomplete SCI (Level T6), diplegic CP and type I OI (Table 2). The subject with OI regularly used only the right Lofstrand crutch for community ambulation purposes. Each instrumented Lofstrand crutch was adjusted to match the height and cuff size to subject's regular crutches. Written parental consent and subject assent was obtained in compliance with IRB requirements. All subjects were recruited from Shriners Hospital in Chicago, IL. Subjects who had undergone orthopaedic surgery in the last one year and had suffered a fracture in the last six months were excluded from participating in the study.

Table 2: Subject specific data

Pathology	Age (years)	Gender	Height (m)	Weight (kg)	Handedness	Weight bearing Extremity
SCI	7	Female	1.2	20.4	Right	Right
CP	11	Female	1.4	24.9	Right	Left
OI	16	Female	1.4	43.8	Right	Right

2.3.6 Data Collection, Processing and Analysis

The subjects were asked to walk at a self-selected pace with the bilateral instrumented Lofstrand crutches on a six-meter walkway for six trials. A Vicon motion analysis system, with 14 infrared cameras, was used to capture 3D motion of the reflective markers placed on the bony landmarks of the subject and the crutches. The motion data were sampled at the rate of 120 Hz. Vicon workstation was used for processing the motion data and generating 3D coordinates of the markers, which were then analyzed using Vicon BodyBuilder. The motion data were filtered using a Woltering filter. Data were averaged over six trials. Foot heel strike to heel strike is defined as a 100% gait cycle with data being processed every 1 % of the gait cycle. Matlab (The MathWorks Inc. Natick, MA) was used for further data analysis.

Cadence, walking speed, stride length and stance duration were calculated for each subject and the mean of six trials was computed. Motion for the thorax, shoulder, elbow and the wrist were evaluated for the sagittal, frontal and transverse planes. Motion seen in all the planes was used for calculating the range of motion. Mean external forces and moments at the crutch tip, handle and cuff were determined for all three planes. Mean joint reaction forces (JRFs) and joint reaction moments (JRMs) were presented for the wrist, elbow and shoulder. Forces and moments are expressed as % body weight (%BW) and % body weight times height (%BW*H) respectively. Peak forces and

moments were the maximum forces and moments seen over the entire gait cycle in a particular plane.

2.4 RESULTS

2.4.1 System Accuracy

The percentage RMS error and STD in the sagittal plane during static validation are reported in Table 3. The least % RMS error of 0.84 % was seen in the lower right load cell for evaluating the forces in the vertical (z) direction. The smallest STD was seen in the lower left load cell for the medial (x) moment. The % RMS error and STD for the dynamic validation between the force plate and load cell are reported in Table 4. Here the left crutch presented the lower % RMS error and STD.

Table 3: Static validation

Forces and Moments		RMS Error (%)		STD (N)	
		Right	Left	Right	Left
Upper load cell	Fz	4.06	1.11	0.11	0.04
	Mx	4.09	4.76	0.01	0.05
Lower load cell	Fz	0.84	0.90	0.05	0.05
	Mx	3.74	5.20	0.03	0.01

Table 4: Dynamic validation

Force	RMS Error (%)		STD (N)	
	Right	Left	Right	Left
Resultant	2.81	1.43	0.55	0.29

2.4.2 Temporal Distance Parameters

The mean cadence, walking speed, stride length and stance duration were compared among the three subjects (Table 5). The subject with OI presented the highest

cadence and walking speed. The subject with SCI presented the lowest walking speed and stride length.

Table 5: Temporal distance parameters

Subject	Cadence (Steps/min)	Walking speed (m/s)	Stride Length (m)	Stance Duration (%)
SCI	97.79	0.53	0.64	68.55
CP	78.29	0.62	0.95	56.31
OI	103.37	0.78	0.91	65.44

On observation of the dynamic crutch data, asymmetry in the crutch gait loading patterns was observed in all subjects (Table 2). Every subject presented a pattern in which one extremity demonstrated higher forces and moments while the other extremity displayed much smaller magnitudes of forces and moments. For ease of comparison between the UEs loading patterns further data was compared based on the extremities presenting higher loads (weight bearing extremity) and lower loads (non-weight bearing extremity)

2.4.3 Upper Extremity Kinematics

The UE kinematic data was compared across all the three subjects. The mean kinematics of the thorax (Figure 8), shoulder, elbow, and crutch angles during crutch gait are displayed (Figures 9-10). Joint ranges of motion (ROM) were calculated for comparison between gait patterns (Figure 11).

2.4.3.1 Thorax

Mean thorax kinematics and the range of motion for all the subjects are presented in the Figure 8. The thorax kinematics is presented along with heel contact and crutch contact. Across all subjects the thorax was in flexion with limited range of motion during complete gait cycle. In the frontal plane, the thorax presented lateral bending to the either

side of the vertical plane for all subjects. In case of the subject with CP, the thorax was rotated in positive direction for 60% of the gait cycle, after which it was rotated in the negative direction for the rest of the gait cycle. The subject with OI presented a thorax motion which was rotated in the negative direction for 0-40% of the gait cycle, followed by positive rotation for rest of the gait cycle.

Maximum and minimum range of motion was seen in the subject with CP and OI respectively. Also, all subjects showed maximum thorax range of motion in the frontal plane.

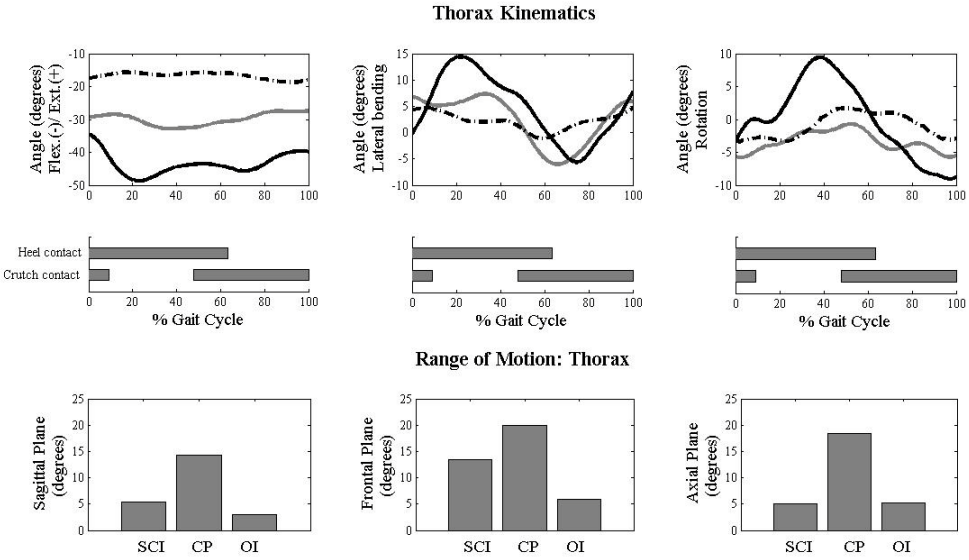

Figure 8**:** Image depicts thorax kinematics and range of motion. Gray line: Subject with SCI; Solid: Subject with CP and Dashed-dot: Subject with OI

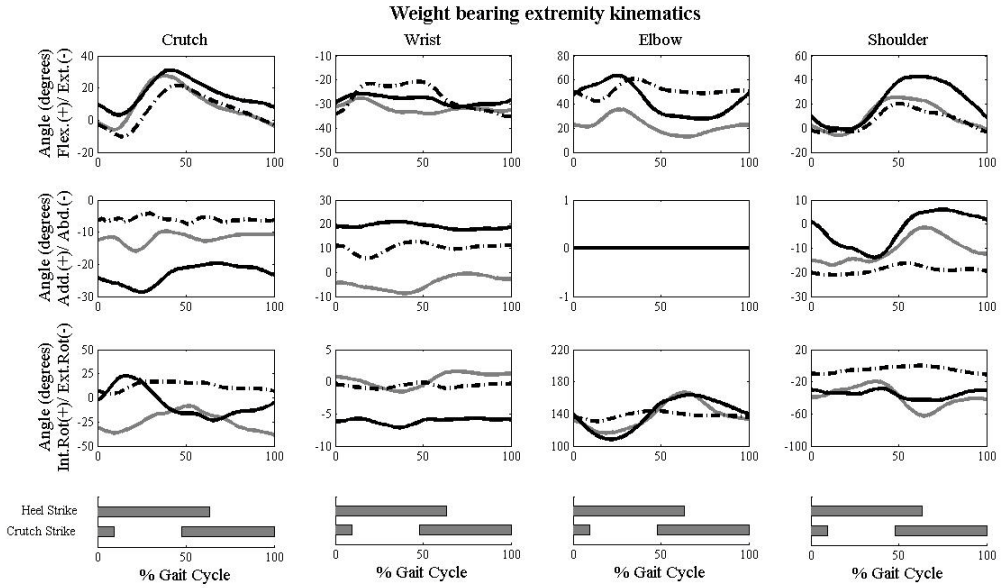

Figure 9: Image depicts crutch, wrist, elbow and shoulder kinematics for the weight bearing extremity. Gray line: Subject with SCI; Solid: Subject with CP and Dashed-dot: Subject with OI

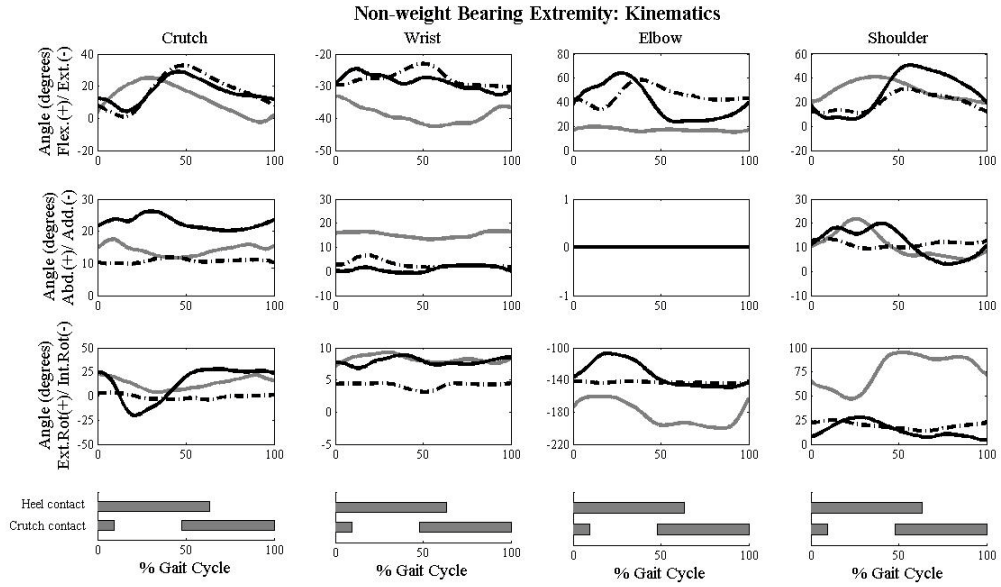

Figure 10: Image depicts crutch, wrist, and elbow and shoulder kinematics for the non-weight bearing extremity. Gray line: Subject with SCI; Solid: Subject with CP and Dashed-dot: Subject with OI

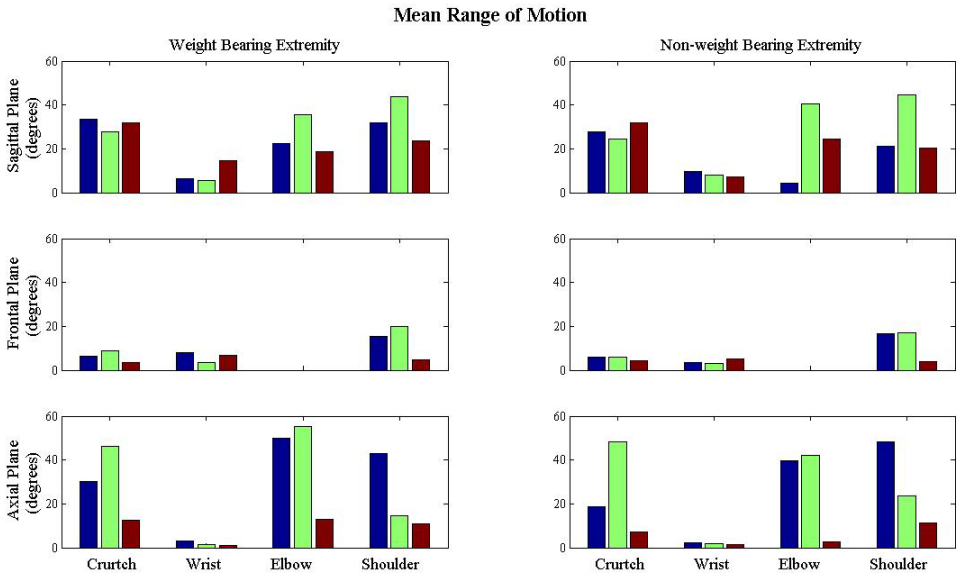

Figure 11: Image depicts crutch, wrist, elbow and shoulder range of motion for the weight bearing and non-weight bearing extremity. Blue: Subject with SCI; green: Subject with CP and red: Subject with OI

2.4.3.2 Shoulder

Mean shoulder kinematics of the weight bearing extremity across all subjects is presented in Figure 9. Shoulder kinematics displayed similar motion across all subjects. Sagittal plane shoulder motion displayed extension 0-5% of gait cycle, this position was maintained until 30% of gait cycle, followed by flexion until 100% of gait cycle. In the frontal plane shoulder motion for the subjects with SCI and OI remained adducted over the entire gait cycle, but for the subject with CP the shoulder was adducted till 50% of gait cycle followed by abduction for the rest of the gait cycle. The shoulder remained externally rotated for the entire gait cycle across all subjects.

Mean shoulder kinematics of the non-weight bearing extremity across all subjects is presented in Figure 10. Sagittal plane shoulder motion in subjects with CP and OI was similar to the shoulder motion of the weight bearing extremity. The subject with SCI

displayed a flexed shoulder for the entire gait cycle. The shoulder was abducted and externally rotated for the entire gait cycle across all subjects.

The range of motion of the shoulder for the weight bearing and the non-weight bearing extremities are presented in Figure 11. The subject with CP and OI presented similar ranges of motion of the shoulder in both the extremities in all planes of motion. In case of subject with SCI, weight bearing extremity presented greater shoulder range of motion in the sagittal plane and reduced range of motion in the other two planes.

2.4.3.3 Elbow

Mean elbow kinematics of the weight bearing extremity across all subjects is presented in Figure 9. Elbow kinematics displayed similar motion across all subjects. Sagittal plane elbow motion displayed flexion for the entire gait cycle. The elbow remained internally rotated for the entire gait cycle across all subjects.

Mean elbow kinematics for the non-weight bearing extremity across all subjects is presented in Figure 10. Sagittal plane elbow motion in all subjects was flexed for the entire gait cycle. The elbows remained internally rotated for the entire gait cycle across all subjects.

The range of motion of the elbow for the weight bearing and the non-weight bearing extremities are presented in Figure 11. Sagittal plane motion of the elbow was higher in the non-weight bearing extremity in subjects with CP and OI. In contrast, the subject with SCI presented higher range of motion at the elbow in the weight bearing extremity. Transverse plane range of motion of the elbow was higher in all three planes of the weight bearing extremity.

2.4.3.4 Wrist

Mean wrist kinematics of the weight bearing extremity across all subjects is presented in Figure 9. Wrist kinematics displayed similar motion across all subjects in the sagittal plane, which was indicative of extension for the entire gait cycle. In the frontal plane and transverse plane, elbow motion for the subjects with CP and OI remained adducted and externally rotated over the entire gait cycle. But for the subject with SCI, the wrist remained abducted for the entire gait cycle. Also, in this subject, the elbow was internally rotated for 0-20%, followed by external rotation, which was maintained till 57% and then was internally rotated for the rest of the gait cycle.

Mean wrist kinematics of the non-weight bearing extremity across all subjects is presented in Figure 10. Sagittal, frontal and transverse plane wrist motion in all subjects was extension, abduction and external rotation, respectively, throughout the entire gait cycle.

The range of motion of the wrist of the weight bearing and the non-weight bearing extremities are presented in Figure 11. Among the UE joints, the wrist showed the least range of motion. In the sagittal plane, subjects with SCI and OI demonstrated higher range of motion on the weight bearing extremity whereas; the subject with CP presented higher range of motion in the non-weight bearing extremity. Range of motion of the elbow in the frontal plane was higher in the weight bearing extremity. The transverse plane range of motion was similar between the weight bearing and non-weight bearing extremities in all the subjects.

2.4.3.5. Crutch

Mean crutch kinematics of the weight bearing extremity across all subjects is presented in Figure 9. Crutch kinematics displayed similar patterns across all subjects in the sagittal plane but their flexion/ extension magnitudes varied across subjects. For the subject with SCI the crutch presented extension for 0-20% of the gait cycle, followed by flexion for the rest of the gait cycle. Crutch motion in the sagittal place for the subject with CP remained in flexion for the entire gait cycle. The subject with OI demonstrated extension for 0-30% of the gait cycle, followed with flexion for the rest of the gait cycle. In the frontal plane crutch motion for all subjects remained titled outwards over the entire gait cycle. Crutch motion in the transverse plane remained externally rotated in the subject with SCI, internally rotated in the subject with OI and for the subject with CP external rotation was observed until 40%, followed by internal rotation for the rest of the gait cycle.

Mean crutch kinematics of the non-weight bearing extremities across all subjects is presented in Figure 10. Sagittal and frontal plane crutch motion in all subjects was flexion and titled outwards for the entire gait cycle. In the transverse plane, crutch motion displayed by the subject with SCI remained externally rotated. Subjects with CP and OI displayed internal rotation of the crutch for 15-40% and 20-90% of the gait cycle respectively; and for the rest of the gait cycle external rotation was observed.

The range of motion of the crutch of the weight bearing and the non-weight bearing extremities are presented in Figure 11. In the sagittal and frontal plane, the weight bearing extremity presented greater range of motion subjects with SCI and OI, but in the OI subject greater range of motion was observed in the non-weight bearing

extremity. Transverse plane motion was greater in the weight bearing extremity in subjects with SCI and OI, whereas, in the subject with CP the non-weight bearing extremity demonstrated greater range of motion

2.4.4 Upper Extremity Kinetics

The UE kinetic data was compared across all the three subjects. Similar to kinematic data all the kinetic data presented was divided based on weight bearing and non-weight bearing extremities. The mean forces of the crutch tip, handle, cuff, wrist, elbow and shoulder during crutch gait are displayed (Figures 12-13 and 18-19). The mean moments of the crutch tip, handle, cuff, wrist, elbow and shoulder during crutch gait are displayed (Figures 15-16 and 21-22). The peak forces and moments for both the extremities are presented in the Figures 14, 17, 20 and 23.

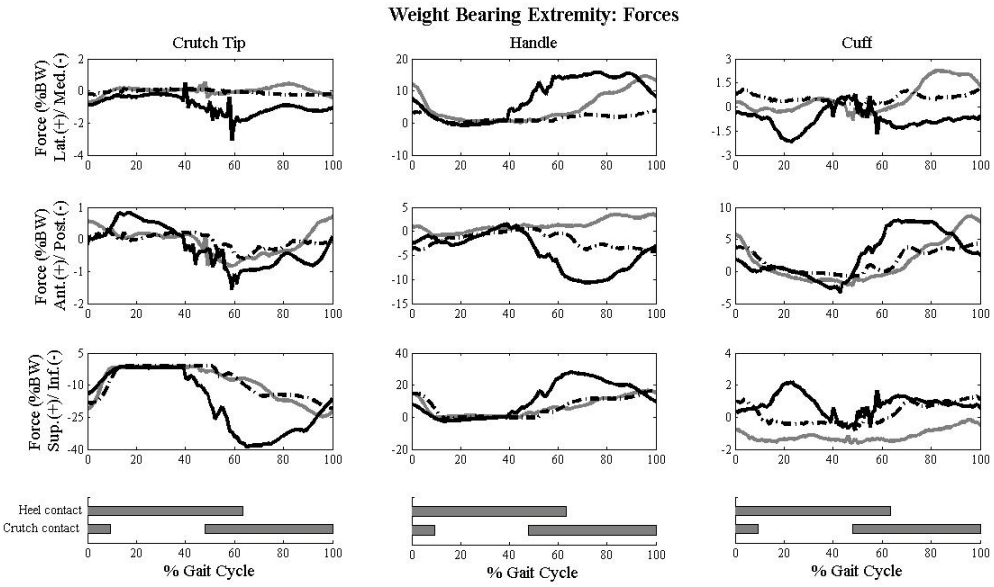

Figure 12: Image depicts crutch tip, handle and cuff forces for the weight bearing extremity. Gray line: Subject with SCI; Solid: Subject with CP and Dashed-dot: Subject with OI

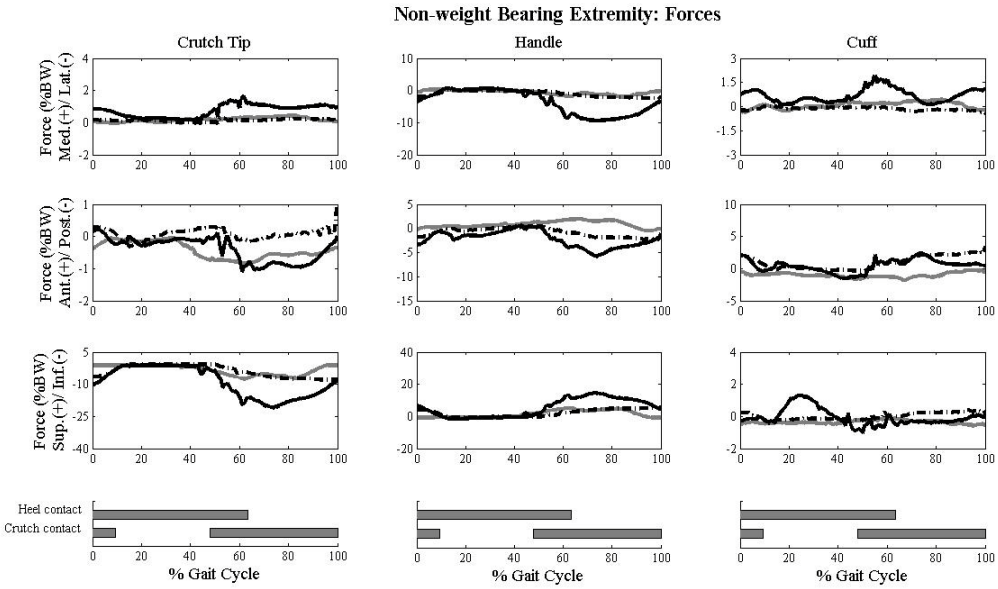

Figure 13: Image depicts crutch tip, handle and cuff forces for the non-weight bearing extremity. Gray line: Subject with SCI; Solid: Subject with CP and Dashed-dot: Subject with OI

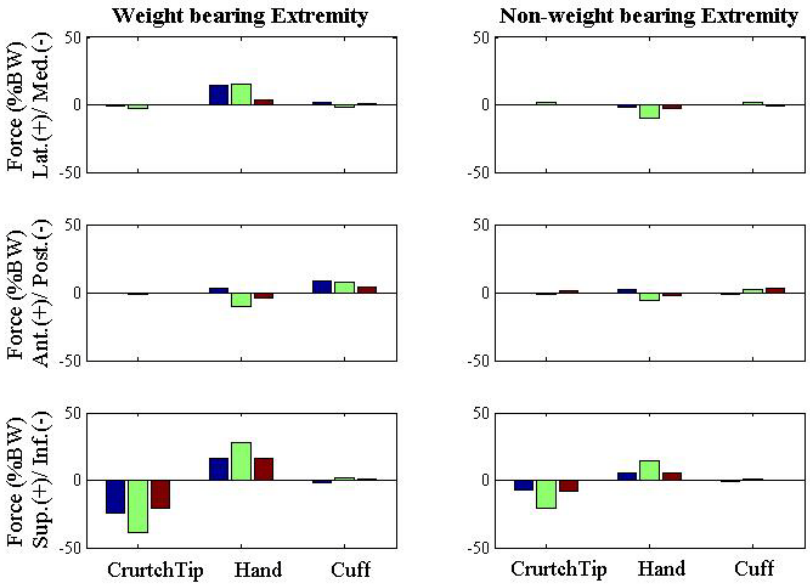

Figure 14: Image depicts peak forces at the crutch tip, handle and cuff for the weight bearing and non-weight bearing extremity. Blue: Subject with SCI; green: Subject with CP and red: Subject with OI

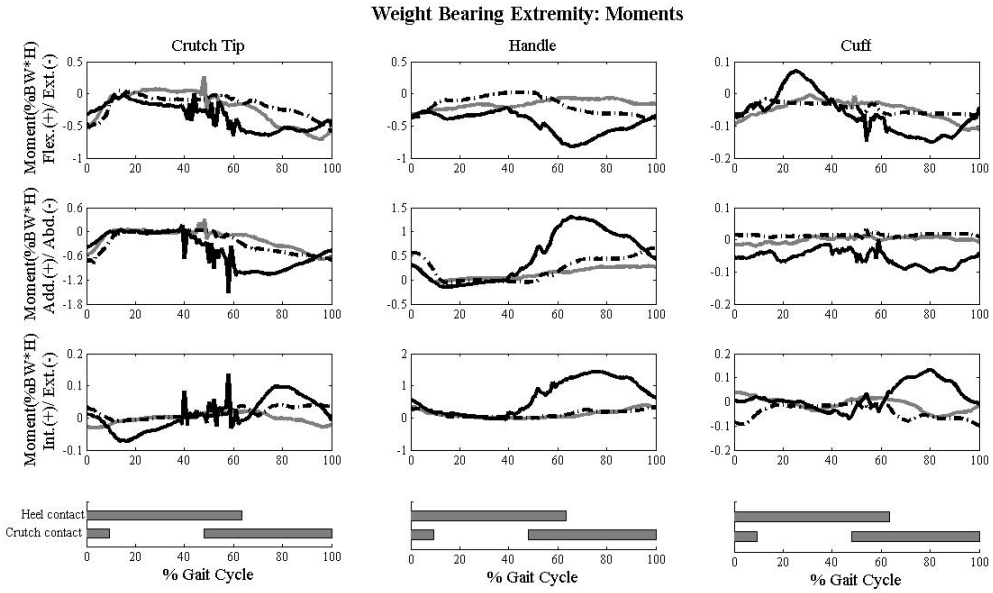

Figure 15: Image depicts crutch tip, handle and cuff moments for the weight bearing extremity. Gray line: Subject with SCI; Solid: Subject with CP and Dashed-dot: Subject with OI

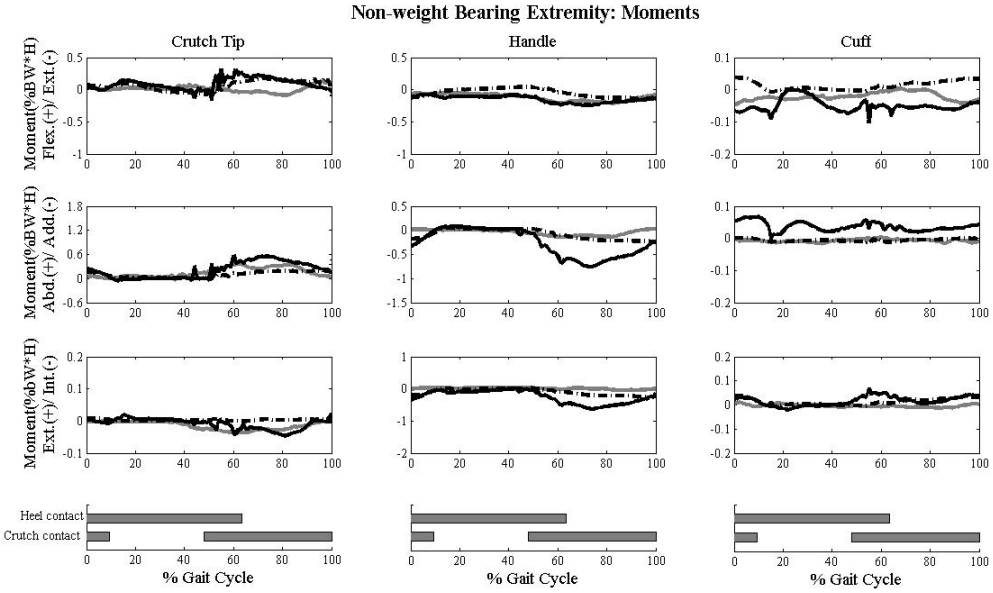

Figure 16: Image depicts crutch tip, handle and cuff moments for the non-weight bearing extremity. Gray line: Subject with SCI; Solid: Subject with CP and Dashed-dot: Subject with OI

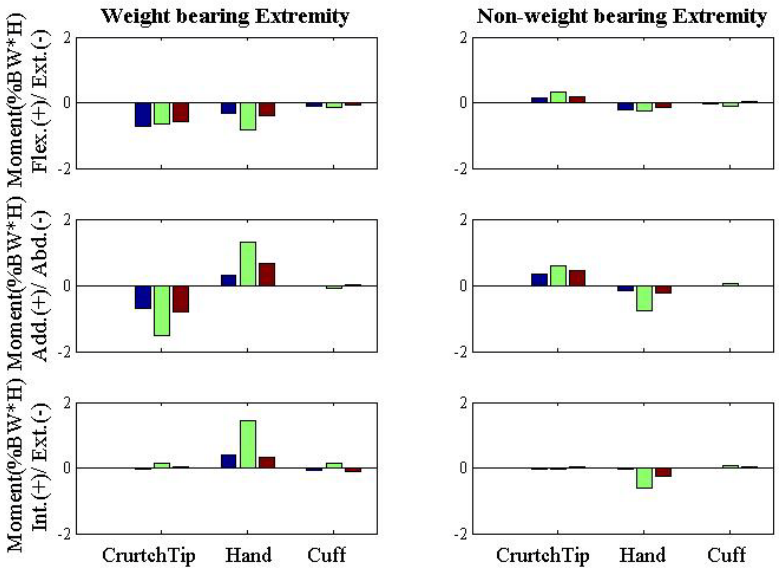

Figure 17: Image depicts peak moments at the crutch tip, handle and cuff for the weight bearing and non-weight bearing extremity. Blue: Subject with SCI; green: Subject with CP and red: Subject with OI

2.4.4.1 Crutch Tip

For the crutch tip forces, among the three directions maximum external force was seen in the superior/inferior direction for both the weight bearing and non-weight bearing extremities (Figures 12-13). Forces in the two shear directions were small. The loading patterns were similar for both the extremities in all subjects. The force on the weight bearing extremity was higher in each subject compared to the non-weight bearing extremity. Highest peak forces were seen in the transverse plane in the subject with CP in both the extremities (Figure 14). Among all subjects superior/inferior forces were the highest.

For the crutch tip moments in both extremities in all subjects, highest abduction moments were seen, followed by the extension moments (Figures 15-16). The weight bearing extremity presented higher moments than the non-weight bearing extremity. Peak moments of about 1% BW* H were observed in all subjects in the frontal and transverse

plane (Figure 17). Highest moments were demonstrated by the subject with CP. Slightly lower moments were seen in the non-weight bearing extremity in comparison to the weight bearing extremity.

2.4.4.2 Handle

The sagittal plane presented highest superiorly directed external forces for both extremities in all subjects (Figures 12-13). Similarly, laterally directed forces were also observed in both extremities across all subjects. The subject with CP was the only one who presented posterior acting forces at the handle. All the forces observed on the weight bearing extremity were larger than that observed in the non-weight bearing extremity. As shown in Figure 14, highest handle forces were seen in the superior/inferior plane. Among subjects, the subject with CP presented the highest forces.

Adduction moments and internal rotation was observed in both extremities in all subjects (Figures 14-15). The subject with CP presented highest moments at the handle. Similar to the crutch tip moments, the weight bearing extremity presented higher moments.

2.4.4.3 Cuff

All subjects presented a force ranging from 5-10% BW during crutch loading in the anterior direction for the weight bearing extremity (Figure 12). This anterior force was also present in the non-weight bearing extremity in subjects with CP and OI but had a lower magnitude. Low cuff moments ranging from -0.2 to 0.2 % BW*H were seen in all subjects. Peak cuff forces were seen in the anterior direction in the weight bearing extremity (Figure 14.). Highest anterior force was seen in the subject with SCI followed by CP and OI.

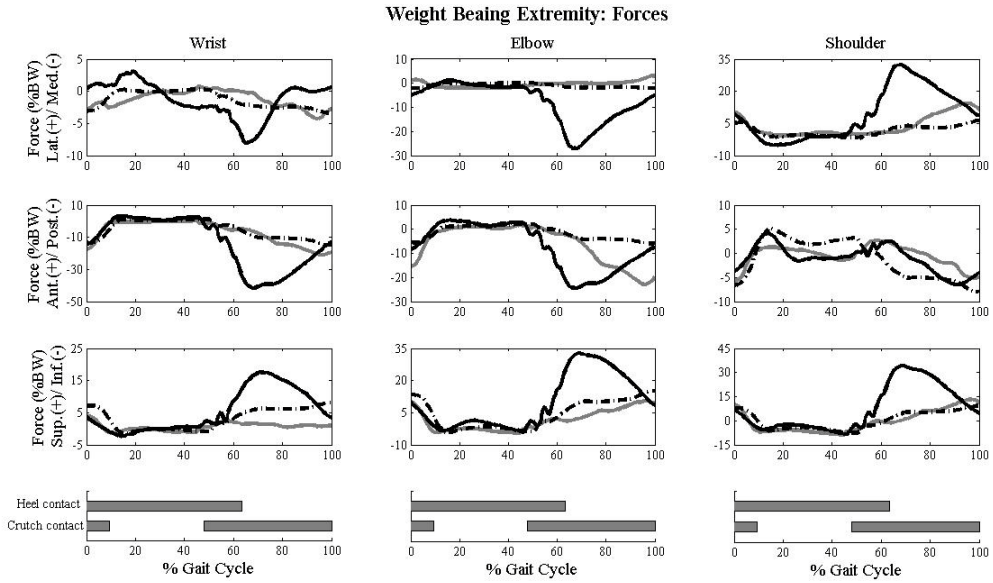

Figure 18: Image depicts wrist, elbow and shoulder forces for the weight bearing extremity. Gray line: Subject with SCI; Solid: Subject with CP and Dashed-dot: Subject with OI

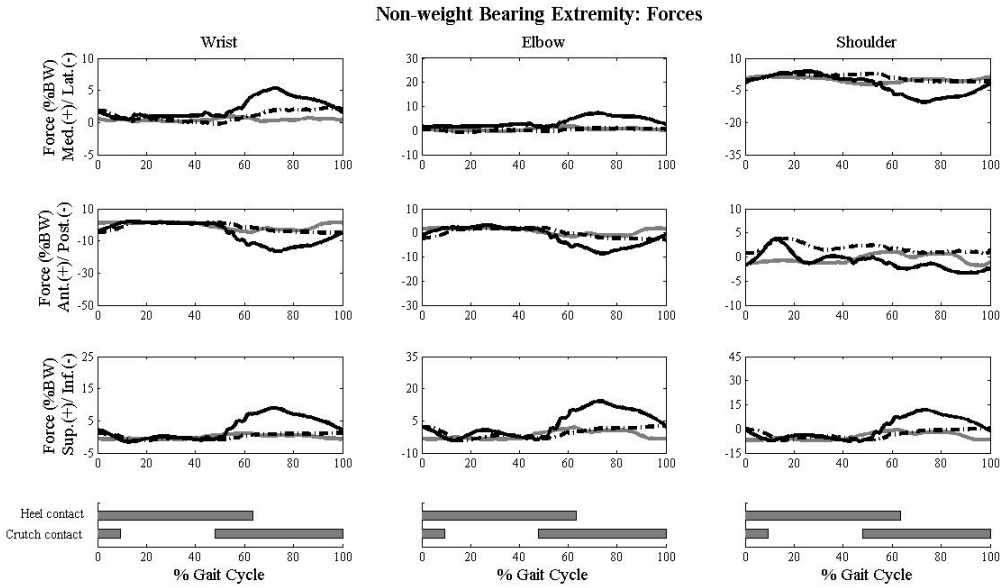

Figure 19: Image depicts wrist, elbow and shoulder forces for the non-weight bearing extremity. Gray line: Subject with SCI; Solid: Subject with CP and Dashed-dot: Subject with OI

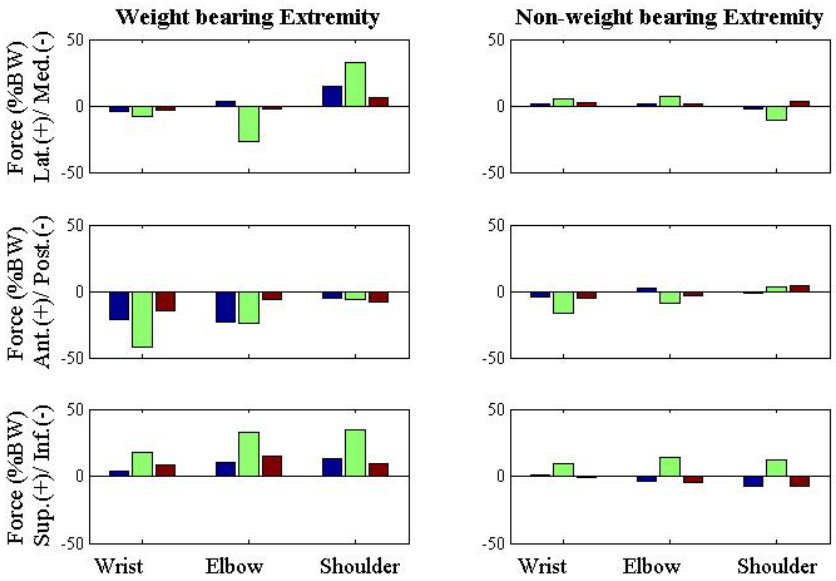

Figure 20: Image depicts peak forces at the wrist, elbow and shoulder for the weight bearing and non-weight bearing extremity. Blue: Subject with SCI; green: Subject with CP and red: Subject with OI

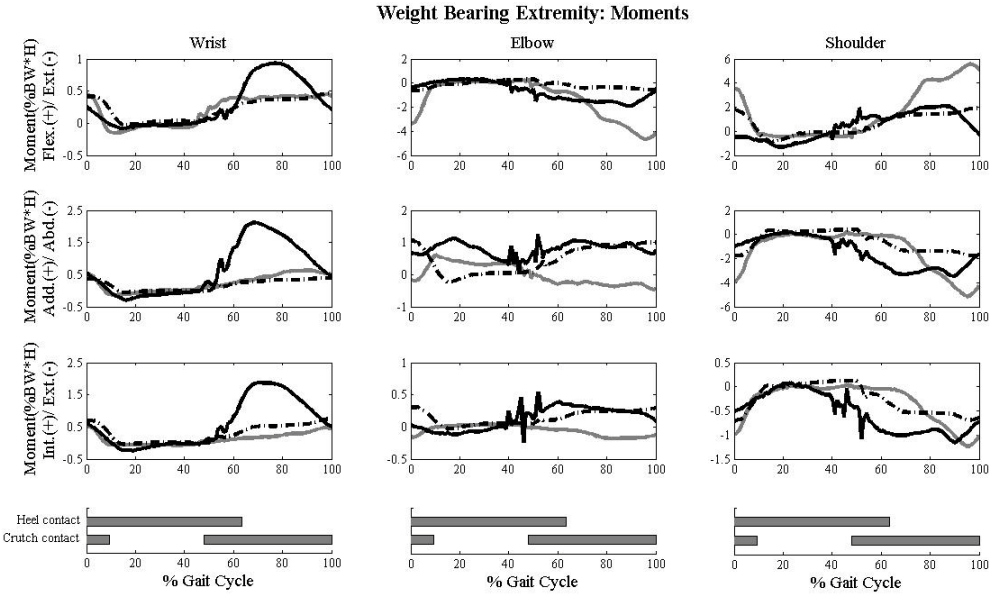

Figure 21: Image depicts wrist, elbow and shoulder moments for the weight bearing extremity. Gray line: Subject with SCI; Solid: Subject with CP and Dashed-dot: Subject with OI

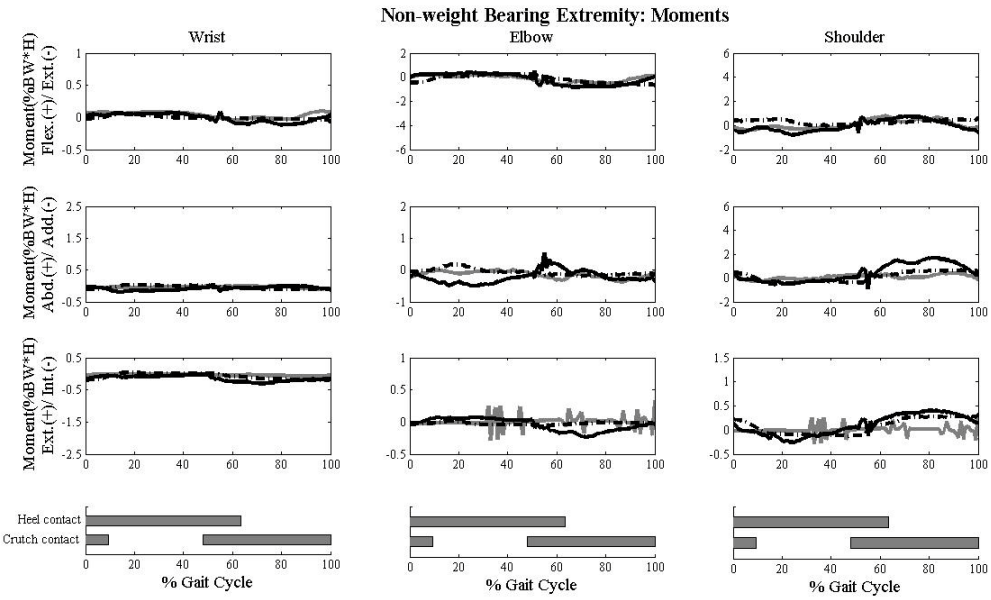

Figure 22: Image depicts wrist, elbow and shoulder moments for the non-weight bearing extremity. Gray line: Subject with SCI; Solid: Subject with CP and Dashed-dot: Subject with OI

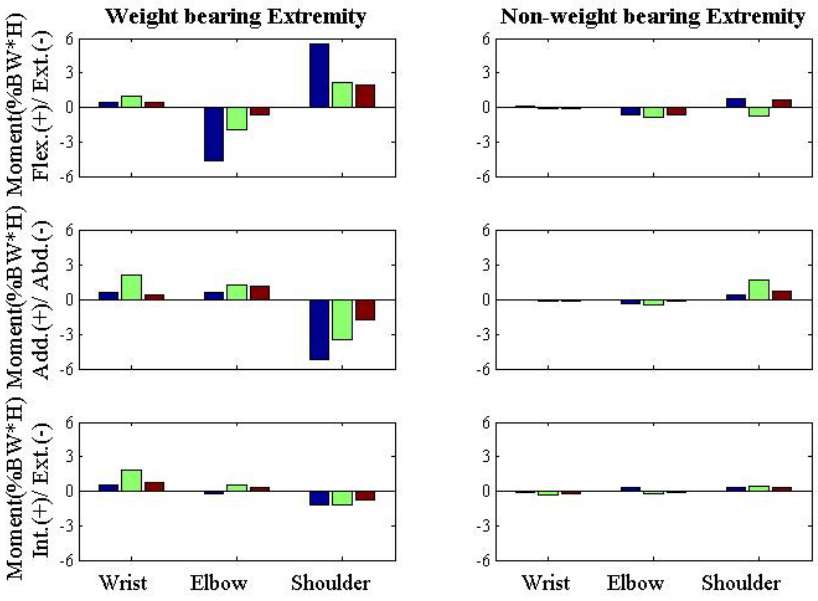

Figure 232: Image depicts peak forces at the wrist, elbow and shoulder for the weight bearing and non-weight bearing extremity. Blue: Subject with SCI; green: Subject with CP and red: Subject with OI

2.4.4.4 Wrist

The joint reaction forces (JRFs) of the wrist are presented in Figures 18-19. The JRF was oriented in the medial, posterior and superior direction across all subjects. The JRFs on the weight bearing extremity were greater than the non-weight baring extremity. Peak forces at the wrist are shown in the Figure 20. Highest forces were seen in the anterior direction in the subject with CP. The weight bearing peak wrist forces were considerably larger than that on the non-weight bearing extremity

As shown in the Figure 21, the joint reaction moments (JRMs) on the sagittal, frontal and transverse planes are presented in the directions of flexion, adduction and internal rotation respectively across all subjects. As compared to the weight bearing extremity the moments seen in the non-weight bearing extremity were extremely small across all the subjects. Similar to the peak forces, the highest peak moments at the wrist were seen in the frontal plane and in the subject with CP (Figure 23).

2.4.4.5 Elbow

High superior and posterior elbow JRFs were observed across all subjects (Figures 18-19). Medially directed elbow JRF was present only in the subject with CP. At the elbow, the subject with CP presented highest peak forces among all subjects in all planes (Figure 20). The peak weight bearing forces were considerably larger.

High extension moments were seen at the elbow in the weight bearing extremity across all subjects (Figure 21). As shown in the Figure 22, JRMs were extremely small in all subjects in their non-weight bearing extremity. High peak extension moments were seen in the subject with SCI, followed by subject with CP and then OI in the weight bearing extremity (Figure 23). The peak moment was small in the other two planes for all

the three subjects. The peak elbow moments were very small in all the three planes in the non-weight extremity.

2.4.4.6 Shoulder

The shoulder JRFs were lateral and superior in direction across all subjects (Figures 18-19). The medially acting JRF in the transverse plane was only present in the weight bearing extremity across all subjects. The magnitude of the shoulder JRFs was greater in the weight bearing extremity. In the sagittal and frontal plane highest forces were seen in the subject with CP followed by SCI and OI (Figure 20). The non-weight bearing forces were considerably lower in all subjects

The shoulder JRMs presented flexion, abduction, and external rotation across all subjects in the weight bearing extremity (Figure 21). Similar to the shoulder JRFs, the shoulder JRMs were greater in the weight bearing extremity. Small shoulder JRMs were present in the non-weight bearing extremity (Figure 22). These JRMs were only present in subjects with CP and OI in the sagittal and frontal plane. Highest peak moments were seen at this joint (Figure 23). The subject with SCI presented highest peak shoulder moments.

2.4.5 Comparison with other studies

2.4.5.1 Kinematics

Table 6: Comparisons of range of motion with previous studies

Range of motion (Sagittal Plane)	Current study			Slavens et al.	Requejo et al.
Pathology	SCI	CP	OI	MM	SCI
Shoulder	31º	44º	24º	~ 45º	~ 30º
Elbow	23º	36º	18º	~ 30º	~ 30º
Wrist	6º	5º	14º	~15º	~ 15º
Crutch	30º	27º	31º	~ 38º	~ 25º

As shown in the table 6, the ranges of motion of the UE joints (shoulder, elbow and wrist) seen in the current study and other similar studies which looked at UE kinematics in Lofstrand crutch-assisted gait are presented.

2.4.5.2. Peak Forces

Table 7: Comparison of peak forces in % Body Weight

Peak Forces in the sagittal plane (%BW)	Current Study			Slavens et al.	Requejo et al.	Haubert et al.
Pathology	SCI	CP	OI	MM	SCI	SCI
Shoulder	13	34	9	24	9	7
Elbow	10	32	15	33	12	-
Wrist	4	17	8	29	12	-

Table 8: Comparisons of peak forces in Newton

Peak Forces in the sagittal plane (N)	Current Study			Slavens et al.	Requejo et al.	Haubert et al.
Pathology	SCI	CP	OI	MM	SCI	SCI
Shoulder	26	83	40	124	89	49
Elbow	20	80	65	137	112	-
Wrist	8	43	35	101	112	-

The absolute peak joint reaction forces in %BW and Newtons seen at shoulder, elbow and wrist as seen in various studies evaluating the UE kinetics are presented in the Table 7 and 8 respectively.

Table 9: Comparison of peak cuff forces in % Body Weight

Peak Cuff Forces (% BW)	Current Study			Requejo et al.
Pathology	SCI	CP	OI	SCI
Transverse plane	8.6	7.9	4.3	1.9
Sagittal plane	1.6	2.2	1.3	1.5
Frontal Plane	2.2	1.3	1.2	0.9

Table 10: Comparisons of peak cuff forces in Newton

Peak Cuff Forces (N)	Current Study			Requejo et al.
Pathology	SCI	CP	OI	SCI
Transverse plane	17.3	19.4	18.4	18.2
Sagittal plane	3.2	5.4	5.6	14.2
Frontal Plane	4.5	4.5	5.1	8.3

The data presented in the Table 9 and 10 are the absolute peak forces acting on the forearm at the point of contact of the cuff in % BW and Newtons respectively,

2.4.5.3. Peak Moments

The absolute peak joint reaction moments in % BW*H and N-m seen at shoulder, elbow and wrist seen in various studies evaluating the UE kinetics are presented in the Table 11 and 12.

Table 11: Comparison of peak moments in % Body Weight into Height

Peak Moments in the sagittal plane (% BW*H)	Current Study			Slavens et al.	Requejo et al.
Pathology	SCI	CP	OI	MM	SCI
Shoulder	5.6	2.1	1.9	6.8	0.8
Elbow	4.7	1.9	0.6	5.6	0.3
Wrist	0.4	0.9	0.5	4.3	0.5

Table 12: Comparisons of peak moments in Newton-meter

Peak Moments in the sagittal plane (N-m)	Current Study			Slavens et al.	Requejo et al.
Pathology	SCI	CP	OI	MM	SCI
Shoulder	13.4	7.2	11.6	36.9	13.3
Elbow	11.2	6.5	3.8	30.4	5.0
Wrist	1.2	3.2	2.8	23.9	7.6

2.4.4. DISCUSSION

The goal of this study was to develop and validate a novel instrumented crutch system capable of evaluating UE dynamics during Lofstrand crutch-assisted. This new

design and model were applied to three pathologies (SCI, CP and OI). As shown in tables 6-12, the results of this study were comparable to the previous studies.

The main strength of this study was the instrumentation of the two six-axis load cells placed on each crutch which allowed full examination the UE joint loading. The placement of the lower load cell just below the handles, instead of the crutch tips reduced inertial loading effects seen in the previous model [21]. This also aided the evaluation of the external forces and moments seen at the handle of the crutch. The load cell placement near the cuff allowed measurement of the cuff forces and moments. Inclusion of this data in the kinetic model enabled accurate estimation of the forces and moments occurring at the wrist and elbow. The accuracy of the system was demonstrated via the validation protocols performed (Table 3-4). The % RMS error and STD for the static validation performed in the sagittal plane presented low differences. The comparison of the resultant forces from the crutch and the force plate presented low % RMS error and STD in case of both right and left crutches. These low differences for both the validation protocols substantiated the accuracy of the crutch system. These differences were higher than that seen by crutch system used in the study done by Requejo et al. [24].

The data from three different pathologies presented the functional aspect of this biomechanical model for studying the UEs. The kinematic model was developed based on previous studies [21, and 28-33]. The kinematics of the UEs showed similar morphologies with the previous studies [21, 24, 35 and 37-40]. ISB recommendations were implemented for the defining coordinate segments of the UEs [22]. All subjects used a two-point gait pattern for ambulation which presents lesser demands on the UEs in comparison to swing-through gait and provide necessary walking speed for faster

ambulation [21]. Among all subjects the crutch was titled out for both the crutches as soon as the crutch support phase started. The wrist and elbow remained extended and flexed, respectively, throughout the gait cycle. The shoulder presented greatest flexion motion during start of the crutch support which was accompanied by abduction to assist in clearance of the crutch tip. In the subject with SCI, the kinematics of the non-weight bearing extremity presented a slightly different motion.

The current system was able to detect that the subject with OI was the least dependent crutch user since she had the least superiorly acting compression forces and flexion moments at the shoulder. This is consistent with an effort to reduce overall skeletal loads to minimize fractures.

The subject with CP was the most dependent crutch user, which is consistent with lowest cadence and higher forces occurring at the shoulder. The forces seen at the crutch for this subject was similar to those seen in the Liggins study for a subject with CP [23].

The subject with SCI presented moderate JRFs for the UEs during crutch ambulation which was comparable to the forces shown by the subject with SCI in the studies done by Melis et. al and Haubert et. al. [5 and 6]. Our study presented high moments at the elbow and shoulder for the subject with SCI. In comparison to the study done by Requejo et al., high moments were only seen at the elbow [24]. This might be due to the varying gait patterns among the two subjects. High abduction moments were seen in the shoulder joint which was similar to the shoulder moments seen in a subject with paraplegia in the study done by Opila et al. [9]. The peak forces and moments reported for the subject with SCI were much lower than the ones shown by Slavens et al. for nine MM subjects. Another important finding of this study was the presence of high

anteriorly directed cuff forces which was in comparison to previous work done by Requejo et al. [24].

Large joint demands were placed on the weight bearing extremity in comparison to the non-weight bearing extremity during crutch-assisted gait. High compressive shoulder loads may lead shoulder pain and pathologies in subjects [9-12]. It may be significant that several joint load patterns exhibited forces exceeding those of typical wheelchair users [41].

Results of this study support the use of this technically validated crutch system to evaluate UE ambulation patterns during Lofstrand crutch-assisted gait. Limitations of the previous studies have included limited number of sensors, sensor location, sensor characteristics and a non-standardized model. These limitations were addressed by designing a novel crutch system that included more sensors placed strategically for complete analysis of the UE dynamics.

A limitation of this study was the small sample size for each of the pathologies. Earlier work by our group indicates that crutch-assisted gait patterns directly affect UE joint load distribution [21]. Thus, the other limitation of the study was that only a two-point gait pattern was studied across all the subjects. To provide conclusions and characterization of UE kinetics during Lofstrand crutch usage will require a larger sample size and usage of other gait patterns such as swing-through, swing-to, three and four-point reciprocal gait patterns.

The current kinetic model will allow study of joint load optimization through activity modification, gait training and crutch re-design. Further study with this system

may also offer valuable insight for crutch prescription, placement patterns and long-term usage effects.

Chapter 3: CONCLUSION

3.1 Summary

Studies evaluating upper extremity (UE) dynamics during assistive gait have been limited. Thus, the goal of this study was to develop a comprehensive three dimensional (3D) biomechanical model to quantify the dynamics of the UEs during Lofstrand crutch-assisted gait. The first aim of the study was to develop a novel instrumented Lofstrand crutch system which is capable of accurately estimating the forces and moments occurring at the points of contact of the crutch. Two six-axis load cells were placed just below and above the handle of the crutch to evaluate the kinetics at the handle and cuff respectively. The crutch system was adjustable for height and forearm size. The system was validated for further usage with the help of static and dynamic validation protocols. This validated system was then applied to three subjects. These subjects presented three different pathologies incomplete spinal cord injury (SCI), diplegic cerebral palsy (CP) and type I osteogenesis imperfecta (OI). The system was capable of evaluating all the tri-axial forces and moments occurring at the crutch tip, handle, cuff, wrist, elbow and shoulder. The cuff forces and moments that have not been completely defined in previous studies were evaluated in this study.

All the three subjects with different pathologies in most cases presented similar kinematics and kinetics. Also, the results from this system were similar to the results by some of the previous work done in this field. Maximum forces in the UEs were seen in the subject with CP. Maximum moments in the UEs were seen in the subject with SCI. The subject with OI presented the least amount of forces and moments in the UEs. Thus, this novel instrumented crutch system can be used for comprehensively studying UE

motion during Lofstrand crutch-assisted gait. This research may ultimately improve crutch prescription and therapeutic planning.

3.2 Future Directions

The study demonstrates a validated model with further potential. The first step would be to evaluate and characterize UE motion in a larger population with same pathologies. It would be worthwhile to add pathologies which make use of Lofstrand crutches such as myelomeningocele. This system could also be applied to subjects presenting similar gait patterns which can help characterize the different gait patterns. UE load prediction with each gait pattern can be used for appropriate prescription in case of long-term crutch users.

The next step would be further analysis of the relationship between functional assessment tools such as energy expenditure index and Pediatric Outcomes Data Collection Instrument (PODCI) and the results from this study. This could establish a basis for crutch prescription and might provide more insight to clinicians. The inclusion of lower extremity motion along with UE motion might be helpful. In terms of faster processing and analysis this system can be made real time. This might allow clinicians to make faster decisions.

The forces and moments from this study can be used as inputs for finite element model of the UE. This model can be useful for fracture prediction especially in case of subjects with OI. There exist no injury criteria for assistive devices in case of subjects with long-term crutch usage. A longitudinal study with a dependent crutch user can be used to determine the long-term crutch effect and injury prevention criteria.

3.3 Concluding Remarks

The study demonstrates a 3D biomechanical model for studying UE dynamics during Lofstrand crutch-assisted gait. The methods described in this paper provide a validated system for measuring UE joint demands. High forces and moments from the sample data further demonstrate the potential for identifying risk factors for joint pathology.

Bibliography

1. Mosqueda T, James M, Petuskey K, Bagley A, Abdala E, Rab G. Kinematic assessment of the upper extremity in brachial plexus birth palsy. Journal of Pediatric Orothopedic. 2006; 24(6):695-699.
2. Harris GF and Smith PA. Human Motion Analysis. New York, IEEE Press. 1996.
3. Goldberg B, LeBlanc M, Edelstein J. Canes, crutches, and walkers. In: Goldberg B, Hsu JD, editors. Atlas of orthoses and assistive devices. 3rd ed. St Louis: Mosby-Year Book. 1997; 557-74.
4. Joyce BM, Kirby RL. Canes, crutches and walkers. Am Fam Physician. 1991; 43:535 -42.
5. Haubert LL, Gutierrez DD, Newsam CJ, Gronley JK, Mulroy SJ and Perry J. A comparison of shoulder joint forces during ambulation with crutches versus a walker in persons with incomplete spinal cord injury. Archives of Physical Medicine and Rehabilitation. 2006; 87: 63-70.
6. Melis EH, Torres-Moreno R, Barbeau H, Lemaire ED. Analysis of assisted-gait characteristics in persons with incomplete spinal cord injury. Spinal Cord. 1999; 37:430-9.
7. Glanze WD, Anderson KN, and Anderson LE, ed (1990). Mosby's Medical, Nursing, and Allied Health Dictionary (3rd ed.). St. Louis, Missouri: The C.V. Mosby Co. p.324
8. Kaye HS, Kang T and LaPlante MP. Mobility Device Use in the United States. Washington, D.C, U.S. Department of Education, National Institute on Disability and Rehabilitation Research. 2000
9. Opila KA, Nicol AC and Paul JP. Upper limb loadings of gait with crutches. Journal of Biomechanical Engineering. 1987; 109:285-290.
10. Lal S. Premature degenerative shoulder changes in spinal cord injury patients. Spinal Cord. 1998; 36:186-189.
11. Sala DA, Leva LM, Kummer FJ and Grant AD. Crutch handle design: effect on palmar loads during ambulation. Archives of Physical Medicine and Rehabilitation. 1998; 79:1473-1476.
12. Sie IH, Waters RL, Adkins RH, Gellman H. Upper extremity pain in the postrehabilitation spinal cord injured patient. Arch Phys Med Rehabil. 1992; 73:44–8.
13. O'Sullivan, Susan B, Raymond P, Siegelman. National Physical Therapy Examination Review and Study Guide. International Educational Resources. 2001; 234.
14. University of Alabama at Birmingham. Spinal Cord: facts and figures at a glance. National Spinal Cord Injury Statistical Center, Birmingham, Alabama. 2008; Report: 1-5
15. Vogel LC, Krajci KA and Anderson CJ. Adults with pediatric-onset spinal cord injury: part 2: musculoskeletal and neurological complications. J Spinal Cord Med. 2002; 25:117-23.
16. CDC, 2006. Centers for Disease Control and Prevention. Improved national prevalence estimates for 18 selected major birth defects--United States, 1999-2001. Morbidity and Mortality Weekly Report (MMWR) 54, 1301-1305.

17. Yeargin-Allsopp M, Van Naarden Braun, K. Prevelance of cerebral palsy in 8-year-old children in the three areas of United States in 2002: A multislide collaboration. Pediatrics: 2008; 121 (3): 547-554.
18. Furukawa A. Factors of influence on the walking ability of children with spastic cerebral palsy. J Phys Ther SCI. 1998: 10 (1): 1-5.
19. Gajko-Galicka A. Mutations in type I collagen genes resulting in osteogenesis imperfecta in humans. Acta Biochimica polonica. 2002; 49(2): 433-441.
20. Osteogenesis Imperfacta OI foundation page [facts about OI page]. 2007 Available from: http://www.oif.org/site/PageServer?pagename=AOI_Facts
21. Slavens BA, et al. Upper extremity dynamics during Lofstrand crutch-assisted gait in children with myelomeningocele. Gait and Posture. 2009; 30: 511-517.
22. Wu G, et al. ISB recommendation on definitions of joint coordinate systems of various joints for the reporting of human joint motion. Part II: Shoulder, Elbow, Wrist and Hand. Journal of Biomechanics. 2005; 38(5):981–992.
23. Liggins AB, Coiro D, Lange GW, Johnston TE, Smith BT, McCarthy JJ. The case of using instrumented crutches during gait analysis. In Bioengineering Conference, Proceedings of the IEEE 28th Annual Northeast. 2002; 15-16.
24. Requejo PS, Wahl DP, Bontrager EL, Newsam CJ, Gronley JK, Mulroy SJ and Perry J. Upper extremity kinetics during Lofstrand crutch-assisted gait. Medical Engineering and Physics. 2005; 27:19-29.
25. Klimaitis A, Carroll G and Owen E. Rapidly progressive destructive arthropathy of the shoulder-a viewpoint on pathogenesis. Journal of Rheumatology. 1988; 15:1859-1862.
26. Glendenning JF, Slavniek E, Forbes WF. An evaluation of devices to aid movement: Part I: canes. Rehabil Dig. 1992; 23(2): 15-16.
27. Kralj AR, Bajd T, Munih M, Turk R. FES gait restoration and balance control in spinal cord-injured patients. Prog Brain Res. 1993; 97: 387-396.
28. Nguyen TC, Baker R. Two methods of calculating thorax kinematics in children with myelomeningocele. Clinical Biomechanics. 2004; 19(10):1060–1065.
29. Rab G, Petuskey K and Bagley A. A method for determination of upper extremity kinematics. Gait and Posture. 2002; 15:113-119.
30. Schmidt R, Disselhorst-Klug C, Silny J and Rau G. A marker-based measurement procedure for unconstrained wrist and elbow motions. Journal of Biomechanics. 1999; 32: 615-621.
31. Poppen, NK and Walker PS. Normal and abnormal motion of the shoulder. Journal of Bone & Joint Surgery. 1976; 58:195-201.
32. Veeger HE, Yu B, An KN and Rozendal RH. Parameters for modeling the upper extremity. Journal of Biomechanics. 1997; 30: 647-652.
33. Roux E, Bouilland S, Godillon-Maquinghen AP and Bouttens D. Evaluation of the global optimization method within the upper limb kinematics analysis. Journal of Biomechanics. 2002; 35:1279-1283.
34. Hingtgen B, McGuire JR, Wang M and Harris GF. An upper extremity kinematic model for evaluation of hemiparetic stroke. Journal of Biomechanics. 2006; 39: 681-688.
35. Zatsiorsky VM. Kinetics of Human Motion. Champaign, IL: Human Kinetics. 2002.

36. Jensen RK. Changes in segment inertia proportions between 4 and 20 years. Journal of Biomechanics. 1989; 22:529-536.
37. Simoneau GG, Harris GF, Hambrook G. In: Upper extremity musculoskeletal loads when using a walker for ambulation. October 21-23, 1999; University of Pittsburgh.; 1999.
38. Bachschmidt RA, Harris GF and Simoneau GG. Walker-assisted gait in rehabilitation: a study of biomechanics and instrumentation. IEEE Transactions on Neural Systems and Rehabilitation Engineering. 2001; 9: 96-105.
39. Strifling, KMB. Analysis and modeling of upper and lower extremity dynamics in children with cerebral palsy using walkers. Doctorate, Marquette University, Milwaukee. 2006.
40. Konop K.A., et al. A biomechanical analysis of upper extremity kinetics in children with cerebral palsy using anterior and posterior walkers. Gait and posture. 2009; 30(3): 265-394.
41. Collinger JL, et al. Shoulder biomechanics during the push phase of wheelchair propulsion: a multisite study of persons with paraplegia. Archives of Physical Medicine and Rehabilitation. 2008; 89:667-76.

Appendices

Appendix 1: Drawings and Photos

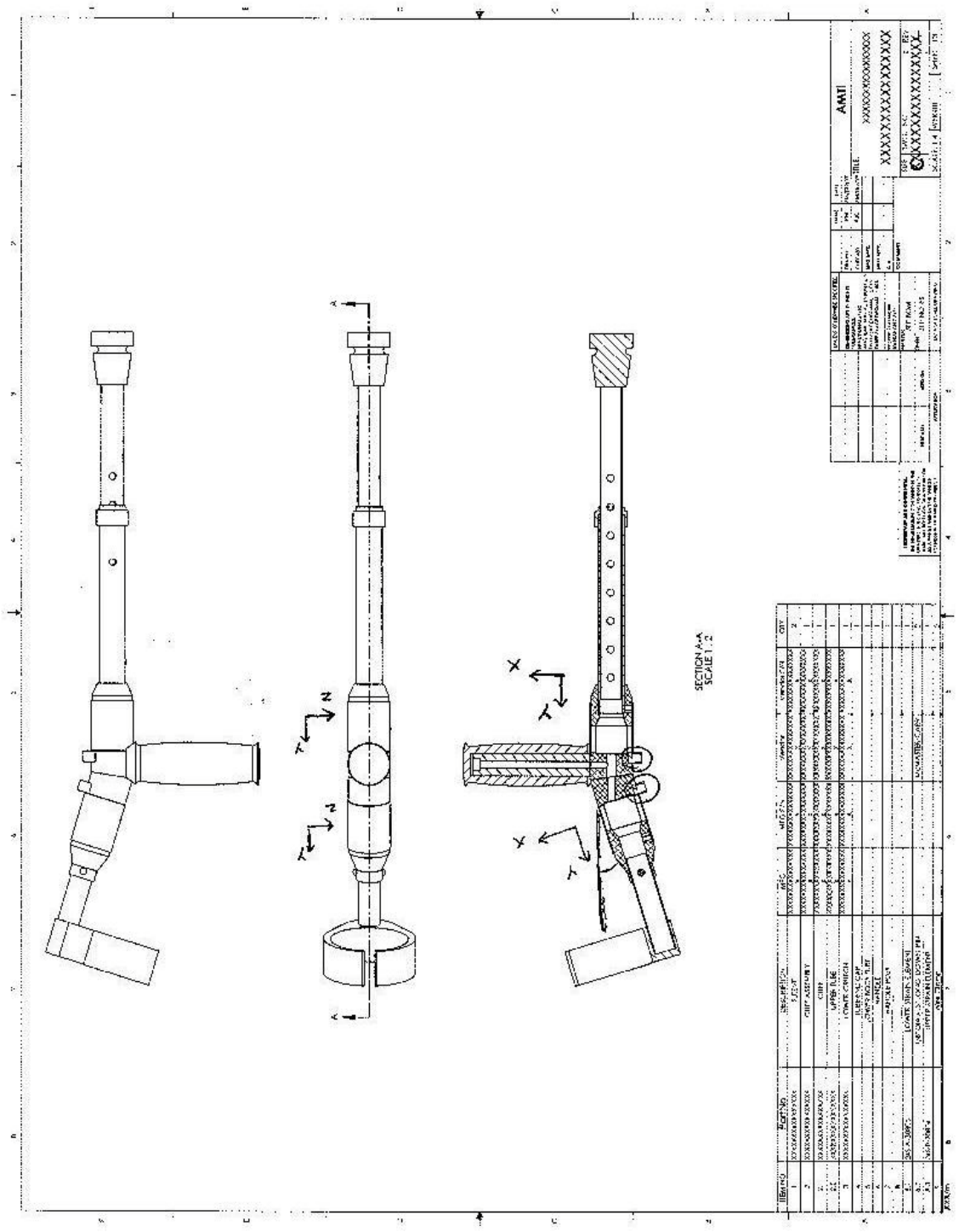

A.1.1 Drawing for the novel instrumented crutch system. (AMTI, Watertowm, MA).

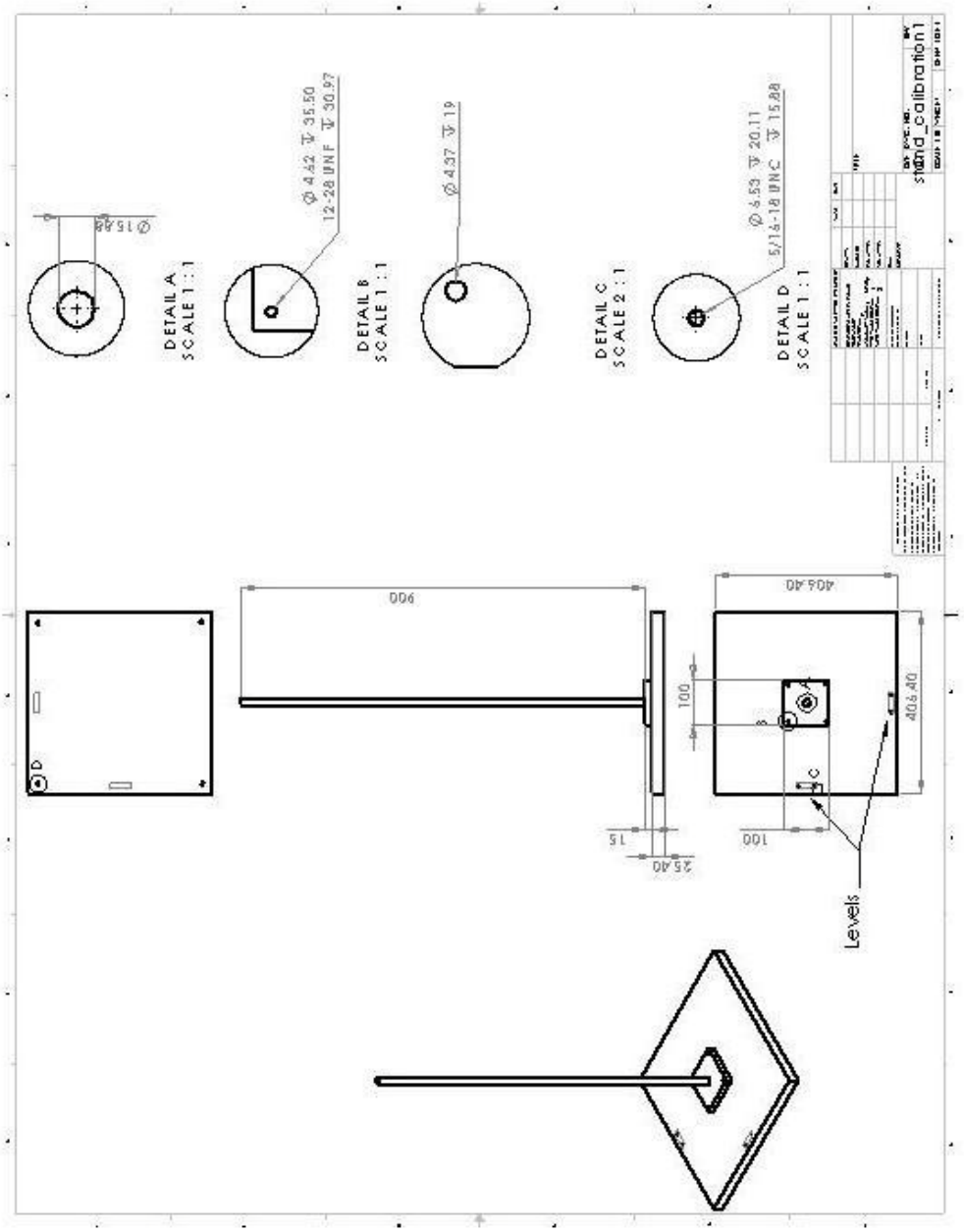

A.1.2 Drawing of the calibration stand.

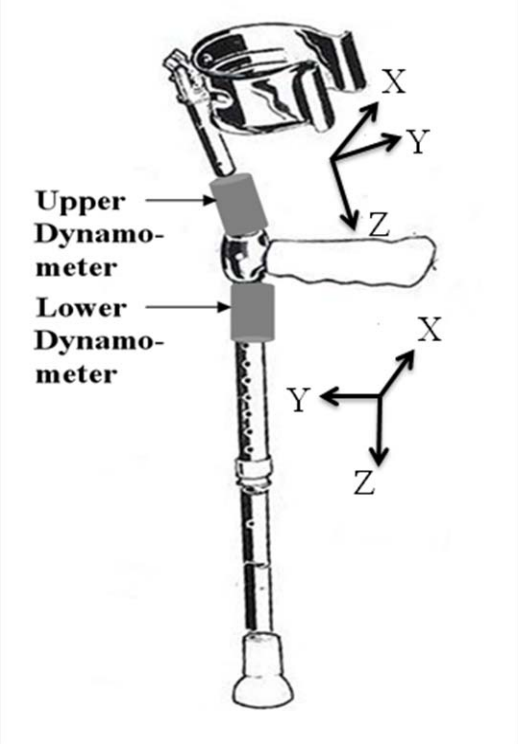

A.1.3 Original axes of the load cells

A.1.4.1 Two lb load applied to the lower sensor in the Y-direction (ISB: X-direction)

A.1.4.2. Two lbs load applied to the upper sensor in the Y-direction (ISB: X-direction)

Appendix 2: Source Code

A.2.1 BodyBuilder (*.mod)

```
{* This is a kinematic model of the upper extremity to be used for evaluating     *}
{* the range of motion and joints angles of the UEs during Crutch gait            *}
{* It uses 18 markers with 7 body segments:thorax, right                          *}
{* upperarm,right forearm,left upperarm, left forearm, and both hands.            *}
{* Markers (5) are placed on the crutches as well.                                *}
{* Neutral position is defined with arms in anatomical position.  0.014m markers*}
{* ================================================== *}

{* ============================================================}
{* Points which may not be present in every trial                 *}
{* ================================================== *}
OPTIONALPOINTS(C7,PX,LCLAV,RCLAV,LACR,LME,LLE,LULN,LRAD,LM3,LM5,LCF,LCB,LCU
,LCL,RACR,RME,RLE,RULN,RRAD,RM3,RM5,RCF,RCB,RCU,RCL)

{* ============================================================================*}
{*                                MACRO SEGVIS                                 *}
{* When called, this macro outputs the origin of the specified segment,        *}
{* along with a point 1m along each axis. Each begins at a point from the      *}
{* origin at zero.                                                             *}
{* ========================================================================== *}

macro SEGVIS(Segment)
ORIGIN#Segment=0(Segment)
AXIS_x#Segment=0(Segment)+(1(Segment)*1)
AXIS_y#Segment=0(Segment)+(2(Segment)*1)
AXIS_z#Segment=0(Segment)+(3(Segment)*1)
OUTPUT(ORIGIN#Segment,AXIS_x#Segment,AXIS_y#Segment,AXIS_z#Segment)
endmacro

macro CROSS (First, Second, Result)
Result = { First(2)*Second(3)-First(3)*Second(2), First(3)*Second(1)-
First(1)*Second(3),First(1)*Second(2)-First(2)*Second(1)}
endmacro

macro DotProduct (One,Two,DotProd)
DotProd = (1(One)*1(Two)+2(One)*2(Two)+3(One)*3(Two))
endmacro

macro MOMENTMULT1 (One, Two,Three,Four,Result)
Result = (1(One)*1(Two)+2(One)*1(Three)+3(One)*1(Four))
endmacro

macro MOMENTMULT2 (One, Two,Three,Four,Result)
Result = (1(One)*2(Two)+2(One)*2(Three)+3(One)*2(Four))
endmacro

macro MOMENTMULT3 (One, Two,Three,Four,Result)
Result = (1(One)*3(Two)+2(One)*3(Three)+3(One)*3(Four))
endmacro

macro Eulerderiv(Angle) {* b/c of ZXY rotation sequence 1=z,2=x,3=y *}
Angle#_dZ=(((Angle(1)[1])-(Angle(1)[-1]))*(120/2))
Angle#_dX=(((Angle(2)[1])-(Angle(2)[-1]))*(120/2))
```

```
Angle#_dY=(((Angle(3)[1])-(Angle(3)[-1]))*(120/2))
Angle#_dt={Angle#_dZ,Angle#_dX,Angle#_dY}
 output(Angle#_dt)
endmacro

macro ANGVEL1(Angle,dAngle) {* b/c of ZXY rotation sequence 1=z,2=x,3=y, units converted to [rad/s]
b/c of Vaughan *}
Angle#_avX=(dAngle(2)*COS(Angle(3))-dAngle(1)*SIN(Angle(3))*COS(Angle(2)))*(3.1415926/180)
Angle#_avY=(dAngle(3)+dAngle(1)*SIN(Angle(2)))*(3.1415926/180)
Angle#_avZ=(dAngle(1)*COS(Angle(3))*COS(Angle(2))+dAngle(2)*SIN(Angle(3)))*(3.1415926/180)
 output(Angle#_avX, Angle#_avY, Angle#_avZ)
endmacro

{* (1/2t) = 1/(2/120) = 120/2 , units of aa = [rad/s^2] *}
macro ANGACCX(Angle,avAngle)
Angle#_aaX=(((avAngle[1])-(avAngle[-1]))*(120/2))
 output(Angle#_aaX)
endmacro

macro ANGACCY(Angle,avAngle)
Angle#_aaY=(((avAngle[1])-(avAngle[-1]))*(120/2))
 output(Angle#_aaY)
endmacro

macro ANGACCZ(Angle,avAngle)
Angle#_aaZ=(((avAngle[1])-(avAngle[-1]))*(120/2))
 output(Angle#_aaZ)
endmacro

macro VCGSEG(Point)
Point#v=(Point[1]-Point[-1])*(120/2)
{* output(Point#v) *}
endmacro

macro ACGSEG(Point)
Point#a=(Point[1]-Point[-1])*(120/2)
 output(Point#a)
endmacro

{* Calculate elements of the ZXY rotation matrix * SIN/COS in degrees,use to get to
global,1=z,2=x,3=y*}
macro ROTMATRIX(Angle)
Angle#_r11_x = -SIN(Angle(1))*SIN(Angle(2))*SIN(Angle(3))+COS(Angle(1))*COS(Angle(3))
Angle#_r12_y = -SIN(Angle(1))*COS(Angle(2))
Angle#_r13_z = SIN(Angle(1))*SIN(Angle(2))*COS(Angle(3))+COS(Angle(1))*SIN(Angle(3))
Angle#_r21_x = COS(Angle(1))*SIN(Angle(2))*SIN(Angle(3))+SIN(Angle(1))*COS(Angle(3))
Angle#_r22_y = COS(Angle(1))*COS(Angle(2))
Angle#_r23_z = -COS(Angle(1))*SIN(Angle(2))*COS(Angle(3))+SIN(Angle(1))*SIN(Angle(3))
Angle#_r31_x = -COS(Angle(2))*SIN(Angle(3))
Angle#_r32_y = SIN(Angle(2))
Angle#_r33_z = COS(Angle(2))*COS(Angle(3))
Angle#_l11_x = -SIN(Angle(1))*SIN(Angle(2))*SIN(Angle(3))+COS(Angle(1))*COS(Angle(3))
Angle#_l12_y = -SIN(Angle(1))*COS(Angle(2))
Angle#_l13_z = SIN(Angle(1))*SIN(Angle(2))*COS(Angle(3))+COS(Angle(1))*SIN(Angle(3))
Angle#_l21_x = COS(Angle(1))*SIN(Angle(2))*SIN(Angle(3))+SIN(Angle(1))*COS(Angle(3))
Angle#_l22_y = COS(Angle(1))*COS(Angle(2))
```

```
Angle#_l23_z = -COS(Angle(1))*SIN(Angle(2))*COS(Angle(3))+SIN(Angle(1))*SIN(Angle(3))
Angle#_l31_x = -COS(Angle(2))*SIN(Angle(3))
Angle#_l32_y = SIN(Angle(2))
Angle#_l33_z = COS(Angle(2))*COS(Angle(3))
endmacro

{* Calculate elements of the transpose of ZXY rotation matrix * SIN/COS in degrees,use to get to local*}
macro TROTMATRIX(Angle)
tAngle#_r11_x = -SIN(Angle(1))*SIN(Angle(2))*SIN(Angle(3))+COS(Angle(1))*COS(Angle(3)
tAngle#_r12_x = COS(Angle(1))*SIN(Angle(2))*SIN(Angle(3))+SIN(Angle(1))*COS(Angle(3))
tAngle#_r13_x = -COS(Angle(2))*SIN(Angle(3))
tAngle#_r21_y = -SIN(Angle(1))*COS(Angle(2))
tAngle#_r22_y = COS(Angle(1))*COS(Angle(2))
tAngle#_r23_y = SIN(Angle(2))
tAngle#_r31_z = SIN(Angle(1))*SIN(Angle(2))*COS(Angle(3))+COS(Angle(1))*SIN(Angle(3))
tAngle#_r32_z = -COS(Angle(1))*SIN(Angle(2))*COS(Angle(3))+SIN(Angle(1))*SIN(Angle(3))
tAngle#_r33_z = COS(Angle(2))*COS(Angle(3))
tAngle#_l11_x =  -SIN(Angle(1))*SIN(Angle(2))*SIN(Angle(3))+COS(Angle(1))*COS(Angle(3)
tAngle#_l12_x = COS(Angle(1))*SIN(Angle(2))*SIN(Angle(3))+SIN(Angle(1))*COS(Angle(3))
tAngle#_l13_x = -COS(Angle(2))*SIN(Angle(3))
tAngle#_l21_y = -SIN(Angle(1))*COS(Angle(2))
tAngle#_l22_y = COS(Angle(1))*COS(Angle(2))
tAngle#_l23_y = SIN(Angle(2))
tAngle#_l31_z =  SIN(Angle(1))*SIN(Angle(2))*COS(Angle(3))+COS(Angle(1))*SIN(Angle(3))
tAngle#_l32_z = -COS(Angle(1))*SIN(Angle(2))*COS(Angle(3))+SIN(Angle(1))*SIN(Angle(3))
tAngle#_l33_z = COS(Angle(2))*COS(Angle(3))
endmacro

{* ============================End of Macros================================== *}

{* ========================================================================== *}
{* Create a global cs with x anterior, z to the right and y proximal        *}
{* ========================================================================== *}
        Gorigin = {0,0,0}
        Global_mod = [Gorigin,{1,0,0},{0,0,-1},xzy]

{* ========================================================================== *}
{*                                THORAX                                    *}
{* Thorax segment has z-axis in line from the center of the hip markers to the *}
{* sternum,y-axis is perpendicular to this from the right acromion to the left *}
{* acromion. Origin is located at the mid point of the acromion markers.      *}
{* ========================================================================== *}
        {* Nguyen and Baker-Thorax Right *}
        Cmid = (LCLAV+RCLAV)/2
        Thr0=(C7+Cmid)/2
        Temp = [PX,C7-PX,Cmid-PX,yxz]
        Ipt = Thr0+0.01*Temp(1)
        Thorax = [Thr0,Cmid-C7,Ipt-Thr0,xyz]

{* ========================================================================== *}
{*                                HUMERUS                                   *}
{* Shoulder joint is below acromion marker, in direction of thorax z-axis.    *}
{* Elbow joint center is in plane of the humeral and elbow markers.           *}
{* Humerus segment has z-axis from elbow to shoulder joint centers,x-axis     *}
{* is from the elbow to wrist joint center. Flexion/Extension occurs about    *}
{* the y-axis. Origin is at the elbow joint center.                           *}
```

```
{* ============================================================================ *}
        {* Shoulder joint centers *}
        LSJC=LACR-(($MarkerDiameter/2)*Thorax(2))-($LShoulderOffset*Thorax(2))
        RSJC=RACR-(($MarkerDiameter/2)*Thorax(2))-($RShoulderOffset*Thorax(2))

        {* Elbow joint centers *}
        REJC = (RLE+RME)/2
        LEJC = (LLE+LME)/2

        {* ISB *}
        RHumerus = [RSJC,RSJC-REJC, RULN-REJC,yzx]
        LHumerus = [LSJC,LSJC-LEJC, LULN-LEJC,yzx]

{* ============================================================================ *}
{*                                FOREARMS                                      *}
{* Wrist joint center is halfway between ulna and radial markers. z axis of the *}
{* forearm is in line with the elbow to wrist joint centers, y axis is in line  *}
{* with the ulna to radius markers. The system is placed so the origin is at    *}
{* the wrist joint center.                                                      *}
{* ============================================================================ *}
        {* ISB *}
        RForearm=[RULN,REJC-RULN,RULN-RRAD,yxz]
        LForearm=[LULN,LEJC-LULN,LRAD-LULN, yxz]

{* ============================================================================ *}
{*                                Hands                                         *}
{* A temporary axis is setup in the hand having a origin at the ulnar joint.    *}
{* With the help of thi temporary axis a virtual point in the anterior direction*}
{* of the 3rd metacarpal marker is established. This virtual point is used to   *}
{* define the center of the hand coordinate system.                             *}
{* ============================================================================ *}
        {* Similar to Requejo's model *}
        RWJC=(RULN + RRAD)/2
        LWJC=(LULN + LRAD)/2

        RHTEMP =[RULN,RULN-RM5,RULN-RRAD, yxz]
        RM3JC = RM3 + (1(RHTEMP)*($RWidthhand/2)) + (1(RHTEMP)*($MarkerDiameter/2))
        RHand = [RM3JC,RWJC-RM3JC, RULN-RRAD,yxz]

        LHTEMP = [LULN,LULN-LM5, LRAD-LULN,yxz]
        LM3JC = LM3 + (1(LHTEMP)*($LWidthhand/2)) + (1(LHTEMP)*($MarkerDiameter/2))
        LHand = [LM3JC,LWJC-LM3JC, LRAD-LULN, yxz]

{* ============================================================================ *}
{*                                Crutches                                      *}
{* The crutches are divided into 3 segments: lower crutch segment, Handle       *}
{* segment and cuff segment.
{* ============================================================================ *}

        RL0 = (RLR+RLL)/2
        LL0 = (LLR+LLL)/2

        RG0 = (RLF+RLB)/2
        LG0 = (LLF+LLB)/2

        RC0 = (RL0+RG0)/2
```

```
LC0 = (LL0+LG0)/2

{*Lower Crutch segment*}

RCrutchLow = [RC0, RLF-RLB, RLR-RLL,xyz]
LCrutchLow = [LC0, LLF-LLB, LLR-LLL,xyz]

{*Handle segment*}

RCrutchMid = [RL0, RLF-RLB, RLR-RLL,xyz]
LCrutchMid = [LL0, LLF-LLB, LLR-LLL,xyz]

RCrutchTemp = ROT(RCrutchMid,3(RCrutchMid),15)
LCrutchTemp = ROT(LCrutchMid,3(LCrutchMid),15)

{*Cuff segment*}

RU0 = RL0 + .0817435*(2(RCrutchTemp))
LU0 = LL0 + .0817435*(2(LCrutchTemp))

RCrutchUp = [RU0, RLF-RLB, RLR-RLL,xyz]
LCrutchUp = [LU0, LLF-LLB, LLR-LLL,xyz]

RCrutchUp = ROT(RCrutchUp,3(RCrutchUp),15)
LCrutchUp = ROT(LCrutchUp,3(LCrutchUp),15)


{* ========================================================================== *}
{* Euler Angles ZXY: Referenced distal to proximal segment or global_mod      *}
{* -1 in fron of the euler equation makes use of floating euler sequence *}
{* ========================================================================== *}
        {* distal axis wrt proximal axis, 1 is for new global since points are already transformed *}
        Trunk=-<1,Thorax, ZXY>
        RShoulder=-<Thorax, RHumerus, ZXY>
        LShoulder=-<Thorax, LHumerus, ZXY>
        RElbow=-<RHumerus, RForearm, ZXY>
        LElbow=-<LHumerus, LForearm, ZXY>
        RWrist=-<RForearm, RHand, ZXY>
        LWrist=-<LForearm, LHand, ZXY>
        RCrutch = -<RHand, RCrutchMid, ZXY>
        LCrutch = -<LHand, LCrutchMid, ZXY>
        RLof_Up = -<1, RCrutchUp, ZXY>
        LLof_Up = -<1, LCrutchUp, ZXY>
        RLof_Mid = -<1, RCrutchMid, ZXY>
        LLof_Mid = -<1, LCrutchMid, ZXY>

{* ========================================================================== *}
{* Virtual Points Output                                                      *}
{* ========================================================================== *}
        OUTPUT(Trunk,RShoulder,LShoulder,RElbow,LElbow,RWrist,LWrist, RCrutch, LCrutch,
RLof_Up, LLof_Up, RLof_Low, LLof_Low)

        SEGVIS(RCrutchMid)
        SEGVIS(LCrutchMid)
        SEGVIS(RCrutchLow)
        SEGVIS(LCrutchLow)
```

```
        SEGVIS(RCrutchUp)
        SEGVIS(LCrutchUp)
        SEGVIS(Thorax)
        SEGVIS(LHumerus)
        SEGVIS(RHumerus)
        SEGVIS(LForearm)
        SEGVIS(RForearm)
        SEGVIS(RHand)
        SEGVIS(LHand)

{* ==============================Start of Kinetics========================== *}

{* Call macros to compute positional changes, angular velocities, and angular accelerations *}
Eulerderiv(RShoulder)
Eulerderiv(LShoulder)
Eulerderiv(RElbow)
Eulerderiv(LElbow)
Eulerderiv(RWrist)
Eulerderiv(LWrist)
Eulerderiv(RCrutch)
Eulerderiv(LCrutch)
Eulerderiv(Trunk)

ANGVEL1(RCrutch,RCrutch_dt)
ANGVEL1(LCrutch,LCrutch_dt)
ANGVEL1(Trunk,Trunk_dt)
ANGVEL1(RShoulder,RShoulder_dt)
ANGVEL1(LShoulder,LShoulder_dt)
ANGVEL1(RElbow,RElbow_dt)
ANGVEL1(LElbow,LElbow_dt)
ANGVEL1(RWrist,RWrist_dt)
ANGVEL1(LWrist,LWrist_dt)

ANGACCX(RCrutch, RCrutch_avX)
ANGACCY(RCrutch, RCrutch_avY)
ANGACCZ(RCrutch, RCrutch_avZ)
ANGACCX(LCrutch, LCrutch_avX)
ANGACCY(LCrutch, LCrutch_avY)
ANGACCZ(LCrutch, LCrutch_avZ)

ANGACCX(Trunk, Trunk_avX)
ANGACCY(Trunk, Trunk_avY)
ANGACCZ(Trunk, Trunk_avZ)
ANGACCX(RShoulder, RShoulder_avX)
ANGACCY(RShoulder, RShoulder_avY)
ANGACCZ(RShoulder, RShoulder_avZ)
ANGACCX(LShoulder, LShoulder_avX)
ANGACCY(LShoulder, LShoulder_avY)
ANGACCZ(LShoulder, LShoulder_avZ)
ANGACCX(RElbow, RElbow_avX)
ANGACCY(RElbow, RElbow_avY)
ANGACCZ(RElbow, RElbow_avZ)
ANGACCX(LElbow, LElbow_avX)
ANGACCY(LElbow, LElbow_avY)
ANGACCZ(LElbow, LElbow_avZ)
ANGACCX(RWrist, RWrist_avX)
```

```
ANGACCY(RWrist, RWrist_avY)
ANGACCZ(RWrist, RWrist_avZ)
ANGACCX(LWrist, LWrist_avX)
ANGACCY(LWrist, LWrist_avY)
ANGACCZ(LWrist, LWrist_avZ)

{* Center of gravity computations for the humeri, forearms, and hands from Clauser (1),(2),(3) are from
local XYZ *}
RHumerus_cgX = RSJC(1)-0.4418*(RSJC(1)-REJC(1))
RHumerus_cgY = RSJC(2)-0.4418*(RSJC(2)-REJC(2))
RHumerus_cgZ = RSJC(3)-0.4418*(RSJC(3)-REJC(3))
RHumerus_cg = {RHumerus_cgX, RHumerus_cgY, RHumerus_cgZ}
LHumerus_cgX = LSJC(1)-0.4418*(LSJC(1)-LEJC(1))
LHumerus_cgY = LSJC(2)-0.4418*(LSJC(2)-LEJC(2))
LHumerus_cgZ = LSJC(3)-0.4418*(LSJC(3)-LEJC(3))
LHumerus_cg = {LHumerus_cgX, LHumerus_cgY, LHumerus_cgZ}
RForearm_cgX = REJC(1)-0.43223*(REJC(1)-RWJC(1))
RForearm_cgY = REJC(2)-0.43223*(REJC(2)-RWJC(2))
RForearm_cgZ = REJC(3)-0.43223*(REJC(3)-RWJC(3))
RForearm_cg = {RForearm_cgX, RForearm_cgY, RForearm_cgZ}
LForearm_cgX = LEJC(1)-0.43223*(LEJC(1)-LWJC(1))
LForearm_cgY = LEJC(2)-0.43223*(LEJC(2)-LWJC(2))
LForearm_cgZ = LEJC(3)-0.43223*(LEJC(3)-LWJC(3))
LForearm_cg = {LForearm_cgX, LForearm_cgY, LForearm_cgZ}
RHand_cgX = RWJC(1)-0.4085*(RWJC(1)-RM3(1))
RHand_cgY = RWJC(2)-0.4085*(RWJC(2)-RM3(2))
RHand_cgZ = RWJC(3)-0.4085*(RWJC(3)-RM3(3))
RHand_cg = {RHand_cgX, RHand_cgY, RHand_cgZ}
LHand_cgX = LWJC(1)-0.4085*(LWJC(1)-LM3(1))
LHand_cgY = LWJC(2)-0.4085*(LWJC(2)-LM3(2))
LHand_cgZ = LWJC(3)-0.4085*(LWJC(3)-LM3(3))
LHand_cg = {LHand_cgX, LHand_cgY, LHand_cgZ}

RCrutchLow_cg = RC0
LCrutchLow_cg = LC0

RCrutchUp_cg = RU0 - .0405*RCrutchUp(2)+ (.032+$markerdiameter)*RCrutchUp(1)
LCrutchUp_cg = LU0 - .0405*LCrutchUp(2)+ (.032+$markerdiameter)*LCrutchUp(1)


RCrutchMid_cg = RL0 + .036*RCrutchMid(2) + .025*RCrutchMid(1)
LCrutchMid_cg = LL0 + .036*LCrutchMid(2) + .025*LCrutchMid(1)          {* cog[m]; (2) for Y-
axis:vertical *}

RUPF = RUU + .04*RCrutchUp(1)          {* point of action for the cuff force*}
LUPF = LUU + .04*LCrutchUp(1)

Output(RHumerus_cg,LHumerus_cg,RForearm_cg,LForearm_cg,RHand_cg,LHand_cg,RCrutchUp_cg,LC
rutchUp_cg,RCrutchMid_cg,LCrutchMid_cg,RCrutchLow_cg,LCrutchLow_cg)

{* Call macros to compute center of gravity velocities and accelerations *}
VCGSEG(RHumerus_cgX)
VCGSEG(RHumerus_cgY)
VCGSEG(RHumerus_cgZ)
VCGSEG(LHumerus_cgX)
VCGSEG(LHumerus_cgY)
```

```
VCGSEG(LHumerus_cgZ)
VCGSEG(RForearm_cgX)
VCGSEG(RForearm_cgY)
VCGSEG(RForearm_cgZ)
VCGSEG(LForearm_cgX)
VCGSEG(LForearm_cgY)
VCGSEG(LForearm_cgZ)
VCGSEG(RHand_cgX)
VCGSEG(RHand_cgY)
VCGSEG(RHand_cgZ)
VCGSEG(LHand_cgX)
VCGSEG(LHand_cgY)
VCGSEG(LHand_cgZ)
VCGSEG(RCrutchUp_cg)
VCGSEG(LCrutchUp_cg)
VCGSEG(RCrutchLow_cg)
VCGSEG(LCrutchLow_cg)
VCGSEG(RCrutchMid_cg)
VCGSEG(LCrutchMid_cg)

ACGSEG(RHumerus_cgXv)
ACGSEG(RHumerus_cgYv)
ACGSEG(RHumerus_cgZv)
RHumerus_cga={RHumerus_cgXva, RHumerus_cgYva, RHumerus_cgZva}
ACGSEG(LHumerus_cgXv)
ACGSEG(LHumerus_cgYv)
ACGSEG(LHumerus_cgZv)
LHumerus_cga={LHumerus_cgXva, LHumerus_cgYva, LHumerus_cgZva}
ACGSEG(RForearm_cgXv)
ACGSEG(RForearm_cgYv)
ACGSEG(RForearm_cgZv)
RForearm_cga={RForearm_cgXva, RForearm_cgYva, RForearm_cgZva}
ACGSEG(LForearm_cgXv)
ACGSEG(LForearm_cgYv)
ACGSEG(LForearm_cgZv)
LForearm_cga={LForearm_cgXva, LForearm_cgYva, LForearm_cgZva}
ACGSEG(RHand_cgXv)
ACGSEG(RHand_cgYv)
ACGSEG(RHand_cgZv)
RHand_cga={RHand_cgXva, RHand_cgYva, RHand_cgZva}
ACGSEG(LHand_cgXv)
ACGSEG(LHand_cgYv)
ACGSEG(LHand_cgZv)
LHand_cga={LHand_cgXva, LHand_cgYva, LHand_cgZva}

ACGSEG(RCrutchUp_cgv)
RCrutchUp_cga=RCrutchUp_cgva
ACGSEG(LCrutchUp_cgv)
LCrutchUp_cga=LCrutchUp_cgva
ACGSEG(RCrutchLow_cgv)
RCrutchLow_cga=RCrutchLow_cgva
ACGSEG(LCrutchLow_cgv)
LCrutchLow_cga=LCrutchLow_cgva
ACGSEG(RCrutchMid_cgv)
RCrutchMid_cga=RCrutchMid_cgva
ACGSEG(LCrutch_G_cgv)
```

```
LCrutchMid_cga=LCrutchMid_cgva

{* Right upper sensor = amplifier 1
Right Lower sensor = amplifier 3
left upper sensor = amplifier 5
left lower sensor = amplifier 6*}

{* ========== Need BB patch to read in forces and moments============================== *}
ForcePlate1 = |ForcePlate1(1),ForcePlate1(2),RU0|    {* Connect at crutch segment, this is where COP is
calculated *}
CONNECT(RCrutchUp,ForcePlate1,1)
Force1=ForcePlate1(1)
Moment1=ForcePlate1(2)
ForcePlate2 = |ForcePlate2(1),ForcePlate2(2),RL0|    {* Connect at crutch segment,this is where COP is
calculated *}
CONNECT(RCrutchLow,ForcePlate2,1)
Force2=ForcePlate2(1)
Moment2=ForcePlate2(2)

ForcePlate3 = |ForcePlate3(1),ForcePlate3(2),LU0|    {* Connect at crutch segment, this is where COP is
calculated *}
CONNECT(LCrutchUp,ForcePlate3,1)
Force3=ForcePlate3(1)
Moment3=ForcePlate3(2)
ForcePlate4 = |ForcePlate4(1), ForcePlate4(2),LL0|    {* Connect at crutch segment,this is where COP is
calculated *}
CONNECT(LCrutchLow,ForcePlate4,1)
Force4=ForcePlate4(1)
Moment4=ForcePlate4(2)
Output(Force1,Moment1,Force2,Moment2,Force3,Moment3,Force4,Moment4)


{* Change to match local kinematic coordinate system setup: Y:up,X:forward,Z:right,Walking in +X *}

{* Blue Crutches *}

{* +X WALKING DIRECTION *}
Force1X = Force1(2)                {* Right Upper Force in N *}
Force1Y = -Force1(3)
Force1Z = -Force1(1)

Force2X = -Force2(2)               {* Right Lower Force in N *}
Force2Y = -Force2(3)
Force2Z = -Force2(1)

Force3X = Force3(2)                {* Left Upper Force in N *}
Force3Y = -Force3(3)
Force3Z = -Force3(1)

Force4X = -Force4(2)               {* Left Lower Force in N *}
Force4Y = -Force4(3)
Force4Z = -Force4(1)

Moment1X = Moment1(2)/1000     {* Right Upper Moment in Nmm converted to Nm*}
Moment1Y = -Moment1(3)/1000
Moment1Z = -Moment1(1)/1000
```

```
Moment2X = -Moment2(2)/1000    {* Right Lower Moment in Nmm converted to Nm *}
Moment2Y = -Moment2(3)/1000
Moment2Z = -Moment2(1)/1000

Moment3X = Moment3(2)/1000     {* Left Upper Moment in Nmm converted to Nm*}
Moment3Y = -Moment3(3)/1000
Moment3Z = -Moment3(1)/1000

Moment4X = -Moment4(2)/1000    {* Left Lower Moment in Nmm converted to Nm*}
Moment4Y = -Moment4(3)/1000
Moment4Z = -Moment4(1)/1000

{* Force1local = {Force1X,Force1Y,Force1Z} *}

{* -X WALKING DIRECTION *}

{*Force1X = -Force1(2)              {* Right Upper Force in N *}
Force1Y = -Force1(3)
Force1Z = Force1(1)

Force2X = Force2(2)                {* Right Lower Force in N *}
Force2Y = -Force2(3)
Force2Z = Force2(1)

Force3X = -Force3(2)               {* Left Upper Force in N *}
Force3Y = -Force3(3)
Force3Z = Force3(1)

Force4X = Force4(2)                {* Left Lower Force in N *}
Force4Y = -Force4(3)
Force4Z = Force4(1)

Moment1X = -Moment1(2)/1000    {* Right Upper Moment in Nmm converted to Nm*}
Moment1Y = -Moment1(3)/1000
Moment1Z = Moment1(1)/1000

Moment2X = Moment2(2)/1000     {* Right Lower Moment in Nmm converted to Nm *}
Moment2Y = -Moment2(3)/1000
Moment2Z = Moment2(1)/1000

Moment3X = -Moment3(2)/1000    {* Left Upper Moment in Nmm converted to Nm*}
Moment3Y = -Moment3(3)/1000
Moment3Z = Moment3(1)/1000

Moment4X = Moment4(2)/1000     {* Left Lower Moment in Nmm converted to Nm*}
Moment4Y = -Moment4(3)/1000
Moment4Z = Moment4(1)/1000*}

Output(Force1X,Force1Y,Force1Z,Force2X,Force2Y,Force2Z,Force3X,Force3Y,Force3Z,Force4X,Force4
Y,Force4Z,Moment1X,Moment1Y,Moment1Z,Moment2X,Moment2Y,Moment2Z,Moment3X,Moment3Y
,Moment3Z,Moment4X,Moment4Y,Moment4Z)

{*Multiply now by R, get to global, angle must be relative to global *}
ROTMATRIX(RLof_Up)
Force1iX_g = Force1X*RLof_Up_r11_x
```

```
Force1iY_g = Force1X*RLof_Up_r21_x
Force1iZ_g = Force1X*RLof_Up_r31_x
Force1X_g={Force1iX_g,Force1iY_g,Force1iZ_g}

Force1jX_g = Force1Y*RLof_Up_r12_y
Force1jY_g = Force1Y*RLof_Up_r22_y
Force1jZ_g = Force1Y*RLof_Up_r32_y
Force1Y_g={Force1jX_g ,Force1jY_g,Force1jZ_g}

Force1kX_g = Force1Z*RLof_Up_r13_z
Force1kY_g = Force1Z*RLof_Up_r23_z
Force1kZ_g = Force1Z*RLof_Up_r33_z
Force1Z_g={Force1kX_g ,Force1kY_g,Force1kZ_g}

ROTMATRIX(RLof_Mid)
Force2iX_g = Force2X*RLof_Mid_r11_x
Force2iY_g = Force2X*RLof_Mid_r21_x
Force2iZ_g = Force2X*RLof_Mid_r31_x
Force2X_g={Force2iX_g,Force2iY_g,Force2iZ_g}

Force2jX_g = Force2Y*RLof_Mid_r12_y
Force2jY_g = Force2Y*RLof_Mid_r22_y
Force2jZ_g = Force2Y*RLof_Mid_r32_y
Force2Y_g={Force2jX_g ,Force2jY_g,Force2jZ_g}

Force2kX_g = Force2Z*RLof_Mid_r13_z
Force2kY_g = Force2Z*RLof_Mid_r23_z
Force2kZ_g = Force2Z*RLof_Mid_r33_z
Force2Z_g={Force2kX_g ,Force2kY_g,Force2kZ_g}

{* Or could do this to get to global, test_RCrutchXg is same as -Force1lab(1)  *}
{*MOMENTMULT1(Force1local,RCrutch(1),RCrutch(2),RCrutch(3),test_RCrutchXg) *}
{*Output(test_RCrutchXg) *}

{*Multiply now by R, get to global, angle must be relative to global *}

ROTMATRIX(LLof_Up)
Force3iX_g = Force3X*LLof_Up_l11_x
Force3iY_g = Force3X*LLof_Up_l21_x
Force3iZ_g = Force3X*LLof_Up_l31_x
Force3X_g={Force3iX_g,Force3iY_g,Force3iZ_g}

Force3jX_g = Force3Y*LLof_Up_l12_y
Force3jY_g = Force3Y*LLof_Up_l22_y
Force3jZ_g = Force3Y*LLof_Up_l32_y
Force3Y_g={Force3jX_g ,Force3jY_g,Force3jZ_g}

Force3kX_g = Force3Z*LLof_Up_l13_z
Force3kY_g = Force3Z*LLof_Up_l23_z
Force3kZ_g = Force3Z*LLof_Up_l33_z
Force3Z_g={Force3kX_g ,Force3kY_g,Force3kZ_g}

ROTMATRIX(LLof_Mid)
Force4iX_g = Force4X*LLof_Mid_l11_x
Force4iY_g = Force4X*LLof_Mid_l21_x
Force4iZ_g = Force4X*LLof_Mid_l31_x
```

```
Force4X_g={Force4iX_g,Force4iY_g,Force4iZ_g}

Force4jX_g = Force4Y*LLof_Mid_l12_y
Force4jY_g = Force4Y*LLof_Mid_l22_y
Force4jZ_g = Force4Y*LLof_Mid_l32_y
Force4Y_g={Force4jX_g ,Force4jY_g,Force4jZ_g}

Force4kX_g = Force4Z*LLof_Mid_l13_z
Force4kY_g = Force4Z*LLof_Mid_l23_z
Force4kZ_g = Force4Z*LLof_Mid_l33_z
Force4Z_g={Force4kX_g ,Force4kY_g,Force4kZ_g}


{* Flip from sensor output *}
Force1lab = -(Force1X_g + Force1Y_g + Force1Z_g)
Force2lab = -(Force2X_g + Force2Y_g + Force2Z_g)

Force3lab = -(Force3X_g + Force3Y_g + Force3Z_g)
Force4lab = -(Force4X_g + Force4Y_g + Force4Z_g)

OUTPUT(Force1lab,Force2lab,Force3lab,Force4lab)


I={1,0,0}
J={0,1,0}
K={0,0,1}

{*=======CRUTCH TIP FORCES=== wtcrutch (mass of seg) in kg, cga in m/s2, to get force in N.*}

FRCX = -$wtcrutch_low*RCrutchLow_cga(1) - Force2lab(1)
FRCY = -$wtcrutch_low*(RCrutchLow_cga(2) + 9.81) - Force2lab(2) {* 9.81m/s2 is gravity in vertical
axis *}
FRCZ = -$wtcrutch_low*RCrutchLow_cga(3) - Force2lab(3)
FRCL = {FRCX,FRCY,FRCZ}                                          {* _G=global force *}
FRCrutch = FRCX*I+FRCY*J+FRCZ*K
FRCrutch_G_norm = (FRCrutch/$wt)*100 {* expressed as a percent of Body Weight *}
DotProduct(FRCrutch,RCrutchLow(1),FRCrutchAntPos)        {*multiply by columns (transpose) *}
DotProduct(FRCrutch,RCrutchLow(2),FRCrutchPrxDis)
DotProduct(FRCrutch,RCrutchLow(3),FRCrutchMedLat)
FRCS = {FRCrutchAntPos,FRCrutchPrxDis,FRCrutchMedLat}
FRCrutch_L_norm = (FRCS/$wt)*100   {* local force expressed as a percent of BW *}
OUTPUT(FRCL,FRCrutch,FRCrutch_G_norm,FRCS,FRCrutch_L_norm)

FLCX = -$wtcrutch_low*LCrutchLow_cga(1) - Force4lab(1)
FLCY = -$wtcrutch_low*(LCrutchLow_cga(2) + 9.81) - Force4lab(2)
FLCZ = -$wtcrutch_low*LCrutchLow_cga(3) - Force4lab(3)
FLCL = {FLCX,FLCY,FLCZ}                                          {* _G=global force *}
FLCrutch = FLCX*I+FLCY*J+FLCZ*K
FLCrutch_G_norm = (FLCrutch/$wt)*100
DotProduct(FLCrutch,LCrutchLow(1),FLCrutchAntPos)
DotProduct(FLCrutch,LCrutchLow(2),FLCrutchPrxDis)
DotProduct(FLCrutch,LCrutchLow(3),FLCrutchMedLat)
FLCS = {FLCrutchAntPos,FLCrutchPrxDis,FLCrutchMedLat}            {* _L=local force *}
FLCrutch_L_norm = (FLCS/$wt)*100
OUTPUT(FLCL,FLCrutch,FLCrutch_G_norm,FLCS,FLCrutch_L_norm)
```

```
{*==========Hand FORCES========= wtcrutch (mass of seg) in kg, cga in m/s2, to get force in N.*}

FRHX = -$wtcrutch_mid*RCrutchMid_cga(1) + Force2lab(1)-COS($CRUTCH_ANGLE)*Force1lab(1)
FRHY = -$wtcrutch_mid*(RCrutchMid_cga(2) + 9.81) + Force2lab(2)-
COS($CRUTCH_ANGLE)*Force1lab(2) {* 9.81m/s2 is gravity in vertical axis *}
FRHZ = -$wtcrutch_mid*RCrutchMid_cga(3) + Force1lab(3)-Force2lab(3)
FRHL = {FRHX,FRHY,FRHZ}                         {* _G=global force *}
FRHand = FRHX*I+FRHY*J+FRHZ*K
FRHand_G_norm = (FRHand/$wt)*100                {* expressed as a percent of Body Weight *}
DotProduct(FRHand,RCrutchMid(1),FRHandAntPos)           {*multiply by columns (transpose) *}
DotProduct(FRHand,RCrutchMid(2),FRHandPrxDis)
DotProduct(FRHand,RCrutchMid(3),FRHandMedLat)
FRHS = {FRHandAntPos,FRHandPrxDis,FRHandMedLat}
FRHand_L_norm = (FRHS/$wt)*100                  {* local force expressed as a percent of BW *}
OUTPUT(FRHL,FRHand,FRHand_G_norm,FRHS,FRHand_L_norm)

FLHX = -$wtcrutch_mid*LCrutchMid_cga(1) + Force4lab(1)-COS($CRUTCH_ANGLE)*Force3lab(1)
FLHY = -$wtcrutch_mid*(LCrutchMid_cga(2) + 9.81) + Force4lab(2)-
COS($CRUTCH_ANGLE)*Force3lab(2)                 {* 9.81m/s2 is gravity in vertical axis *}
FLHZ = -$wtcrutch_mid*LCrutchMid_cga(3) + Force3lab(3)-Force4lab(3)
FLHL = {FLHX,FLHY,FLHZ}                         {* _G=global force *}
FLHand = FLHX*I+FLHY*J+FLHZ*K
FLHand_G_norm = (FLHand/$wt)*100                {* expressed as a percent of Body Weight *}
DotProduct(FLHand,LCrutchMid(1),FLHandAntPos)  {*multiply by columns (transpose) *}
DotProduct(FLHand,LCrutchMid(2),FLHandPrxDis)
DotProduct(FLHand,LCrutchMid(3),FLHandMedLat)
FLHS = {FLHandAntPos,FLHandPrxDis,FLHandMedLat}
FLHand_L_norm = (FLHS/$wt)*100                  {* local force expressed as a percent of BW *}
OUTPUT(FLHL,FLHAND,FLHand_G_norm,FLHS,FLHand_L_norm)

{*==========Cuff FORCES======== wtcrutch (mass of seg) in kg, cga in m/s2, to get force in N.*}

FRCXU = -$wtcrutch_up*RCrutchUp_cga(1) + Force1lab(1)
FRCYU = -$wtcrutch_up*(RCrutchUp_cga(2) + 9.81) + Force1lab(2)   {* 9.81m/s2 is gravity in vertical
axis *}
FRCZU = -$wtcrutch_up*RCrutchUp_cga(3) + Force1lab(3)
FRCU = {FRCXU,FRCYU,FRCZU}                              {* _G=global force *}
FRCrutchUp = FRCXU*I+FRCYU*J+FRCZU*K
FRCrutchUp_G_norm = (FRCrutchUp/$wt)*100        {* expressed as a percent of Body Weight *}
DotProduct(FRCrutchUp,RCrutchUp(1),FRCrutchUpAntPosU) {*multiply by columns (transpose) *}
DotProduct(FRCrutchUp,RCrutchUp(2),FRCrutchUpPrxDisU)
DotProduct(FRCrutchUp,RCrutchUp(3),FRCrutchUpMedLatU)
FRCSU = {FRCrutchUpAntPosU,FRCrutchUpPrxDisU,FRCrutchUpMedLatU}
FRCrutchUp_L_norm = (FRCSU/$wt)*100   {* local force expressed as a percent of BW *}
OUTPUT(FRCU,FRCrutchUp,FRCrutchUp_G_norm,FRCSU,FRCrutchUp_L_norm)

FLCXU = -$wtcrutchUp*LCrutchUp_cga(1) + Force3lab(1)
FLCYU = -$wtcrutchUp*(LCrutchUp_cga(2) + 9.81) + Force3lab(2)    {* 9.81m/s2 is gravity in vertical
axis *}
FLCZU = -$wtcrutchUp*LCrutchUp_cga(3) + Force3lab(3)
FLCU = {FLCXU,FLCYU,FLCZU}                                      {* _G=global force *}
FLCrutchUp = FLCXU*I+FLCYU*J+FLCZU*K
FLCrutchUp_G_norm = (FLCrutchUp/$wt)*100        {* expressed as a percent of Body Weight *}
DotProduct(FLCrutchUp,LCrutchUp(1),FLCrutchAntPosU)    {*multiply by columns (transpose) *}
DotProduct(FLCrutchUp,LCrutchUp(2),FLCrutchPrxDisU)
```

```
DotProduct(FLCrutchUp,LCrutchUp(3),FLCrutchMedLatU)
FLCSU = {FLCrutchAntPosU,FLCrutchPrxDisU,FLCrutchMedLatU}
FLCrutchUp_L_norm = (FLCSU/$wt)*100          {* local force expressed as a percent of BW *}
OUTPUT(FLCU,FLCrutchUp,FLCrutchUp_G_norm,FLCSU,FLCrutchUp_L_norm)

{* ==========WRIST FORCES================== *}

FRWX = -$mh*RHand_cga(1) + FRHL(1)

FRWY = -$mh*(RHand_cga(2) + 9.81) + FRHL(2)
FRWZ = -$mh*RHand_cga(3) + FRHL(3)
FRWL = {FRWX,FRWY,FRWZ}                                    {* global force *}
FRWrist=FRWX*I+FRWY*J+FRWZ*K
FRWrist_G_norm = (FRWrist/$wt)*100
DotProduct(FRWrist,RHand(1),FRWristAntPos)
DotProduct(FRWrist,RHand(2),FRWristPrxDis)
DotProduct(FRWrist,RHand(3),FRWristMedLat)
FRWS={FRWristAntPos,FRWristPrxDis,FRWristMedLat}           {* local force *}
FRWrist_L_norm = (FRWS/$wt)*100
OUTPUT(FRWL,FRWrist,FRWrist_G_norm,FRWS, FRWrist_L_norm)


FLWX = -$mh*LHand_cga(1) + FLHL(1)
FLWY = -$mh*(LHand_cga(2) + 9.81) + FLHL(2)
FLWZ = -$mh*LHand_cga(3) + FLHL(3)
FLWL = {FLWX,FLWY,FLWZ}
FLWrist=FLWX*I+FLWY*J+FLWZ*K                               {* global force *}
FLWrist_G_norm = (FLWrist/$wt)*100
DotProduct(FLWrist,LHand(1),FLWristAntPos)
DotProduct(FLWrist,LHand(2),FLWristPrxDis)
DotProduct(FLWrist,LHand(3),FLWristMedLat)
FLWS={FLWristAntPos,FLWristPrxDis,FLWristMedLat}           {* local force *}
FLWrist_L_norm = (FLWS/$wt)*100
OUTPUT(FLWL,FLWrist,FLWrist_G_norm,FLWS,FLWrist_L_norm)

{* ==========ELBOW FORCES================== *}

FREX = -$mfa*RForearm_cga(1) + FRWL(1)+FRCU(1)
FREY = -$mfa*(RForearm_cga(2) + 9.81) + FRWL(2)+FRCU(2)
FREZ = -$mfa*RForearm_cga(3) + FRWL(3)+FRCU(3)
FREL = {FREX, FREY, FREZ}
FRElbow=FREX*I+FREY*J+FREZ*K                               {* global force *}
FRElbow_G_norm = (FRElbow/$wt)*100
DotProduct(FRElbow,RForearm(1),FRElbowAntPos)
DotProduct(FRElbow,RForearm(2),FRElbowPrxDis)
DotProduct(FRElbow,RForearm(3),FRElbowMedLat)
FRES={FRElbowAntPos,FRElbowPrxDis,FRElbowMedLat}           {* local force *}
FRElbow_L_norm = (FRES/$wt)*100
OUTPUT(FREL,FRElbow,FRElbow_G_norm,FRES, FRElbow_L_norm)

FLEX = -$mfa*LForearm_cga(1) + FLWL(1)+FLCU(1)
FLEY = -$mfa*(LForearm_cga(2) + 9.81) + FLWL(2)+FLCU(2)
FLEZ = -$mfa*LForearm_cga(3) + FLWL(3)+FLCU(3)
FLEL = {FLEX, FLEY, FLEZ}
FLElbow=FLEX*I+FLEY*J+FLEZ*K                               {* global force *}
FLElbow_G_norm = (FLElbow/$wt)*100
```

```
DotProduct(FLElbow,LForearm(1),FLElbowAntPos)
DotProduct(FLElbow,LForearm(2),FLElbowPrxDis)
DotProduct(FLElbow,LForearm(3),FLElbowMedLat)
FLES={FLElbowAntPos,FLElbowPrxDis,FLElbowMedLat}              {* local force *}
FLElbow_L_norm = (FLES/$wt)*100
OUTPUT(FLEL,FLElbow,FLElbow_G_norm,FLES,FLElbow_L_norm)

{* ==========SHOULDER FORCES================== *}

FRSX = -$mua*RHumerus_cga(1) + FREL(1)
FRSY = -$mua*(RHumerus_cga(2) + 9.81) + FREL(2)
FRSZ = -$mua*RHumerus_cga(3) + FREL(3)
FRSL = {FRSX, FRSY, FRSZ}
FRShoulder=FRSX*I+FRSY*J+FRSZ*K                               {* global force *}
FRShoulder_G_norm = (FRShoulder/$wt)*100
DotProduct(FRShoulder,RHumerus(1),FRShoulderAntPos)
DotProduct(FRShoulder,RHumerus(2),FRShoulderPrxDis)
DotProduct(FRShoulder,RHumerus(3),FRShoulderMedLat)
FRSS={FRShoulderAntPos,FRShoulderPrxDis,FRShoulderMedLat}     {* local force *}
FRShoulder_L_norm = (FRSS/$wt)*100
OUTPUT(FRSL,FRShoulder,FRShoulder_G_norm,FRSS, FRShoulder_L_norm)

FLSX = -$mua*LHumerus_cga(1) + FLEL(1)
FLSY = -$mua*(LHumerus_cga(2) + 9.81) + FLEL(2)
FLSZ = -$mua*LHumerus_cga(3) + FLEL(3)
FLSL = {FLSX, FLSY, FLSZ}
FLShoulder=FLSX*I+FLSY*J+FLSZ*K                               {* global force *}
FLShoulder_G_norm = (FLShoulder/$wt)*100
DotProduct(FLShoulder,LHumerus(1),FLShoulderAntPos)
DotProduct(FLShoulder,LHumerus(2),FLShoulderPrxDis)
DotProduct(FLShoulder,LHumerus(3),FLShoulderMedLat)
FLSS={FLShoulderAntPos,FLShoulderPrxDis,FLShoulderMedLat}     {* local force *}
FLShoulder_L_norm = (FLSS/$wt)*100
OUTPUT(FLSL,FLShoulder,FLShoulder_G_norm,FLSS, FLShoulder_L_norm)

{* ==========END OF FORCES================== *}


{* MOMENTS given in local, convert to global using R *}
Moment1iX_g = Moment1X*RLof_Up_r11_x
Moment1iY_g = Moment1X*RLof_Up_r21_x
Moment1iZ_g = Moment1X*RLof_Up_r31_x
Moment1X_g = {Moment1iX_g, Moment1iY_g, Moment1iZ_g}
Moment1jX_g = Moment1Y*RLof_Up_r12_y
Moment1jY_g = Moment1Y*RLof_Up_r22_y
Moment1jZ_g = Moment1Y*RLof_Up_r32_y
Moment1Y_g = {Moment1jX_g, Moment1jY_g, Moment1jZ_g}
Moment1kX_g = Moment1Z*RLof_Up_r13_z
Moment1kY_g = Moment1Z*RLof_Up_r23_z
Moment1kZ_g = Moment1Z*RLof_Up_r33_z
Moment1Z_g = {Moment1kX_g,Moment1kY_g, Moment1kZ_g}

Moment2iX_g = Moment2X*RLof_Mid_r11_x
Moment2iY_g = Moment2X*RLof_Mid_r21_x
Moment2iZ_g = Moment2X*RLof_Mid_r31_x
Moment2X_g = {Moment2iX_g, Moment2iY_g, Moment2iZ_g}
```

```
Moment2jX_g = Moment2Y*RLof_Mid_r12_y
Moment2jY_g = Moment2Y*RLof_Mid_r22_y
Moment2jZ_g = Moment2Y*RLof_Mid_r32_y
Moment2Y_g = {Moment2jX_g, Moment2jY_g, Moment2jZ_g}
Moment2kX_g = Moment2Z*RLof_Mid_r13_z
Moment2kY_g = Moment2Z*RLof_Mid_r23_z
Moment2kZ_g = Moment2Z*RLof_Mid_r33_z
Moment2Z_g = {Moment2kX_g,Moment2kY_g, Moment2kZ_g}

Moment3iX_g = Moment3X*LLof_Up_l11_x
Moment3iY_g = Moment3X*LLof_Up_l21_x
Moment3iZ_g = Moment3X*LLof_Up_l31_x
Moment3X_g = {Moment3iX_g, Moment3iY_g, Moment3iZ_g}
Moment3jX_g = Moment3Y*LLof_Up_l12_y
Moment3jY_g = Moment3Y*LLof_Up_l22_y
Moment3jZ_g = Moment3Y*LLof_Up_l32_y
Moment3Y_g = {Moment3jX_g, Moment3jY_g, Moment3jZ_g}
Moment3kX_g = Moment3Z*LLof_Up_l13_z
Moment3kY_g = Moment3Z*LLof_Up_l23_z
Moment3kZ_g = Moment3Z*LLof_Up_l33_z
Moment3Z_g = {Moment3kX_g, Moment3kY_g, Moment3kZ_g}

Moment4iX_g = Moment4X*LLof_Mid_l11_x
Moment4iY_g = Moment4X*LLof_Mid_l21_x
Moment4iZ_g = Moment4X*LLof_Mid_l31_x
Moment4X_g = {Moment4iX_g, Moment4iY_g, Moment4iZ_g}
Moment4jX_g = Moment4Y*LLof_Mid_l12_y
Moment4jY_g = Moment4Y*LLof_Mid_l22_y
Moment4jZ_g = Moment4Y*LLof_Mid_l32_y
Moment4Y_g = {Moment4jX_g, Moment4jY_g, Moment4jZ_g}
Moment4kX_g = Moment4Z*LLof_Mid_l13_z
Moment4kY_g = Moment4Z*LLof_Mid_l23_z
Moment4kZ_g = Moment4Z*LLof_Mid_l33_z
Moment4Z_g = {Moment4kX_g, Moment4kY_g, Moment4kZ_g}

Moment1lab = -(Moment1X_g + Moment1Y_g + Moment1Z_g)
Moment2lab = -(Moment2X_g + Moment2Y_g + Moment2Z_g)
Moment3lab = -(Moment3X_g + Moment3Y_g + Moment3Z_g)
Moment4lab = -(Moment4X_g + Moment4Y_g + Moment4Z_g)
OUTPUT(Moment1lab,Moment2lab,Moment3lab,Moment4lab)

{* Rate of change of angular momentum,resultant moments, eqn 5.35 Zatsiorsky
in local, angle wrt proximal segment; Iy:long, Ix=Iz:transverse I=[kg*m^2], aa=[rad/s^2],av=[rad/s],
H=Nm *}

HRCLX= $IxcL*RCrutch_aaX - ($IycL-$IzcL)*RCrutch_avY*RCrutch_avZ
HRCLY= $IycL*RCrutch_aaY - ($IzcL-$IxcL)*RCrutch_avZ*RCrutch_avX
HRCLZ= $IzcL*RCrutch_aaZ - ($IxcL-$IycL)*RCrutch_avX*RCrutch_avY
HRCL = {HRCLX,HRCLY,HRCLZ}

HLCLX= $IxcL*LCrutch_aaX - ($IycL-$IzcL)*LCrutch_avY*LCrutch_avZ
HLCLY= $IycL*LCrutch_aaY - ($IzcL-$IxcL)*LCrutch_avZ*LCrutch_avX
HLCLZ= $IzcL*LCrutch_aaZ - ($IxcL-$IycL)*LCrutch_avX*LCrutch_avY
HLCL = {HLCLX,HLCLY,HLCLZ}

HRHX = $Ixuar*RShoulder_aaX - ($Iyuar-$Izuar)*RShoulder_avY*RShoulder_avZ
```

```
HRHY = $Iyuar*RShoulder_aaY - ($Izuar-$Ixuar)*RShoulder_avZ*RShoulder_avX
HRHZ = $Izuar*RShoulder_aaZ - ($Ixuar-$Iyuar)*RShoulder_avX*RShoulder_avY
HRH = {HRHX, HRHY, HRHZ}

HLHX = $Ixual*LShoulder_aaX - ($Iyual-$Izual)*LShoulder_avY*LShoulder_avZ
HLHY = $Iyual*LShoulder_aaY - ($Izual-$Ixual)*LShoulder_avZ*LShoulder_avX
HLHZ = $Izual*LShoulder_aaZ - ($Ixual-$Iyual)*LShoulder_avX*LShoulder_avY
HLH = {HLHX, HLHY, HLHZ}

HRFX = $Ixfar*RElbow_aaX - ($Iyfar-$Izfar)*RElbow_avY*RElbow_avZ
HRFY = $Iyfar*RElbow_aaY - ($Izfar-$Ixuar)*RElbow_avZ*RElbow_avX
HRFZ = $Izfar*RElbow_aaZ - ($Ixfar-$Iyfar)*RElbow_avX*RElbow_avY
HRF = {HRFX, HRFY, HRFZ}

HLFX = $Ixfal*LElbow_aaX - ($Iyfal-$Izfal)*LElbow_avY*LElbow_avZ
HLFY = $Iyfal*LElbow_aaY - ($Izfal-$Ixual)*LElbow_avZ*LElbow_avX
HLFZ = $Izfal*LElbow_aaZ - ($Ixfal-$Iyfal)*LElbow_avX*LElbow_avY
HLF = {HLFX, HLFY, HLFZ}

HRHdX = $Ixhr*RWrist_aaX - ($Iyhr-$Izhr)*RWrist_avY*RWrist_avZ
HRHdY = $Iyhr*RWrist_aaY - ($Izhr-$Ixhr)*RWrist_avZ*RWrist_avX
HRHdZ = $Izhr*RWrist_aaZ - ($Ixhr-$Iyhr)*RWrist_avX*RWrist_avY
HRHd = {HRHdX, HRHdY, HRHdZ}

HLHdX = $Ixhl*LWrist_aaX - ($Iyhl-$Izhl)*LWrist_avY*LWrist_avZ
HLHdY = $Iyhl*LWrist_aaY - ($Izhl-$Ixhl)*LWrist_avZ*LWrist_avX
HLHdZ = $Izhl*LWrist_aaZ - ($Ixhl-$Iyhl)*LWrist_avX*LWrist_avY
HLHd = {HLHdX, HLHdY, HLHdZ}

OUTPUT(HLHd,HRHd,HLF,HRF,HLH,HRH,HLCL,HRCL)
OUTPUT($Ixuar,$Iyuar,$Izuar,$Ixfar,$Iyfar,$Izfar,$Ixhr,$Iyhr,$Izhr,$IxcL,$IycL,$IzcL)


{* Moments *}

{* RIGHT CRUTCH LOWER SEGMENT *}

RCLprox = RL0-RCrutchLow_cg                    {* Use marker on hand [m]*}
RCLdist = RG0-RCrutchLow_cg

CROSS(RCLprox,Force2lab,MRCTip_cg1)                    {* Nm *}
CROSS(RCLdist,FRCL,MRCTip_cg2)

MresRCL = -Moment2lab - MRCTip_cg1 - MRCTip_cg2 {* global position *}

uMresRCL = MresRCL(1)*I+MresRCL(2)*J+MresRCL(3)*K
DotProduct(uMresRCL,RCrutchLow(3),MresRCLSZ)        {* change to local *}
DotProduct(uMresRCL,RCrutchLow(1),MresRCLSX)
DotProduct(uMresRCL,RCrutchLow(2),MresRCLSY)
MresRCLS = {MresRCLSX,MresRCLSY,MresRCLSZ}        {* Now in local *}

MRCLS = MresRCLS {* H is local, H is equal to moments (change all H signs), Nm *}
MRCLSx = MRCLS(1)
MRCLSy = MRCLS(2)
MRCLSz = MRCLS(3)
MRCLS_final = {MRCLSx,MRCLSy,MRCLSz}                {* L=local *}
```

```
MRCLow_L_norm = 100*MRCLS_final/($wt*$height)          {* Normalized as percent bodyweight time
height, *100 to get percent great than 1 *}

MOMENTMULT1(MRCLS_final,RCrutchLow(1),RCrutchLow(2),RCrutchLow(3),MRCL1) {* Change
to global by multiplying by [R] *}
MOMENTMULT2(MRCLS_final,RCrutchLow(1),RCrutchLow(2),RCrutchLow(3),MRCL2)
MOMENTMULT3(MRCLS_final,RCrutchLow(1),RCrutchLow(2),RCrutchLow(3),MRCL3)
MRCL={MRCL1,MRCL2,MRCL3}  {* G=global *}

MRCLow_G_norm=100*MRCL/($wt*$height)                   {* expressed as %BW*HT(N*m) *}

OUTPUT(MRCL,uMresRCL,MRCLS,MRCLow_G_norm,MRCLow_L_norm, MRCLS_final)

{* LEFT CRUTCH LOWER SEGMENT *}

LCLprox = LL0-LCrutchLow_cg                            {* Use LM3 vs LCU *}
LCLdist = LG0-LCrutchLow_cg

CROSS(LCLprox,Force4lab,MLCTip_cg1)                    {* Nm *}
CROSS(LCLdist,FLCL,MLCTip_cg2)

MresLCL = -Moment4lab - MLCTip_cg1 - MLCTip_cg2        {* global position Nm *}

uMresLCL = MresLCL(1)*I+MresLCL(2)*J+MresLCL(3)*K
DotProduct(uMresLCL,LCrutchLow(3),MresLCLSZ)           {* change order,2,3,1 *}
DotProduct(uMresLCL,LCrutchLow(1),MresLCLSX)
DotProduct(uMresLCL,LCrutchLow(2),MresLCLSY)
MresLCLS = {MresLCLSX,MresLCLSY,MresLCLSZ}

MLCLS = MresLCLS                                       {* Nm *}
MLCLSx = MLCLS(1)
MLCLSy = MLCLS(2)
MLCLSz = MLCLS(3)
MLCLS_final = {MLCLSx,MLCLSy,MLCLSz}
MLCLow_L_norm = 100*MLCLS_final/($wt*$height)          {* G=global *}

MOMENTMULT1(MLCLS_final,LCrutchLow(1),LCrutchLow(2),LCrutchLow(3),MLCL1)
MOMENTMULT2(MLCLS_final,LCrutchLow(1),LCrutchLow(2),LCrutchLow(3),MLCL2)
MOMENTMULT3(MLCLS_final,LCrutchLow(1),LCrutchLow(2),LCrutchLow(3),MLCL3)
MLCL={MLCL1,MLCL2,MLCL3}

MLCLow_G_norm=100*MLCL/($wt*$height)
OUTPUT(MLCL,uMresLCL,MLCLS,MLCLow_G_norm,MLCLow_L_norm, MLCLS_final)

{* RIGHT CRUTCH MID SEGMENT *}

RChand = RM3-RCrutchMid_cg                     {* Use marker on hand [m]*}
RClow = RL0-RCrutchMid_cg
RCup = RU0-RCrutchMid_cg

CROSS(RChand,FRHL,MRCrutch_cg1)                {* Nm *}
CROSS(RCup,Force1lab,MRCrutch_cg2)
CROSS(RClow,Force2lab,MRCrutch_cg3)
```

```
MresRHL = - Moment1lab + Moment2lab - MRCrutch_cg1 - MRCrutch_cg2 + MRCrutch_cg3 {* global
position *}

uMresRHL = MresRHL(1)*I+MresRHL(2)*J+MresRHL(3)*K
DotProduct(uMresRHL,RCrutchMid(3),MresRHSZ)          {* change to local *}
DotProduct(uMresRHL,RCrutchMid(1),MresRHSX)
DotProduct(uMresRHL,RCrutchMid(2),MresRHSY)
MresRHS = {MresRHSX,MresRHSY,MresRHSZ}               {* Now in local *}

MRHS = HRCL + MresRHS {* H is local, H is equal to moments (change all H signs), Nm *}
MRHSx = MRHS(1)
MRHSy = MRHS(2)
MRHSz = MRHS(3)
MRHS_final = {MRHSx,MRHSy,MRHSz}                     {* L=local *}

MRHand_L_norm = 100*MRHS_final/($wt*$height)         {* Normalized as percent bodyweight time
height, *100 to get percent great than 1 *}

MOMENTMULT1(MRHS_final,RCrutchMid(1),RCrutchMid(2),RCrutchMid(3),MRHL1) {* Change to
global by multiplying by [R] *}
MOMENTMULT2(MRHS_final,RCrutchMid(1),RCrutchMid(2),RCrutchMid(3),MRHL2)
MOMENTMULT3(MRHS_final,RCrutchMid(1),RCrutchMid(2),RCrutchMid(3),MRHL3)
MRHL={MRHL1,MRHL2,MRHL3}                             {* G=global *}

MRHand_G_norm=100*MRHL/($wt*$height)                 {* expressed as %BW*HT(N*m) *}

OUTPUT(MRHL,MRHand_G_norm,uMresRHL,MRHS,MRHand_L_norm, MRHS_final)

{* LEFT CRUTCH MID SEGMENT*}
LChand = LM3-LCrutchMid_cg                           {* Use LM3 vs LCU *}
LClow = LL0-LCrutchMid_cg
LCup = LU0-LCrutchMid_cg

CROSS(LChand,FLHL,MLCrutch_cg1)                      {* Nm *}
CROSS(LCup,Force3lab,MLCrutch_cg2)
CROSS(LClow,Force4lab,MLCrutch_cg3)

MresLHL = -Moment3lab +Moment4lab - MLCrutch_cg1 - MLCrutch_cg2 + MLCrutch_cg3 {* global
position Nm *}
uMresLHL = MresLHL(1)*I+MresLHL(2)*J+MresLHL(3)*K

DotProduct(uMresLHL,LCrutchMid(3),MresLHSZ)          {* change order,2,3,1 *}
DotProduct(uMresLHL,LCrutchMid(1),MresLHSX)
DotProduct(uMresLHL,LCrutchMid(2),MresLHSY)
MresLHS = {MresLHSX,MresLHSY,MresLHSZ}

MLHS = HLCL + MresLHS                                {* Nm *}
MLHSx = MLHS(1)
MLHSy = MLHS(2)
MLHSz = MLHS(3)
MLHS_final = {MLHSx,MLHSy,MLHSz}
MLHand_L_norm = 100*MLHS_final/($wt*$height)         {* G=global *}

MOMENTMULT1(MLHS_final,LCrutchMid(1),LCrutchMid(2),LCrutchMid(3),MLHL1)
MOMENTMULT2(MLHS_final,LCrutchMid(1),LCrutchMid(2),LCrutchMid(3),MLHL2)
MOMENTMULT3(MLHS_final,LCrutchMid(1),LCrutchMid(2),LCrutchMid(3),MLHL3)
```

```
MLHL={MLHL1,MLHL2,MLHL3}

MLHand_G_norm=100*MLHL/($wt*$height)
OUTPUT(MLHL,MLHand_G_norm,uMresLHL,MLHS,MLHand_L_norm, MLHS_final)

{* RIGHT CUFF *}

RCprox = RUPF-RCrutchUp_cg                    {* Use marker on hand [m]*}
RCdist = RU0-RCrutchUp_cg

CROSS(RCprox,FRCU,MRCuff_cg1)                 {* Nm *}
CROSS(RCdist,Force1lab,MRCuff_cg2)

MresRCU = Moment1lab - MRCuff_cg1 + MRCuff_cg2    {* global position *}

uMresRCU = MresRCU(1)*I+MresRCU(2)*J+MresRCU(3)*K
DotProduct(uMresRCU,RCrutchUp(3),MresRCUSZ)   {* change to local *}
DotProduct(uMresRCU,RCrutchUp(1),MresRCUSX)
DotProduct(uMresRCU,RCrutchUp(2),MresRCUSY)
MresRCUS = {MresRCUSX,MresRCUSY,MresRCUSZ}    {* Now in local *}

MRCUS = MresRCUS {* H is local, H is equal to moments (change all H signs), Nm *}
MRCUSx = MRCUS(1)
MRCUSy = MRCUS(2)
MRCUSz = MRCUS(3)
MRCUS_final = {MRCUSx,MRCUSy,MRCUSz}          {* L=local *}

MRCuff_L_norm = 100*MRCUS_final/($wt*$height)     {* Normalized as percent bodyweight time
height, *100 to get percent great than 1 *}

MOMENTMULT1(MRCUS_final,RCrutchUp(1),RCrutchUp(2),RCrutchUp(3),MRCU1) {* Change to
global by multiplying by [R] *}
MOMENTMULT2(MRCUS_final,RCrutchUp(1),RCrutchUp(2),RCrutchUp(3),MRCU2)
MOMENTMULT3(MRCUS_final,RCrutchUp(1),RCrutchUp(2),RCrutchUp(3),MRCU3)
MRCU={MRCU1,MRCU2,MRCU3}                      {* G=global *}

MRCuff_G_norm=100*MRCU/($wt*$height)          {* expressed as %BW*HT(N*m) *}

OUTPUT(MRCU,uMresRCU,MRCUS,MRCuff_G_norm,MRCuff_L_norm, MRCUS_final)

{* LEFT CUFF *}

LCprox = LUPF-LCrutchUp_cg                    {* Use LM3 vs LCU *}
LCdist = LU0-LCrutchUp_cg

CROSS(LCprox,FLCU,MLCuff_cg1)                 {* Nm *}
CROSS(LCdist,Force3lab,MLCuff_cg2)

MresLCU = Moment3lab - MLCuff_cg1 + MLCuff_cg2    {* global position Nm *}

uMresLCU = MresLCU(1)*I+MresLCU(2)*J+MresLCU(3)*K
DotProduct(uMresLCU,LCrutchUp(3),MresLCUSZ)   {* change order,2,3,1 *}
DotProduct(uMresLCU,LCrutchUp(1),MresLCUSX)
DotProduct(uMresLCU,LCrutchUp(2),MresLCUSY)
MresLCUS = {MresLCUSX,MresLCUSY,MresLCUSZ}
```

```
MLCUS = MresLCUS                                    {* Nm *}
MLCUSx = MLCUS(1)
MLCUSy = MLCUS(2)
MLCUSz = MLCUS(3)
MLCUS_final = {MLCUSx,MLCUSy,MLCUSz}
MLCuff_L_norm = 100*MLCUS_final/($wt*$height)       {* G=global *}

MOMENTMULT1(MLCUS_final,LCrutchUp(1),LCrutchUp(2),LCrutchUp(3),MLCU1)
MOMENTMULT2(MLCUS_final,LCrutchUp(1),LCrutchUp(2),LCrutchUp(3),MLCU2)
MOMENTMULT3(MLCUS_final,LCrutchUp(1),LCrutchUp(2),LCrutchUp(3),MLCU3)
MLCL={MLCU1,MLCU2,MLCU3}

MLCuff_G_norm=100*MLCU/($wt*$height)
OUTPUT(MLCU,uMresLCU,MLCUS,MLCuff_G_norm,MLCuff_L_norm, MLCUS_final)


{* RIGHT WRIST *}

RWprox = RWJC - RHand_cg
RWdist = RM3 - RHand_cg

CROSS(RWprox, FRWL, MRWrist_cg1)                    {* Nm *}
CROSS(RWdist, FRHL, MRWrist_cg2)

MresRW_G = MRHL - MRWrist_cg1 + MRWrist_cg2         {* global position *}

uMresRW_G = MresRW_G(1)*I+MresRW_G(2)*J+MresRW_G(3)*K
DotProduct(uMresRW_G,RHand(1),MresRWSX)             {* L=LOCAL,S=segmental *}
DotProduct(uMresRW_G,RHand(2),MresRWSY)
DotProduct(uMresRW_G,RHand(3),MresRWSZ)
MresRWS={MresRWSX,MresRWSY,MresRWSZ}
MRWS = HRHd + MresRWS                               {* Nm *}

MRWSx=MRWS(1)
MRWSy=MRWS(2)
MRWSz=MRWS(3)
MRWS_final={MRWSx,MRWSy,MRWSz}
MRWrist_L_norm=100*MRWS_final/($wt*$height)         {* G=global *}

MOMENTMULT1(MRWS_final,RHand(1),RHand(2),RHand(3),MRWL1)
MOMENTMULT2(MRWS_final,RHand(1),RHand(2),RHand(3),MRWL2)
MOMENTMULT3(MRWS_final,RHand(1),RHand(2),RHand(3),MRWL3)
MRWL={MRWL1,MRWL2,MRWL3}

MRWrist_G_norm=100*MRWL/($wt*$height)
OUTPUT(MRWL,uMresRW_G,MRWS,MRWrist_G_norm,MRWrist_L_norm,MRWS_final)

{* LEFT WRIST *}
LWprox = LWJC - LHand_cg
LWdist = LM3 - LHand_cg

CROSS(LWprox, FLWL, MLWrist_cg1)                    {* Nm *}
CROSS(LWdist, FLHL, MLWrist_cg2)

MresLWL = MLHL - MLWrist_cg1 + MLWrist_cg2          {* global position Nm *}
```

```
uMresLWL = MresLWL(1)*I+MresLWL(2)*J+MresLWL(3)*K
DotProduct(uMresLWL,LHand(1),MresLWSX)
DotProduct(uMresLWL,LHand(2),MresLWSY)
DotProduct(uMresLWL,LHand(3),MresLWSZ)
MresLWS={MresLWSX,MresLWSY,MresLWSZ}

MLWS = HLHd + MresLWS                                   {* Nm *}
MLWSx=MLWS(1)
MLWSy=MLWS(2)
MLWSz=MLWS(3)
MLWS_final={MLWSx,MLWSy,MLWSz}
MLWrist_L_norm=100*MLWS_final/($wt*$height)             {* G=global *}

MOMENTMULT1(MLWS_final,LHand(1),LHand(2),LHand(3),MLWL1)
MOMENTMULT2(MLWS_final,LHand(1),LHand(2),LHand(3),MLWL2)
MOMENTMULT3(MLWS_final,LHand(1),LHand(2),LHand(3),MLWL3)
MLWL={MLWL1,MLWL2,MLWL3}

MLWrist_G_norm=100*MLWL/($wt*$height)
OUTPUT(MLWL,uMresLWL,MLWS,MLWrist_G_norm,MLWrist_L_norm,MLWS_final)

{* RIGHT ELBOW *}

REprox = REJC - RForearm_cg
REdist = RWJC - RForearm_cg
REcuff = RUPF - RForearm_cg

CROSS(REprox, FREL, MRElbow_cg1)                        {* Nm *}
CROSS(REdist, FRWL, MRElbow_cg2)
CROSS(REcuff, FRCU, MRElbow_cg3)

MresREL = MRWL + MRCL - MRElbow_cg1 + MRElbow_cg2 + MRElbow_cg3 {* global position Nm
*}

uMresREL = MresREL(1)*I+MresREL(2)*J+MresREL(3)*K
DotProduct(uMresREL,RForearm(1),MresRESX)
DotProduct(uMresREL,RForearm(2),MresRESY)
DotProduct(uMresREL,RForearm(3),MresRESZ)
MresRES = {MresRESX, MresRESY, MresRESZ}

MRES = HRF + MresRES                                    {* Nm *}
MRESx=MRES(1)
MRESy=MRES(2)
MRESz=MRES(3)
MRES_final={MRESx,MRESy,MRESz}
MRElbow_L_norm = 100*MRES_final/($wt*$height)           {* G=global *}

MOMENTMULT1(MRES_final,RForearm(1),RForearm(2),RForearm(3),MREL1)
MOMENTMULT2(MRES_final,RForearm(1),RForearm(2),RForearm(3),MREL2)
MOMENTMULT3(MRES_final,RForearm(1),RForearm(2),RForearm(3),MREL3)
MREL={MREL1,MREL2,MREL3}
MRElbow_G_norm=100*MREL/($wt*$height)

OUTPUT(MREL,uMresREL,MRES,MRElbow_G_norm,MRElbow_L_norm,MRES_final)

{* LEFT ELBOW *}
```

```
LEprox = LEJC - LForearm_cg
LEdist = LWJC - LForearm_cg
LEcuff = LUPF - LForearm_cg

CROSS(LEprox, FLEL, MLElbow_cg1)                    {* Nm *}
CROSS(LEdist, FLWL, MLElbow_cg2)
CROSS(LEcuff, FLCU, MLElbow_cg3)

MresLEL = MLWL + MLCL - MLElbow_cg1 + MLElbow_cg2 + MLElbow_cg3 {* global position *}

uMresLEL = MresLEL(1)*I+MresLEL(2)*J+MresLEL(3)*K
DotProduct(uMresLEL,LForearm(1),MresLESX)           {* convert to local *}
DotProduct(uMresLEL,LForearm(2),MresLESY)
DotProduct(uMresLEL,LForearm(3),MresLESZ)
MresLES = {MresLESX, MresLESY, MresLESZ}

MLES = HLF + MresLES                                {* Nm *}
MLESx=MLES(1)
MLESy=MLES(2)
MLESz=MLES(3)
MLES_final={MLESx,MLESy,MLESz}
MLElbow_L_norm = 100*MLES_final/($wt*$height)       {* G=global *}

MOMENTMULT1(MLES_final,LForearm(1),LForearm(2),LForearm(3),MLEL1)
MOMENTMULT2(MLES_final,LForearm(1),LForearm(2),LForearm(3),MLEL2)
MOMENTMULT3(MLES_final,LForearm(1),LForearm(2),LForearm(3),MLEL3)
MLEL={MLEL1,MLEL2,MLEL3}
MLElbow_G_norm=100*MLEL/($wt*$height)

OUTPUT(MLEL,uMresLEL,MLES,MLElbow_G_norm,MLElbow_L_norm,MLES_final)

{* RIGHT SHOULDER *}

RSprox = RSJC - RHumerus_cg
RSdist = REJC - RHumerus_cg

CROSS(RSprox, FRSL, MRShoulder_cg1)                 {* Nm *}
CROSS(RSdist, FREL, MRShoulder_cg2)

MresRSL = MREL - MRShoulder_cg1 + MRShoulder_cg2 {* global position Nm *}

uMresRSL = MresRSL(1)*I+MresRSL(2)*J+MresRSL(3)*K
DotProduct(uMresRSL,RHumerus(1),MresRSSX)
DotProduct(uMresRSL,RHumerus(2),MresRSSY)
DotProduct(uMresRSL,RHumerus(3),MresRSSZ)
MresRSS = {MresRSSX, MresRSSY, MresRSSZ}

MRSS = HRH + MresRSS                                {* Nm *}
MRSSx=MRSS(1)
MRSSy=MRSS(2)
MRSSz=MRSS(3)
MRSS_final={MRSSx,MRSSy,MRSSz}
MRShoulder_L_norm = 100*MRSS_final/($wt*$height)    {* G=global *}

MOMENTMULT1(MRSS_final,RHumerus(1),RHumerus(2),RHumerus(3),MRSL1)
MOMENTMULT2(MRSS_final,RHumerus(1),RHumerus(2),RHumerus(3),MRSL2)
```

```
MOMENTMULT3(MRSS_final,RHumerus(1),RHumerus(2),RHumerus(3),MRSL3)
MRSL={MRSL1,MRSL2,MRSL3}
MRShoulder_G_norm=100*MRSL/($wt*$height)

OUTPUT(uMresRSL,MRSS,MRSL,MRShoulder_G_norm,MRShoulder_L_norm,MRSS_final)

{* LEFT SHOULDER *}

LSprox = LSJC - LHumerus_cg
LSdist = LEJC - LHumerus_cg

CROSS(LSprox, FLSL, MLShoulder_cg1)                    {* Nm *}
CROSS(LSdist, FLEL, MLShoulder_cg2)

MresLSL = MLEL - MLShoulder_cg1 + MLShoulder_cg2 {* global position Nm *}

uMresLSL = MresLSL(1)*I+MresLSL(2)*J+MresLSL(3)*K
DotProduct(uMresLSL,LHumerus(1),MresLSSX)
DotProduct(uMresLSL,LHumerus(2),MresLSSY)
DotProduct(uMresLSL,LHumerus(3),MresLSSZ)
MresLSS = {MresLSSX, MresLSSY, MresLSSZ}

MLSS = HLH + MresLSS                                   {* Nm *}
MLSSx=MLSS(1)
MLSSy=MLSS(2)
MLSSz=MLSS(3)
MLSS_final={MLSSx,MLSSy,MLSSz}
MLShoulder_L_norm = 100*MLSS_final/($wt*$height)       {* G=global *}

MOMENTMULT1(MLSS_final,LHumerus(1),LHumerus(2),LHumerus(3),MLSL1)
MOMENTMULT2(MLSS_final,LHumerus(1),LHumerus(2),LHumerus(3),MLSL2)
MOMENTMULT3(MLSS_final,LHumerus(1),LHumerus(2),LHumerus(3),MLSL3)
MLSL={MLSL1,MLSL2,MLSL3}
MLShoulder_G_norm=100*MLSL/($wt*$height)

OUTPUT(uMresLSL,MLSS,MLSL,MLShoulder_G_norm,MLShoulder_L_norm,MLSS_final)
```

A.2.2 Paramaters (*.mp)

```
$MarkerDiameter = 0.014
$ForceThreshold= 1
$SamplingRate = 120
$FTL = 120
$pi= 3.14156


$LShoulderOffset = (0.28/(2*3.14156))
$RShoulderOffset = (0.28/(2*3.14156))
$RWidthHand = 0.02
$LWidthHand = 0.02


$CRUTCH_ANGLE = 15

$wtcrutch_low =0.234
$wtcrutch_mid = 0.15795
$wtcrutch_up = 0.1718152

$age = 11
$Weight =  54.89
$wt= $Weight * 4.4482
$kwt = 24.9
$height = 1.384

$mua =(0.02344+ (0.00069558*$age))*$kwt
$mfa =(0.0134+ (0.00031268*$age))*$kwt
$mh = 0.0088*$kwt

{* ========================================================================== *}
{*        Humerus                    *******Measure for each subject in m ******                    *}
{* ========================================================================== *}

$lhe = 0.285      {* lhe = length of left shoulder center to left elbow center in m *}
$lsc = 0.28       {* lsc = circumference of the left shoulder in m                  *}
$lhc = 0.19       {* lhc = circumference of the maximum left humerus segment in m *}
$lec = 0.185      {* lec = circumference of the left elbow in m                        *}
$led = 0.06       {* led = diameter of the left elbow in m                  *}

$rhe = 0.285      {* rhe = length right shoulder center to right elbow center in m *}
$rsc = 0.28       {* rsc = circumference of the right shoulder in m                 *}
$rhc = 0.19       {* rhc = circumference of the maximum right humerus segment in m *}
$rec = 0.185      {* rec = circumference of the right elbow in m                       *}
$red = 0.06       {* red = diameter of the right elbow in m                 *}

{* ========================================================================== *}
{*        FOREARM                        Measure for each subject              *}
{* ========================================================================== *}

$lew = 0.21       {* lew = length of left elbow center to left wrist center in m *}
$lfc = 0.17       {* lfc = circumference of the maximum left forearm segment in m *}
$lwc = 0.13       {* lwc = circumference of the left wrist in m                        *}
$lwd = 0.05       {* lwd = diameter of the left wrist in m                  *}
```

```
$rew = 0.21        {* rew = length of right elbow center to right wrist center in m *}
$rfc = 0.17        {* rfc = circumference of the maximum right forearm segment in m *}
$rwc = 0.13        {* rwc = circumference of the right wrist in m                    *}
$rwd = 0.05        {* rwd = diameter of the right wrist in m                  *}

{* ========================================================================= *}
{*         HAND   *******Measure for each subject******                      *}
{* ========================================================================= *}

$lwm = 0.15        {* lhm = length of left wrist center to tip of left metacarpal-phalangeal III in m *}
$lmc = 0.16        {* lmc = circumference of the left metacarpal-phalangeal joints in m          *}

$rwm = 0.15        {* rhm = length of right wrist center to tip of right metacarpal-phalangeal III in m *}
$rmc = 0.16        {* rmc = circumference of the right metacarpal-phalangeal joints in m          *}

{* ========================================================================= *}
{* perimeters                                                                *}
{* ========================================================================= *}

{* Yeadon & Morlock *}

$pual= (($lsc + (2*$lhc) + $lec)/4)  {* pual = perimeter of left humerus in m taken from Yeadon &
Morlock *}
$pfal= (($lec + (2*$lfc) + $lwc)/4)  {* pfal = perimeter of left forearm in m taken from Yeadon & Morlock
*}
$phl= (($lwc + $lmc)/2)              {* phl = perimeter of left hand in m taken from Yeadon & Morlock *}

$puar= (($rsc + (2*$rhc) + $rec)/4) {* puar = perimeter of right humerus in m taken from Yeadon &
Morlock *}
$pfar= (($rec + (2*$rfc) + $rwc)/4) {* pfar = perimeter of right forearm in m taken from Yeadon &
Morlock *}
$phr= (($rwc + $rmc)/2)              {* phr = perimeter of right hand in m taken from Yeadon & Morlock *}

{* ========================================================================= *}
{* INERTIA kg*m^2 taken from Yeadon & Morlock J Biomech (1989) 22:683-9  LOCAL SEGMENT
PARAMETERS Y is longitudinal axis *}
{* ========================================================================= *}

$Ixual= (0.5*0.979*$pual*$pual*$pual*$pual*$lhe) + (6.11*$pual*$pual*$lhe*$lhe*$lhe) {* left upper
arm *}
$Izual= (0.5*0.979*$pual*$pual*$pual*$pual*$lhe) + (6.11*$pual*$pual*$lhe*$lhe*$lhe)
$Iyual= 0.979*$pual*$pual*$pual*$pual*$lhe

$Ixfal= (0.5*0.810*$pfal*$pfal*$pfal*$pfal*$lew) + (4.98*$pfal*$pfal*$lew*$lew*$lew) {* left forearm
*}
$Izfal= (0.5*0.810*$pfal*$pfal*$pfal*$pfal*$lew) + (4.98*$pfal*$pfal*$lew*$lew*$lew)
$Iyfal= 0.810*$pfal*$pfal*$pfal*$pfal*$lew

$Ixhl= (0.5*1.309*$phl*$phl*$phl*$phl*$lwm) + (7.68*$phl*$phl*$lwm*$lwm*$lwm) {* left hand *}
$Izhl= (0.5*1.309*$phl*$phl*$phl*$phl*$lwm) + (7.68*$phl*$phl*$lwm*$lwm*$lwm)
$Iyhl= 1.309*$phl*$phl*$phl*$phl*$lwm

$Ixuar= (0.5*0.979*$puar*$puar*$puar*$puar*$rhe) + (6.11*$puar*$puar*$rhe*$rhe*$rhe) {* right
upper arm *}
$Izuar= (0.5*0.979*$puar*$puar*$puar*$puar*$rhe) + (6.11*$puar*$puar*$rhe*$rhe*$rhe)
$Iyuar= 0.979*$puar*$puar*$puar*$puar*$rhe
```

```
$Ixfar= (0.5*0.810*$pfar*$pfar*$pfar*$pfar*$rew) + (4.98*$pfar*$pfar*$rew*$rew*$rew) {* right
forearm *}
$Izfar= (0.5*0.810*$pfar*$pfar*$pfar*$pfar*$rew) + (4.98*$pfar*$pfar*$rew*$rew*$rew)
$Iyfar= 0.810*$pfar*$pfar*$pfar*$pfar*$rew

$Ixhr= (0.5*1.309*$phr*$phr*$phr*$phr*$rwm) + (7.68*$phr*$phr*$rwm*$rwm*$rwm) {* right hand
*}
$Izhr= (0.5*1.309*$phr*$phr*$phr*$phr*$rwm) + (7.68*$phr*$phr*$rwm*$rwm*$rwm)
$Iyhr= 1.309*$phr*$phr*$phr*$phr*$rwm

{* $IxcU = 0.000304187 *}
{* $IzcU = 0.000304187 *}
{* $IycU = 0.000202935 *}

$IxcL = 8.35279E-05
$IzcL = 0.000139322
$IycL = 0.000297127
```

A.2.3 Markers (*.mkr)

```
!MKR#2
[Autolabel]
C7      Spinal Process C7
LACR    Left Acromium
LCLAV Left Clavicle
RACR    Right Acromium
RCLAV Right Clavicle
LLE     Left Lateral Epicondyle
LME     Left Medial Epicondyle
PX      Xiphoid Process
RME     Right Medial Epicondyle
RLE     Right Lateral Epicondyle
LRAD    Left Radial Styloid
LULN    Left Ulnar Styloid
LM3     Head of third metacarpal (Left Hand)
LM5     Head of fifth metacarpal placed laterally (Left Hand)
LUU     Left Crutch Upper
LLL     Left Crutch Lower Left
LLR     Left Crutch Lower Right
LLF     Left Crutch Lower Forward
LLB     Left Crutch Lower Backward
RRAD    Right Radial Styloid
RULN    Right Ulnar Styloid
RM3     Head of third metacarpal (Right Hand)
RM5     Head of fifth metacarpal placed laterally (Right Hand)
RUU     Right Crutch Upper
RLL     Right Crutch Lower Left
RLR     Right Crutch Lower Right
RLF     Right Crutch Lower Forward
RLB     Right Crutch Lower Backward

Thorax= C7,PX,LCLAV,RCLAV,LACR,RACR
RUpperarm= RACR,RLE,RME
LUpperarm= LACR,LLE,LME
RForearm= RLE,RME,RRAD,RULN
LForearm= LLE,LME,LRAD,LULN
RHand= RM3,RM5,RRAD,RULN
LHand= LM3,LM5,LRAD,LULN
RCrutchLow= RLF,RLB,RLR,RLL
LCrutchLow= LLF,LLB,LLR,LLL
RCrutchUp= RLF,RLB,RLR,RLL
LCrutchUp= LLF,LLB,LLR,LLL

Thorax,RUpperarm
RUpperarm,RForearm
RForearm,RHand
Thorax,LUpperarm
LUpperarm,LForearm
LForearm,LHand

#[Output Markers]
#C7      Spinal Process C7
#PX      Xiphoid Process
#LCLAV          Left Clavicle
#LACR  Left Acromium
```

```
#LME    Left Medial Epicondyle
#LLE    Left Lateral Epicondyle
#LULN   Left Ulnar Styloid
#LRAD   Left Radial Styloid
#LM3    Head of third metacarpal (Left Hand)
#LM5    Head of fifth metacarpal placed laterally (Left Hand)
#LLF    Left Crutch Lower Forward
#LLB    Left Crutch Lower Backward
#LLR    Left Crutch Lower Right
#LLL    Left Crutch Lower Left

#RCLAV          Right Clavicle
#RACR   Right Acromium
#RME    Right Medial Epicondyle
#RLE    Right Lateral Epicondyle
#RULN   Right Ulnar Styloid
#RRAD   Right Radial Styloid
#RM3    Head of third metacarpal (Right Hand)
#RM5    Head of fifth metacarpal placed laterally (Right Hand)
#RLF    Right Crutch Lower Forward
#RLB    Right Crutch Lower Backward
#RLR    Right Crutch Lower Right
#RLL    Right Crutch Lower Left

PX,     C7
C7,     RCLAV
C7,     LCLAV
PX,     LCLAV
PX,     RCLAV
LCLAV,RCLAV
LACR,   LCLAV
RACR,   C7
LACR,   C7
RACR,   RCLAV
LACR,   LCLAV
RACR,   RASI
LACR,   LASI
RASI,   LASI
LASI,   LACR
RASI,   RACR
PX,     RASI
PX,     LASI
LACR,   LLE
LACR,   LME
LLE,    LME
LLE,    LRAD
LME,    LULN
LULN,   LRAD
LM3,    LM5
LM3,    LRAD
LM5,    LULN
RACR,   RLE
RACR,   RME
RLE,    RME
RLE,    RRAD
RME,    RULN
```

RULN, RRAD
RM3, RM5
RM3, RRAD
RM5, RULN
RLF, RLB
RLR, RLL
LLF, LLB
LLR, LLL

[Angles]
Trunk
RShoulder
LShoulder
RElbow
LElbow
RWrist
LWrist
RLof_Up
LLof_Up
RLof_Low
LLof_Low

#[Forces]
#FRCrutch_L_norm
#FRWrist_L_norm
#FRElbow_L_norm
#FRShoulder_L_norm
#FLCrutch_L_norm
#FLWrist_L_norm
#FLElbow_L_norm
#FLShoulder_L_norm

#[Moments]
#MRCrutch_L_norm
#MRWrist_L_norm
#MRElbow_L_norm
#MRShoulder_L_norm
#MLCrutch_L_norm
#MLWrist_L_norm
#MLElbow_L_norm
#MLShoulder_L_norm

[Segment Axes]
ORIGINGlobal_mod
AXIS_xGlobal_mod
AXIS_yGlobal_mod
AXIS_zGlobal_mod

ORIGINThorax
AXIS_xThorax
AXIS_yThorax
AXIS_zThorax

ORIGINLHumerus
AXIS_xLHumerus
AXIS_yLHumerus

AXIS_zLHumerus

ORIGINRHumerus
AXIS_xRHumerus
AXIS_yRHumerus
AXIS_zRHumerus

ORIGINLForearm
AXIS_xLForearm
AXIS_yLForearm
AXIS_zLForearm

ORIGINRForearm
AXIS_xRForearm
AXIS_yRForearm
AXIS_zRForearm

ORIGINRHand
AXIS_xRHand
AXIS_yRHand
AXIS_zRHand

ORIGINLHand
AXIS_xLHand
AXIS_yLHand
AXIS_zLHand

ORIGINRCrutchUp
AXIS_xRCrutchUp
AXIS_yRCrutchUp
AXIS_zRCrutchUp

ORIGINLCrutchUp
AXIS_xLCrutchUp
AXIS_yLCrutchUp
AXIS_zLCrutchUp

ORIGINRCrutchLow
AXIS_xRCrutchLow
AXIS_yRCrutchLow
AXIS_zRCrutchLow

ORIGINLCrutchLow
AXIS_xLCrutchLow
AXIS_yLCrutchLow
AXIS_zLCrutchLow

ORIGINGlobal_mod,AXIS_xGlobal_mod
ORIGINGlobal_mod,AXIS_yGlobal_mod
ORIGINGlobal_mod,AXIS_zGlobal_mod

ORIGINThorax,AXIS_xThorax
ORIGINThorax,AXIS_yThorax
ORIGINThorax,AXIS_zThorax

ORIGINLForearm,AXIS_xLForearm
ORIGINLForearm,AXIS_yLForearm
ORIGINLForearm,AXIS_zLForearm

ORIGINRForearm,AXIS_xRForearm
ORIGINRForearm,AXIS_yRForearm
ORIGINRForearm,AXIS_zRForearm

ORIGINLHumerus,AXIS_xLHumerus
ORIGINLHumerus,AXIS_yLHumerus
ORIGINLHumerus,AXIS_zLHumerus

ORIGINRHumerus,AXIS_xRHumerus
ORIGINRHumerus,AXIS_yRHumerus
ORIGINRHumerus,AXIS_zRHumerus

ORIGINRHand,AXIS_xRHand
ORIGINRHand,AXIS_yRHand
ORIGINRHand,AXIS_zRHand

ORIGINLHand,AXIS_xLHand
ORIGINLHand,AXIS_yLHand
ORIGINLHand,AXIS_zLHand

ORIGINRCrutchUp,AXIS_xRCrutchUp
ORIGINRCrutchUp,AXIS_yRCrutchUp
ORIGINRCrutchUp,AXIS_zRCrutchUp

ORIGINLCrutchUp,AXIS_xLCrutchUp
ORIGINLCrutchUp,AXIS_yLCrutchUp
ORIGINLCrutchUp,AXIS_zLCrutchUp

ORIGINRCrutchLow,AXIS_xRCrutchLow
ORIGINRCrutchLow,AXIS_yRCrutchLow
ORIGINRCrutchLow,AXIS_zRCrutchLow

ORIGINLCrutchLow,AXIS_xLCrutchLow
ORIGINLCrutchLow,AXIS_yLCrutchLow
ORIGINLCrutchLow,AXIS_zLCrutchLow